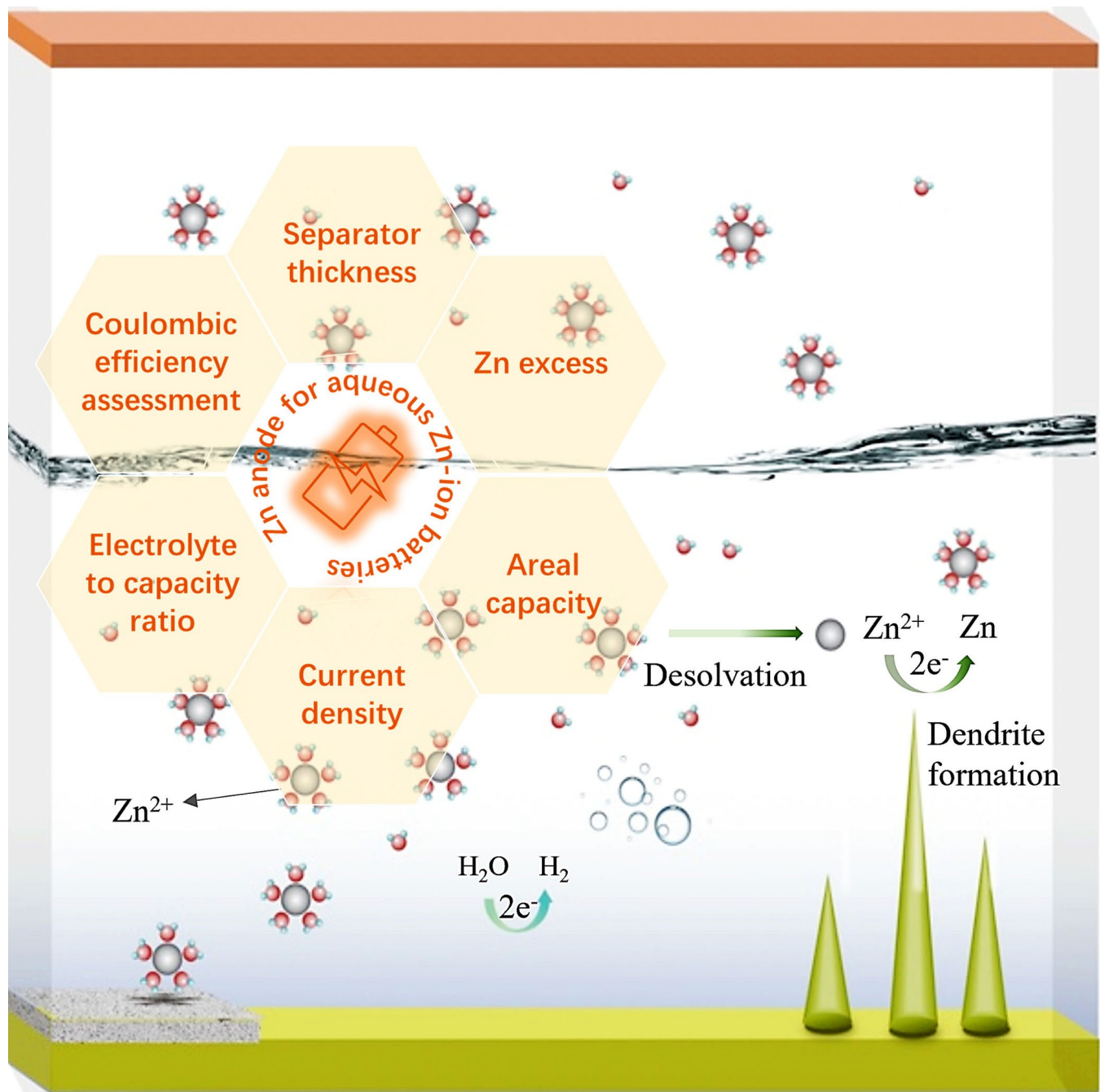


Understanding and Performance of the Zinc Anode Cycling in Aqueous Zinc-Ion Batteries and a Roadmap for the Future

Yuan Shang^[a] and Dipan Kundu*^[a, b]



By virtue of environmental benignity, inherent safety, and affordable cost of raw materials, aqueous zinc-ion batteries (AZIBs) have witnessed tremendous upheaval in research interest and are considered to have enormous potential for stationary and renewable storage applications. Yet, the high activity of Zn in aqueous electrolytes triggers metal corrosion and hydrogen evolution, which, together with dendrite formation on zinc surface during its electrodeposition, leads to poor Coulombic efficiency and rapid short-circuit failure during cycling. Therefore, to divulge a critical and in-depth understanding of these underlying issues, (electro)chemical behavior of the Zn metal in aqueous electrolytes and corresponding

theories are first discussed in this review. This is followed by a thorough discussion of various strategies, categorized based on the intrinsic mechanism, for the suppression of dendrite and parasitic side reactions that are ultimately intertwined. Finally, strategic recommendations are provided as a roadmap to coordinate research and development efforts, and the energy density analyses of a representative AZIB cell is presented to highlight technical and functional needs for the practical development of the technology. This review is expected to provide a comprehensive understanding of the Zn metal anode development for AZIBs and draw attention to pertinent criteria for performance assessment.

1. Introduction

Electrochemical energy storage devices based on batteries coupled with rapidly developing renewable energy resources (e.g., solar and wind) is seen as one of the key enabling solutions to avert the grave environmental issues facing humankind today.^[1] Batteries are deemed vital for balancing the fluctuation in renewable energy generation that complicates renewable integration with the electrical grid.^[2] Non-aqueous rechargeable lithium-ion batteries (LIBs) are the frontrunner thanks to their high energy density, extended lifespan, and market readiness, which have helped them outweigh competitions in portable electronics and electric vehicle applications. Yet, the cost of the LIB technologies, safety concerns associated with the use of flammable and toxic organic electrolytes and worries over the future cost of lithium and sustainability of raw materials resources dissuades their application for stationary and large-scale storage.^[3] Considering these bottlenecks for LIBs, developing safer and cheaper alternatives with considerable energy density is imperative.

Electrochemically inert and high energy density anodes with water-based electrolytes have been envisaged as feasible solutions. As a result, aqueous batteries based on iron,^[4] aluminum,^[5] and zinc^[6] have attracted considerable attention. Among those, aqueous zinc-ion batteries (AZIBs) are being intensively investigated due to their resource availability, safety,

and environmental benignity. A typical AZIB prototype is composed of an inorganic/organic Zn^{2+} storing (or anion storing) cathode, a Zn metal anode, and a Zn^{2+} salt solution in water as the electrolyte (typical pH of 3 to 6). The charge storage mechanism is complex on the cathode side, involving Zn^{2+} intercalation reaction, chemical conversion reaction, and co-intercalation of protons. On the other side, the Zn anode reaction can be simplified as the electrochemical Zn dissolution/deposition. To date, massive efforts have been devoted to investigating cathode materials. Considerable progress has been achieved with respect to cathode performance with manganese oxide-based materials,^[7] vanadium oxide-based material,^[8] and Prussian blue analogues.^[9] At this point, along with achieving scalability of the cathode performance, the issue that appears to hold back the next stage of development is the Zn anode stability and cyclability, particularly, when somewhat practical cycling conditions are applied.

Zinc is not only non-toxic and relatively inexpensive, but it is also compatible with aqueous electrolytes despite its quite negative reduction potential (-0.76 V vs. standard hydrogen electrode). A large kinetic overpotential for hydrogen evolution on zinc means even at the low electrochemical potential of Zn cycling, a fierce reaction with water-based electrolyte is avoided, enhancing the stability window of even standard aqueous electrolytes to ~ 2 V.^[10] Besides, the divalent redox of the Zn renders a high theoretical capacity of 5849 mAh cm^{-3} . Despite these positive attributes, Zn metal anode development for AZIBs is still at an early stage, and there are intricate issues concerning the aqueous Zn/Zn^{2+} cycling, which impede the feasibility of scale-up. The 'Achilles' heel' for the zinc metal anode is eventually its thermodynamic instability in aqueous electrolytes, which triggers hydrogen evolution reaction (HER), consequent corrosion, and dendrite formation (Figure 1).^[10,11] On the one hand, the decomposition of the electrolyte and the loss of active zinc due to HER and Zn corrosion, respectively, severely affect Zn's reversibility, and thus Coulombic efficiency. Ensuing surface irregularities along with inherent surface and crystalline inhomogeneities, on the other hand, induces heterogeneous nucleation of Zn, triggering dendrite growth, leading to rapid cell failure by a short circuit.^[12] To make the matter worse, the dendritic deposition enhances the accessible anode surface area to the electrolyte, thereby exacerbating HER

[a] Y. Shang, Dr. D. Kundu
School of Chemical Engineering
UNSW Sydney
Kensington, NSW 2052, Australia
E-mail: d.kundu@unsw.edu.au

[b] Dr. D. Kundu
School of Mechanical and Manufacturing Engineering
UNSW Sydney
Kensington, NSW 2052, Australia

 Supporting information for this article is available on the WWW under
<https://doi.org/10.1002/batt.202100394>

 An invited contribution to a Special Collection dedicated to Aqueous Electrolyte Batteries.

 © 2022 The Authors. *Batteries & Supercaps* published by Wiley-VCH GmbH. This is an open access article under the terms of the Creative Commons Attribution Non-Commercial License, which permits use, distribution and reproduction in any medium, provided the original work is properly cited and is not used for commercial purposes.

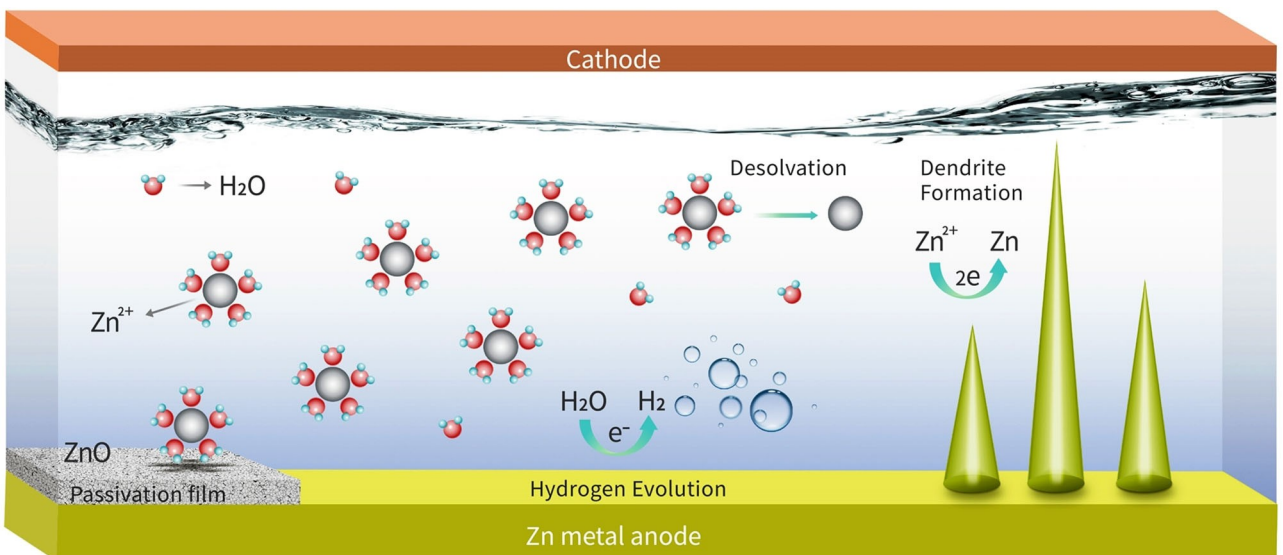


Figure 1. Schematic illustration of potential issues related to the Zn metal anode cycling in AZIBs.

and corrosion. In turn, the sluggish Zn^{2+} migration through the passivation byproducts further worsens the heterogeneous deposition of Zn, sparking further dendritic structure formation. This mutual reinforcement between HER/corrosion and dendrite formation severely affects the cycling performance and appeals for serious attention for a comprehensive understanding of the underlying issues and the development of rational strategies with a practical outlook.^[13]

Many studies have been undertaken in the past few years to improve the tolerance of the Zn anode to corrosion and dendrite formation focusing on strategies as highlighted in Figure 2, and some notable advancement has been made. As there are already several reviews summarizing the different approaches to stabilize Zn anode, it is of great importance to have a comprehensive critique on the topic from the perspective of intrinsic chemical-electrochemical attributes and mechanisms of the reversible Zn^{2+}/Zn electrochemistry, which we try to do here. Apart from numerically boosting the lifespan of Zn anode, and thus AZIBs, it is essential to keep practical considerations in mind in designing feasible strategies. However, this is often overlooked in most studies. In this review, first up, we discuss the (electro)chemistry and dendritic issues of zinc metal under different pH environments and correspond-

ing theories. Subsequently, different strategies for suppressing side reactions (HER and corrosion) and dendrite formation are systematically reviewed and summarized. In order to address the wide variation in performance between studies - even for the unoptimized reference electrochemical system - and assess the viability of the innovative approaches, we make some recommendations in regard to some of the critical aspects like current density, areal capacity, inter-electrode distance and the electrochemical protocol, which are either overlooked or ignored, leading to inconsistencies that impede proper understanding and advancement. Finally, we present an analysis of the volumetric and gravimetric energy densities for a representative AZIB cell chemistry as a function of a few critical cell parameters, which highlights some of the requirements we should consider for a realistic and balanced perspective while evaluating and presenting breakthrough research ideas to foster the practical development of the AZIB technology.



Yuan Shang received his B.S. degree from the Powder Metallurgy Research Institute at Central South University and M.S. from the School of Photovoltaic and Renewable Energy Engineering at University New South Wales (UNSW). Now, he is a Ph.D. candidate in the School of Chemical Engineering at UNSW under the supervision of Dr. Dipan Kundu. At present, his research interest concerns the practical development of the Zn anode for aqueous Zn-ion batteries.



Dipan Kundu received his Ph.D. from ETH Zurich in 2012 and was a postdoctoral scientist with Prof. Linda Nazar at the University Waterloo between 2013 and 2016. Later he was a group leader at ETH (2017–2019), endowed by Swiss National Science Foundation Ambizione grant. He joined the University of New South Wales (UNSW Sydney) as a Senior Lecturer at the end of 2019. His research experience and interests span the areas of solid-state electrochemistry, materials science, Li-ion and beyond Li-ion batteries.

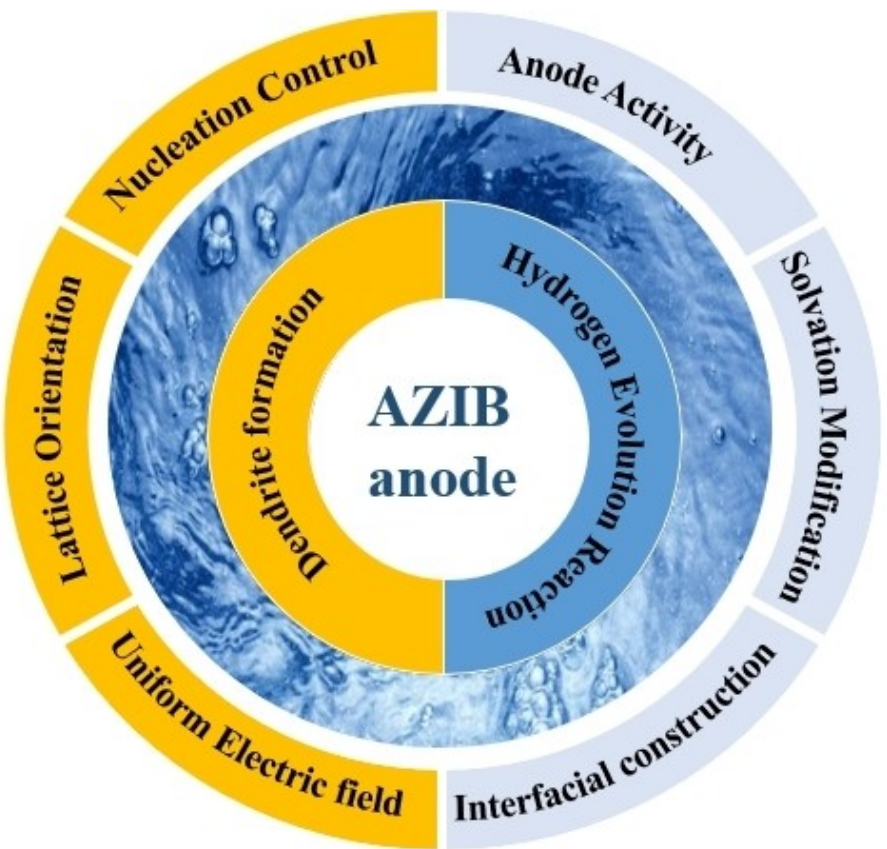


Figure 2. Schematic highlighting the strategies implemented to improve the Zn metal anode cycling from mechanistic perspectives.

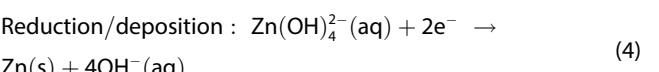
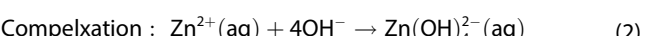
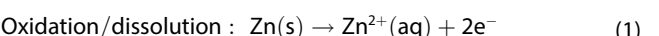
2. (Electro)chemistry of Zn and Associated Reactions

The electrochemistry of zinc anode is intimately correlated with the electrolyte, affecting Zn's chemical behavior through the nature of the solute and the pH. In this context, it is worthwhile to classify Zn's reaction steps and byproducts at different pH in detail to provide an insightful understanding of the Zn anode in aqueous electrolytes. Even though AZIBs typically employ electrolytes of mildly acidic pH (~3–5), the pH of many optimized electrolytes hover around the neutral value, and therefore here we look into the behavior of Zn in both acidic and alkaline media.

2.1. Behavior of the Zn anode in alkaline media

The thermodynamic stability of Zn metal in different pH ranges is generalized by the Pourbaix diagram (Figure 3a).^[14] Theoretically, during the zinc battery discharge (dissolution of zinc), electrons from the oxidation of zinc metal are transferred to the cathode through the external circuit. This process is not all plain sailing; accompanied by side reactions, the efficiency and reversibility are vastly diminished. In strongly alkaline systems such as zinc-air and Zn–MnO₂ batteries, the hydroxyl ions present near the surface of the anode complexes with

dissolving Zn²⁺ to form Zn(OH)₄²⁻ which then decomposes to ZnO [Reactions (1–3)]. The corresponding electrochemical and chemical reactions are:



The presence of complexation and precipitation process makes the dissolution of zinc much more complex than deposition,^[11a] which only involves the decomposition of Zn(OH)₄²⁻ back into Zn [Reaction (4)].^[14] Consequently, the detailed (electro)chemical reactions for dissolution are still controversial.^[15] Concerning the precipitation process, the common understanding is that when Zn(OH)₄²⁻ concentration exceeds the local solubility limit, the zinc oxide (ZnO) is precipitated [Reactions (2) and (3)].^[16] On the contrary, another theory – the adsorption model – proposes that the protons are rejected from adsorbed species such as adsorbed ZnOH,

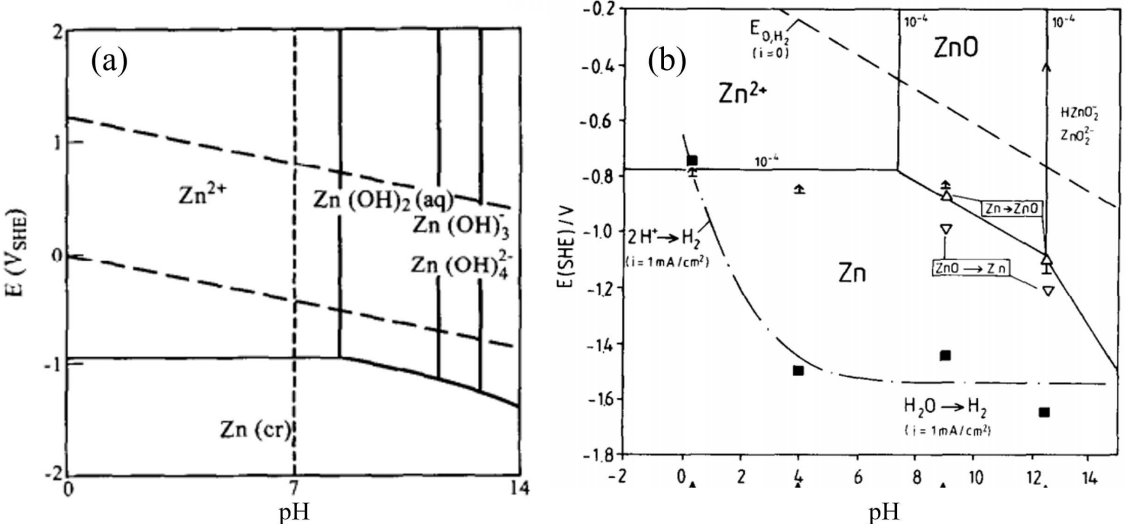
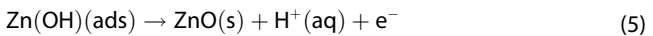
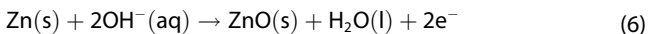


Figure 3. a) Pourbaix diagram of the $\text{Zn}/\text{H}_2\text{O}$ system.^[14] Reproduced with permission from Ref. [14]. Copyright (1996) Elsevier. b) Pourbaix diagram of the $\text{Zn}/\text{H}_2\text{O}$ system considering the overpotential.^[20] Reproduced with permission from Ref. [20]. Copyright (1990) Elsevier.

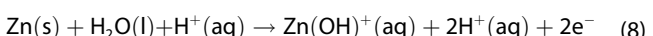
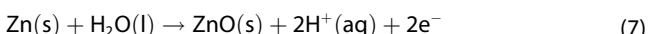
denoted as $\text{ZnOH}(\text{ads})$ at a specific critical potential, leading to the formation of ZnO [Reaction (5)].^[17]



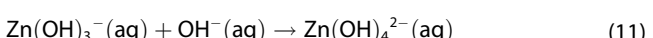
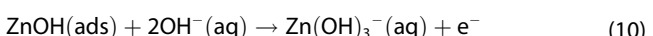
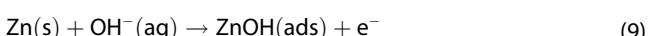
Moreover, the precipitation process is described through a nucleation-growth model that assumes that the passivation layer is formed by direct reaction of zinc with hydroxy anions [Reaction (6)].^[18]



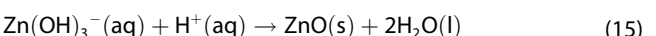
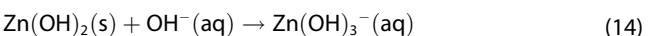
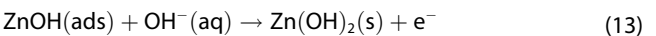
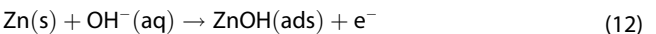
Since the chemistry of Zn metal in alkaline electrolytes is susceptible to OH^- concentration, it is essential to differentiate possible reactions according to electrolyte pH. In this context, a comprehensive study was conducted by Thomas et al.,^[19] inferring that in a mildly alkaline environment ($\text{pH } 7\text{--}10$), the dissolution products are mainly composed of ZnO and $\text{Zn}(\text{OH})^+$. These two corrosion products are formed by reaction with water [Reaction (7)] and metal hydrolysis [Reaction (8)] separately.



In the pH range of 11 to 13, zinc undergoes reaction [Reactions (9–11)] to form zinc hydroxy complexes [$\text{Zn}(\text{OH})_3^-$ and $\text{Zn}(\text{OH})_4^{2-}$] where zinc oxide is more thermodynamically stable and act as a passivation layer.



At pH values exceeding 13, different zinc hydroxy complexes exist in this environment, suggesting a unique dissolution mechanism. The adsorbed species [Reaction (12)] can initiate the formation of $\text{Zn}(\text{OH})_2$ [Reaction (13)] and $\text{Zn}(\text{OH})_3^-$ [Reaction (14)], and the local supersaturation of zinc hydroxy complexes may function as a diffusion barrier for OH^- that acts as a self-limiting step for reactions (13) and (14). Eventually, when the $\text{Zn}(\text{OH})_3^-$ reaches the local supersaturation, ZnO precipitates out [Reaction (15)].



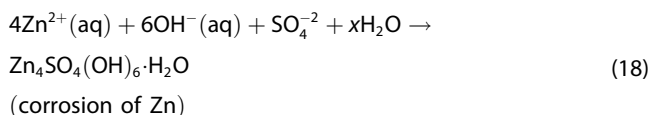
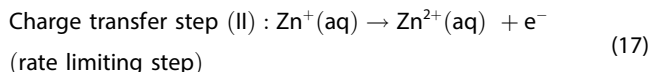
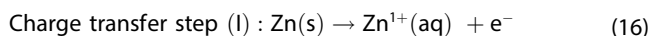
Since no consensus has been reached for the specific mechanism for zinc dissolution, various reaction models are proposed to explain the complexation process, including concentration-dependent mechanism,^[21] step-by-step process mechanism,^[22] and concentration-independent mechanism.^[23] These chemical models and corresponding kinetics have been comprehensively reviewed by Han et al.^[11a]

Despite the complicated and manifold theories, previous studies strongly suggest that the byproducts are the zinc-based oxide/hydroxide film with a duplex structure.^[24] At the initial stage of corrosion, $\text{Zn}(\text{OH})_2$ precipitates on the electrode to build a porous (type 1) film as the inner layer, followed by the formation of a thin and compact ZnO (type 2) film on the exterior surface. Detailed research was conducted by Mokkadem and coworkers, revealing that a thin ZnO film (type 3) also forms at the interface between type 1 and type 2.^[25] Generally, the passivation layers with compact structures could provide a protective effect against zinc degradation and prevent further

corrosion. However, indirect corrosion through dense layers is still possible. In contrast, the porous passivation layer is almost free channels for zinc corrosion, and the degradation of Zn metal is hardly inhibited. Even though the compact passivation could prevent corrosion, mutual effects from the formation of insulating passivation products and diffusion barrier generated by the inner $Zn(OH)_2$ layer would significantly increase the overall impedance of the cell, resulting in sluggish charge transfer during cycling.

2.2. Behavior of the zinc anode in mildly acidic media

Currently, an overwhelming amount of zinc battery research concerns AZIBs, which employ mildly acidic aqueous zinc salt solutions (pH 3–5) as electrolytes, and these studies date back to the work of Yamamoto et al. in the 1980s.^[26] In mildly acidic conditions, the side reaction, such as complexation and precipitation, is suppressed due to the lack of hydroxyl anions, allowing Zn^{2+} to exist in its ionized form. Therefore, the dissolution of Zn metal in a mildly acidic environment is more straightforward than that in an alkaline electrolyte. Here, it is a two-step process involving an ion-transfer step [Reaction (16)] followed by an electron-transfer step [Reaction (17)].^[27] The first charge transfer step typically exhibits fast kinetics; hence, the rate-limiting step is the following step.^[27a] Based on the above discussion, the chemistry of Zn dissolution can be summarized by the following reactions:



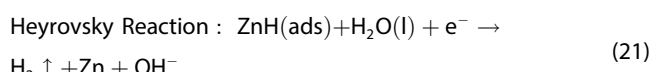
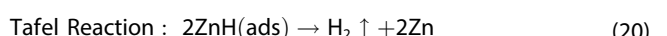
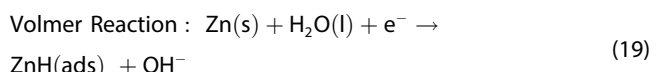
Interestingly, despite the mild acidic chemical environment of AZIB electrolytes, the corrosion of Zn metal is still triggered by OH^- in the form $\text{Zn}_4\text{SO}_4(\text{OH})_6 \cdot \text{H}_2\text{O}$ precipitation that typically presents itself as hexagonal flakes [Reaction (18)]. This OH^- generates both chemically and electrochemically. As zinc has a strong tendency to ionize (higher electrochemical potential) by donating its electron to H^+ of water, OH^- is left behind in the process. Furthermore, the higher equilibrium redox potential of hydrogen evolution (H^+/H) than that for Zn/Zn^{2+} means hydrogen evolution (via H^+ reduction) is inevitable during Zn plating/stripping, and thus OH^- accumulates near the surface to trigger the corrosion. Fortunately, HER on Zn surface is associated with a large kinetic overpotential, enabling the reversible Zn deposition feasible (Figure 3b).^[20] Nonetheless, hydrogen evolution is still rampant in acidic conditions, which not only degrades the reversibility of AZIBs but also raises safety concerns due to hydrogen generation. Many attempts have been made to minimize the HER and optimize the

reversibility of AZIBs,^[28] but rational designs and strategies are still needed to achieve a performance desired for practical application.

2.3. Chemistry of HER in alkaline and mildly acidic media

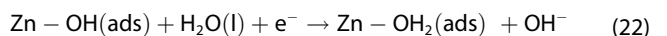
One of the most attractive attributes of AZIBs – the use of inexpensive and safe aqueous electrolytes – introduces a severe problem in the form of HER, which takes place simultaneous to the Zn stripping/plating, depleting the electrolyte solvent and Zn^{2+} . As explained above, the latter happens due to the accumulation of OH^- near the electrode surface, which increases the local pH. If the local pH goes above ~ 5 ,^[29] complexation and precipitation Zn^{2+} occurs in the form of the corrosion product, leading to the degradation of Zn and heterogeneous deposition.^[30] Thus, exploring the specific mechanism of HER on zinc surface is of great significance to gain a deeper insight into the parasitic reactions in AZIBs.

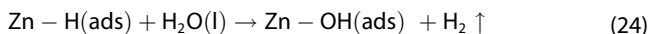
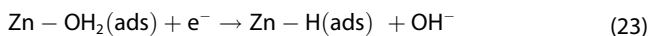
The HER mechanism in alkaline media is well investigated and generally perceived to involve a three-step process,^[31] represented by the following reactions:



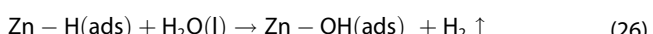
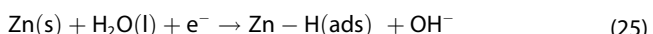
The first step is the electroreduction of water molecules and adsorption of H atom on the surface of the zinc electrode (Volmer Step). This is followed by the desorption of H atoms with hydrogen gas evolution through the electrochemical reaction (Heyrovsky Step) and/or chemical reaction (Tafel Step). As the rate-limiting step is the recombination of adsorbed H atoms (Tafel Step), the kinetics of HER on zinc is susceptible to the nature of the surface. Thus, not surprisingly, a compact passivation layer exhibits more robust anti-corrosion properties than a porous layer or bare Zn metal.

In acidic media, Ichino et al.^[32] have proposed two consecutive steps to describe the HER, consisting of the adsorption of H atom on zinc surface and the reaction between adsorbed H and H^+ to evolve hydrogen. This model, however, has not gained sufficient experimental support, and the well-established model for HER in acidic or alkaline media is still a three-step process. A more comprehensive model has been proposed by Trisovic et al.^[33] based on a three-step process, suggesting HER exhibits different behavior under varying potential. At low potentials, the surface oxide plays a significant role in facilitating hydrogen evolution where the mechanism for HER consists of two electrochemical and one chemical reaction:





Although the reaction model includes discharge reaction (Volmer step), recombination reaction (Tafel step), and chemical desorption (Heyrovsky step), the reaction path is entirely different from the alkaline one. In acidic media, the surface concentration of adsorbed species ($\text{Zn}-\text{OH}_2$ and $\text{Zn}-\text{H}$) and the free energy of adsorption could hugely impact each reaction rate. Moreover, when switching to more negative potentials, the model assumes that hydrogen evolution is controlled through parallel Volmer–Heyrovsky routes:



Apart from the intrinsic mechanism of HER, this reaction is also sensitive to dendritic growth. The appearance of dendrite here is synonymous with the formation of porous and flaky metal with a high specific surface area, which intensifies HER due to more available surface sites. The strong correlation between HER and dendrite formation makes it impossible to bypass the dendrite when discussing HER.

2.4. Dendrite formation and related mechanisms

Reversible Zn deposition and dissolution at the anode side are pivotal to the reversible operation of the Zn-ion system, and thus play a significant role in dictating the cycling performance and Coulombic efficiency of AZIBs. Employing neutral or mildly acidic electrolytes in AZIBs was initially presumed to be adequate to eliminate the Zn corrosion and dendrite issues. However, rapid dendritic failure of ZIBs is still observed in mildly acidic or neutral electrolytes when operated at practical current densities and cycling capacities.^[34] Hence, it is essential to have a rigorous fundamental understanding of the dendrite formation mechanism to pursue improved performance of AZIBs.

2.4.1. The zinc dendrite in AZIBs

Even though the metal “dendrite” in batteries is typically described as fractal and/or mossy growth, it can generally be any irregular shape that can pierce through the separator and cause a short circuit. In alkaline electrolytes, as a critical overpotential is reached under a high current density, the dendrite growth initiates in the form of the spruce tree like shape with sequential formation of the primary trunk and secondary and tertiary branches (Figure 4a and b).^[35] In contrast, the shape of the dendrite in neutral to mildly acidic electrolytes primarily appears as two dimensional (2D) hexagonal platelets without any ramification, slightly mitigating the

issues of separator failure. However, the dendrite is still one of the critical bottlenecks in extending the lifespan of AZIBs.

2.4.2. Dendrite-formation steps and related challenges

Generally, the electrochemical deposition of Zn on the anode surface occurs via three successive steps: Zn^{2+} ion adsorption, 2D growth (deposition/dissolution and diffusion), and three-dimensional (3D) growth process (Figure 4c).^[36] At the initial stage, the electroplating requires a driving force (activation energy) to overcome the energy barrier for Zn^{2+} adsorption and electron transfer (Figure 4d). This is followed by the nucleation and growth steps, which play a critical role in the electroplating process and dictate the deposition quality. Since it is difficult to deconvolute each process by electrode polarization from the voltage profile, the electroplating process is commonly represented by two overpotentials: 1) the nucleation overpotential, which is the magnitude of voltage drop at the onset of Zn deposition, and 2) the plateau overpotential, which refers to the polarization during the steady growth process after nucleation. Both overpotentials are easily discernible in the galvanostatic voltage profile (Figure 4e). Contrarily, the overall plating overpotential in the potentiodynamic method (cyclic voltammetry) is typically ascribed to the nucleation overpotential, and the growth overpotential cannot be observed separately.^[39] Nevertheless, the nucleation overpotential can significantly influence the deposition quality.^[40] Higher nucleation overpotential leads to the formation of a large number of nuclei, resulting in more fine-grained deposits with narrow size distribution. It is believed that the nuclei, instantaneously formed at the beginning, grow at the same rate during the growth period (plateau overpotential), forming uniform zinc crystallites. Typically, dendrite formation takes place due to the electrode surface inhomogeneity that results in varying electric field and mass transport limitation that leads to ion concentration gradient build-up at the electrode-electrolyte interface. The intensity of the electric field at protuberances with large curvature is much greater than the surrounding area. This electric field inhomogeneity leads to a discrepancy of deposition rate between bumps and planar surface (Figure 4f), also known as the “tip effect”.^[38] It is crucial to minimize the electric field density variation and keep it stable during electroplating to eliminate this effect. In addition to the electric field, ion migration also exerts a remarkable impact on the nucleation process as faster ion migration along the surface could accelerate the transportation of Zn^{2+} and reduce the energy barrier for nucleation.^[41] Another vital factor is the crystal growth orientation. The hexagonally close-packed Zn typically crystallizes as hexagonal platelets with (002) and (100)_{hexagonal} facets exposed. After random initial nucleation, the growth should happen through selective addition of zinc to the facet with higher surface energy – i.e., (100) surface^[42] – and thus, lateral growth of the platelets is expected. If this happens in a controlled fashion, the large platelets can stack up and create a dense and basal plane oriented flat and smooth morphology that is conducive for dendrite-free cycling. How-

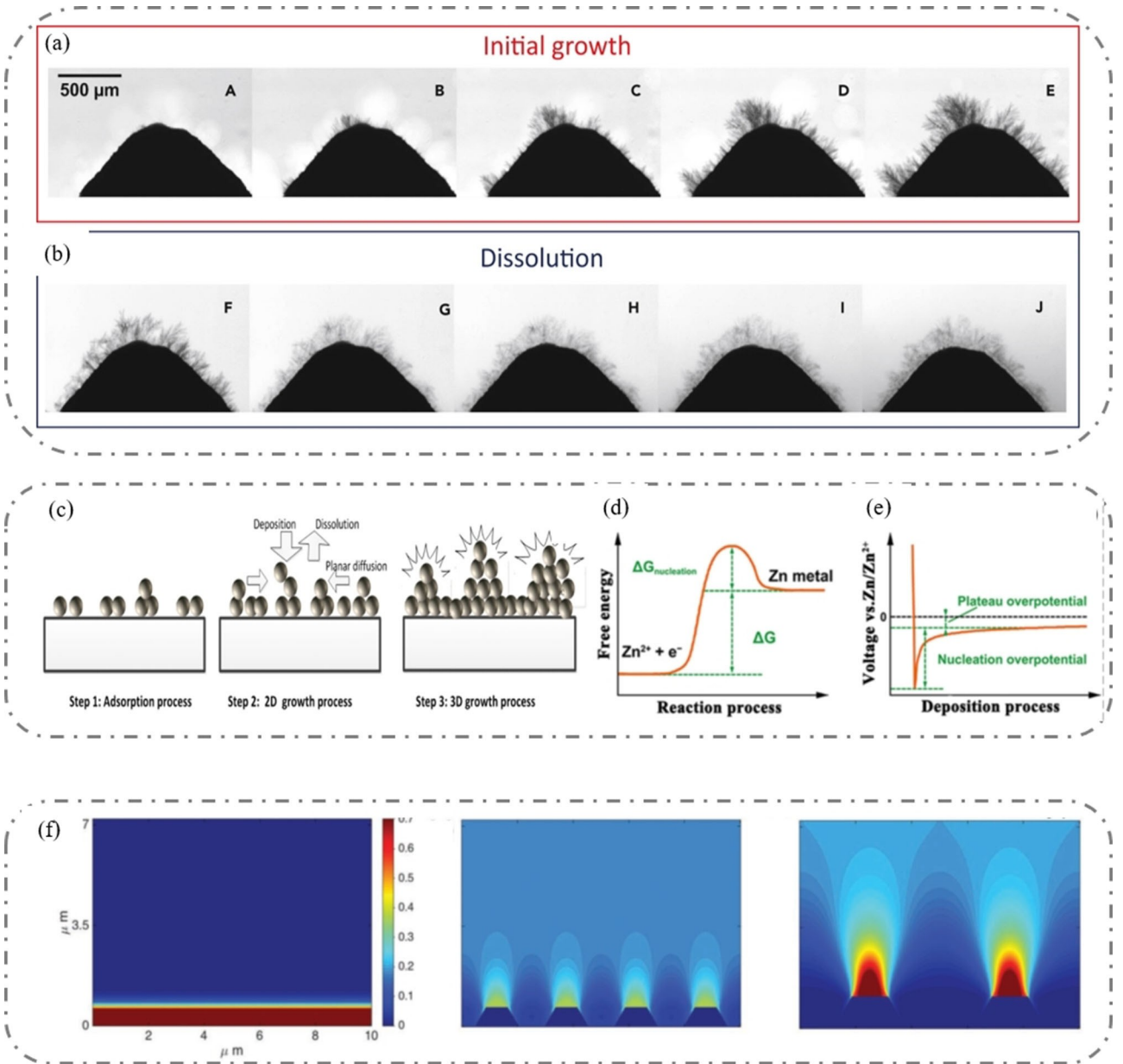


Figure 4. In situ optical microscopy images of dendrite formation at protrusions during a) striping and b) plating.^[35] Reproduced with permission from Ref. [35]. Copyright (2018) Elsevier. c) Schematic illustration of Zn atom deposition on the metal surface.^[36] Reproduced with permission from Ref. [36]. Copyright (2017) American Chemical Society. d) The diagram of the nucleation barrier of the Zn atom. e) The typical voltage profile for Zn deposition.^[37] Reproduced with permission from Ref. [37]. Copyright (2017) American Chemical Society. f) The inhomogeneous distribution of electric field accumulation around the Zn curvatures.^[38] Reproduced with permission from Ref. [38]. Copyright (2019) Wiley-VCH.

ever, dendrite forms and short circuit prevails, meaning the anticipated textured growth is not the reality here.

The heterogeneous deposition of Zn is inevitable in practical conditions due to the buildup concentration gradient of Zn^{2+} at the anode/electrolyte interface. The uneven distribution and deposition of Zn facilitate the perpendicular growth of loose and flaky dendritic structures, providing abundant sites for HER and other corrosion reactions. Besides, the loose contact between substrate and dendrite results in the detachment of dendrite from the substrate, resulting in zinc loss. Dendrite-free Zn anode is urgently needed for the practical development of AZIBs, and focused practical ap-

proaches are going to be needed to eliminate the dendrite problem.

3. Progress in Inhibition of Zinc Dendrite

3.1. Tackling dendrite issues through homogeneous nucleation

Homogeneous nucleation is indispensable to inhibit notorious Zn dendrites. However, during plating, the microscopic inhomogeneity of the Zn surface (e.g., the uneven flatness,

defects, and mismatch on the surface) results in the divergence of the nucleation energy barrier, facilitating the dendrite formation.

3.1.1. Interfacial metal oxide layer

Considerable advances have been made in regard to manipulating nucleation by interfacial engineering.^[43] The artificial interface layer commonly serves as a regulating ion channel to control the Zn^{2+} diffusion and nucleation. The design principles for the synthetic interface layer are mainly based on four factors: ionic conductivity, hydrophilicity, structural porosity, and stability. The inertness is also crucial to avoid the chemical and electrochemical reaction between the layer and the electrolyte/anode. Generally, the protective layer can allow the electrolyte to penetrate and enrich Zn^{2+} in a narrow range from the surface. This prevents reverse transmission of Zn^{2+} , and thus the enriched Zn^{2+} concentration plays a critical role in uniform Zn deposition. Figure 5a and b show the nature of Zn deposition with a nano- $CaCO_3$ coating,^[44] which allows the percolation of the electrolyte and renders a bottom-up and

uniform Zn deposition rather than the preferential deposition at tips. The confining effect of the nanopore in the $CaCO_3$ layer facilitates a homogeneous Zn^{2+} flux, manipulating the Zn^{2+} reduction with low overpotential and excellent lifespan improvement (Figure 5c).

Apart from the inherent properties of the coating layer, the protective effects and ion migration are also determined by the thickness of the layer. Consequently, the application of atomic layer deposition (ALD) has invoked attention due to the possibility of precise thickness control, realizing excellent coverage and conformal deposition. An ultrathin TiO_2 (8 nm) coating on Zn metal through ALD was reported to achieve the uniform growth of Zn and suppress corrosion.^[45] On the one hand, the compact layer avoids direct contact between Zn and electrolyte, physically inhibiting HER and any chemical side reactions. On the other hand, the Zn^{2+} migration through the TiO_2 coating layer is accelerated due to the strong interaction with abundant oxygen bonds. These factors lead to homogeneous nucleation of zinc and endow the Zn anode with dendrite-free morphology after cycling (Figure 5d and e). Besides ALD, the molecular layer deposition (MLD) with self-limiting nature has also been applied to precisely manipulate

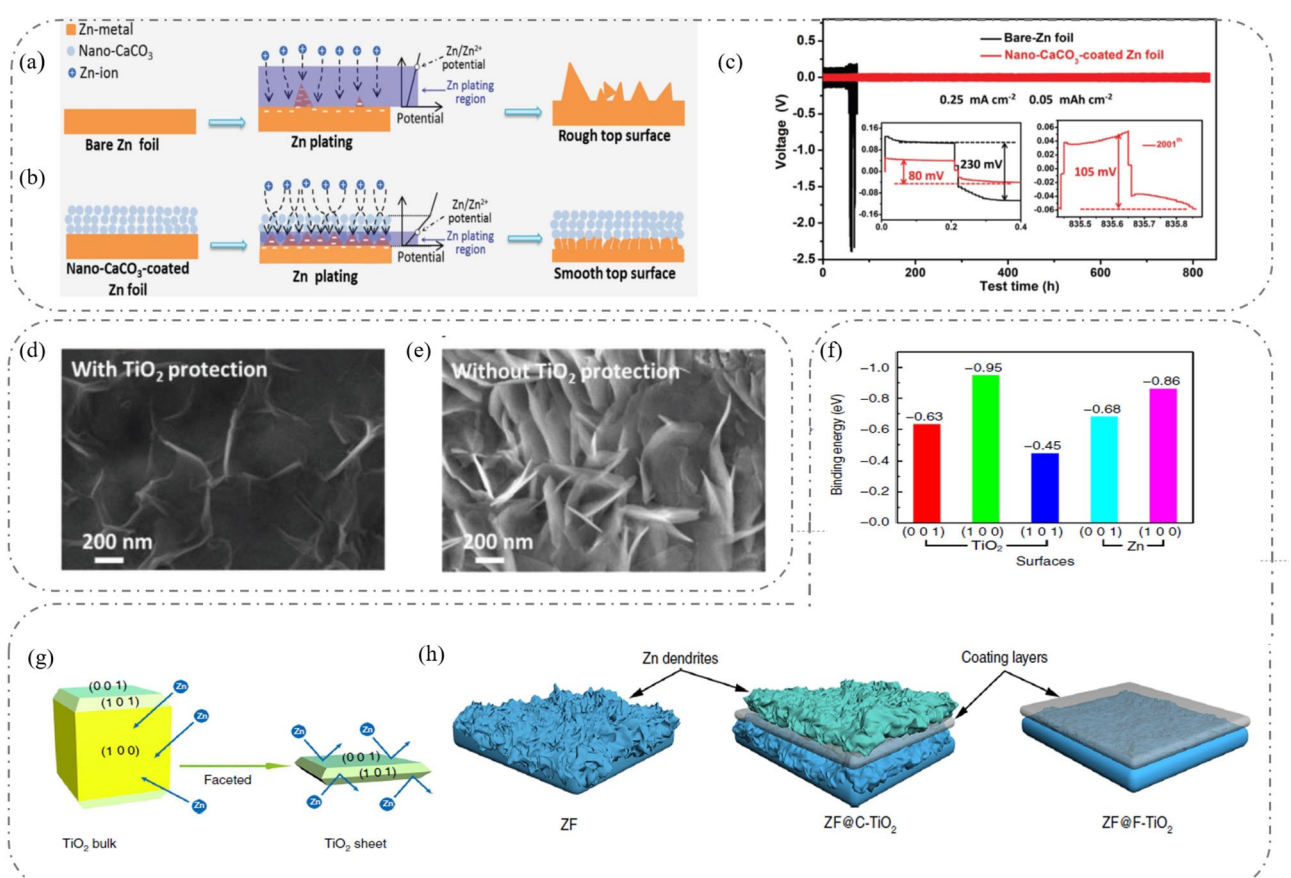


Figure 5. Schematic diagram of the zinc deposition process on a) bare Zn foil and b) nano $CaCO_3$ @Zn anode.^[44] Reproduced with permission from Ref. [44]. Copyright (2018) Wiley-VCH. The SEM images of Zn electrodes after cycling d) with TiO_2 protection and e) without protection.^[45] Reproduced with permission from Ref. [45]. Copyright (2018) Wiley-VCH. f) Binding energies of Zn atom with difference crystallographic facets of Zn and TiO_2 calculated by DFT. g) The interaction between Zn and TiO_2 layers with different exposed facets. h) Schematic diagram about the dendrite formation or suppression with different coating layers.^[46] Reproduced from Ref. [46]. Copyright (2020) The authors, published by Springer Nature.

the thickness of the protective film at the molecular level.^[47] Additionally, more in-depth study about the TiO₂ protective layer was conducted by Zhang et al.^[46] to unveil the underlying interaction between Zn and the crystallographic orientation of the TiO₂ layer. As shown in Figure 5f, the adsorption energy of Zn atoms on the TiO₂ (100) facet is more negative (-0.95 eV) than that for adsorption on Zn (001) and (100) facets (-0.68 eV and -0.86 eV), indicating that Zn is more likely to deposit on the TiO₂ layer rather than on the underlying Zn metal surface. As a result, the Zn dendrite may grow inside the protective layer and weaken the protective effect. For an enhanced protective effect, the commercial anatase TiO₂ (C-TiO₂) with a predominantly exposed (100) plane should be replaced with (Figure 5g) faceted TiO₂ (F-TiO₂) with (001) and (101) facets exposed primarily. The more positive adsorption energies for these two facets (-0.63 and -0.45 eV, respectively) can avoid side reaction or Zn deposition on TiO₂ layers, reinforcing the protective effects (Figure 5h). Thus, Zn@F-TiO₂ exhibits a

superior stripping and plating performance with a long lifespan (460 h at 1 mA cm^{-2} and 1 mAh cm^{-2}). Overall, the innovative study provides an intriguing insight into the fundamental mechanism of metal affinity and can be extended to other strategies related to the interfacial engineering of Zn anode.

Metal oxides have been widely used as an artificial interfacial layer since abundant oxygen atoms enhance the affinity toward Zn atoms and guide uniform nucleation. The unique mechanism of the ZrO₂-coated layer – Maxwell-Wagner polarization or space charge polarization – endowed the Zn anode with excellent cyclability of over 2100 h at 5 mA cm^{-2} and 1 mAh cm^{-2} .^[48] While the high dielectric constant of ZrO₂ enhances its affinity to Zn²⁺, the abundant lone-pair electrons of the oxygen atoms in ZrO₂ function as the nucleation sites for Zn. Both factors contribute to the low energy barrier for nucleation and ensure a homogeneous deposition behavior (Figure 6a and b). Hence, the ZrO₂ coated Zn anode can maintain the stable plating/stripping during cycling and show a

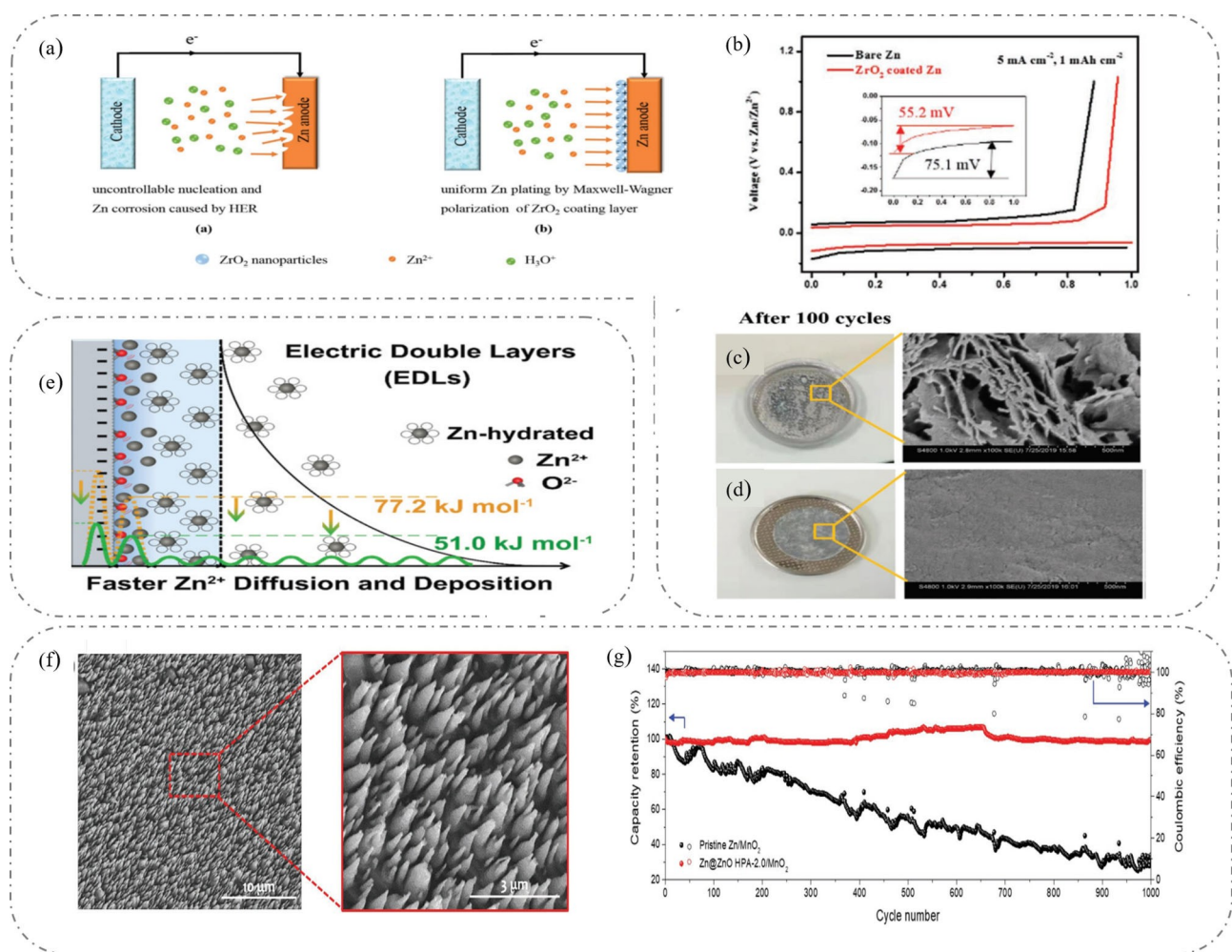


Figure 6. a) Schematics of the stripping/plating process for the bare Zn and ZrO₂@Zn anode. b) Voltage profiles of Zn plating/stripping in asymmetric Zn/Ti (mesh) cell with bare Zn and ZrO₂@Zn anode. Digital and corresponding SEM images for the c) bare Zn and d) ZrO₂@Zn anode after cycling.^[48] Reproduced with permission from Ref. [48]. Copyright (2020) Wiley-VCH. e) Schematic diagram of fast ion diffusion facilitated by nano-porous ZnO coating.^[49] Reproduced with permission from Ref. [49]. Copyright (2020) Royal Society of Chemistry. f) Top-view SEM images of hexagonal pyramid array of ZnO layer. g) Long-term cycling performance of pristine Zn/MnO₂ and ZnO coated Zn/MnO₂ batteries at a current of 9.0 A g^{-1} .^[50] Reproduced with permission from Ref. [50]. Copyright (2020) Wiley-VCH.

smooth topography after cycling compared to the bare Zn anode (Figure 6c and d). The Zn anode cycling stability has also been realized by introducing a thin protective layer at the anode/electrolyte interface to regulate the inner Helmholtz plane (IHP) in the electric double layer (EDL).^[51] In this respect, a three-dimensional nanoporous ZnO-coated Zn anode (3D-ZnO@Zn) was found to be capable of tuning the desolvation step with lower energy consumption in the EDL than for the bare Zn anode (51.0 kJ mol^{-1} vs. 77.2 kJ mol^{-1} ; Figure 6e).^[49] Unlike traditional coating layers with sluggish kinetics, the facile desolvation process stabilizes the charge-transfer step and accelerates zinc deposition kinetics with a lower charge-transfer resistance of 292.7Ω (1240Ω for the bare anode). Since the ZnO with a high Zn^{2+} ionic conductivity effectively expedites the movement of the Zn^{2+} in the layer, some relevant studies have been conducted for this oxide. Besides the nanoporous structure, a unique ZnO layer structure with hexagonal pyramidal arrays (Figure 6f)^[50] was designed, which, thanks to its large electroactive surface area, enables a uniform distribution and plating of zinc. Such a passivation layer rendered an excellent Zn–MnO₂ full cell cycling, with up to 1000 cycles with a capacity retention and Coulombic efficiency of 99.84% and 99.86%, respectively (Figure 6g).

3.1.2. Electronically conductive interfacial layer

Implementing an electronically conductive metallic interface has been investigated as an alternative strategy to tackle charge accumulation and nonuniform electroplating on the Zn metal surface.^[52] Metals with high electronic conductivity and good zincophilicity, such as Cu film^[11d] and Pb film,^[53] can function as heterogeneous seeds to reduce the nucleation energy barrier and provide abundant nucleation sites. If these metals can maintain electrochemical stability during plating/stripping, the Zn atoms can spontaneously adsorb on the surface of the metal seeds thanks to negative adsorption energies. For instance, quasi-isolated Au with nanosized particles (~100 nm diameter) was deposited on the Zn anode through ion beam sputtering method.^[54] The Au particles with high striking energies roughen the surface of Zn (Figure 7a and b), facilitating adequate distribution of nucleation seeds to realize even deposition. A compact, well-distributed, and flake-like morphology of Zn (Figure 7c) confirms homogeneous nucleation and growth. Such Au-decorated anode can lower the overpotential and exhibits long-term stability of up to 2000 h (Figure 7d).

Even though Au sputtering method is facile to operate, the high cost of Au, the applied low current density (0.25 mA cm^{-2}), and a very small areal capacity (0.05 mAh cm^{-2}) raise questions around the practicality of the strategy. Clearly, the application

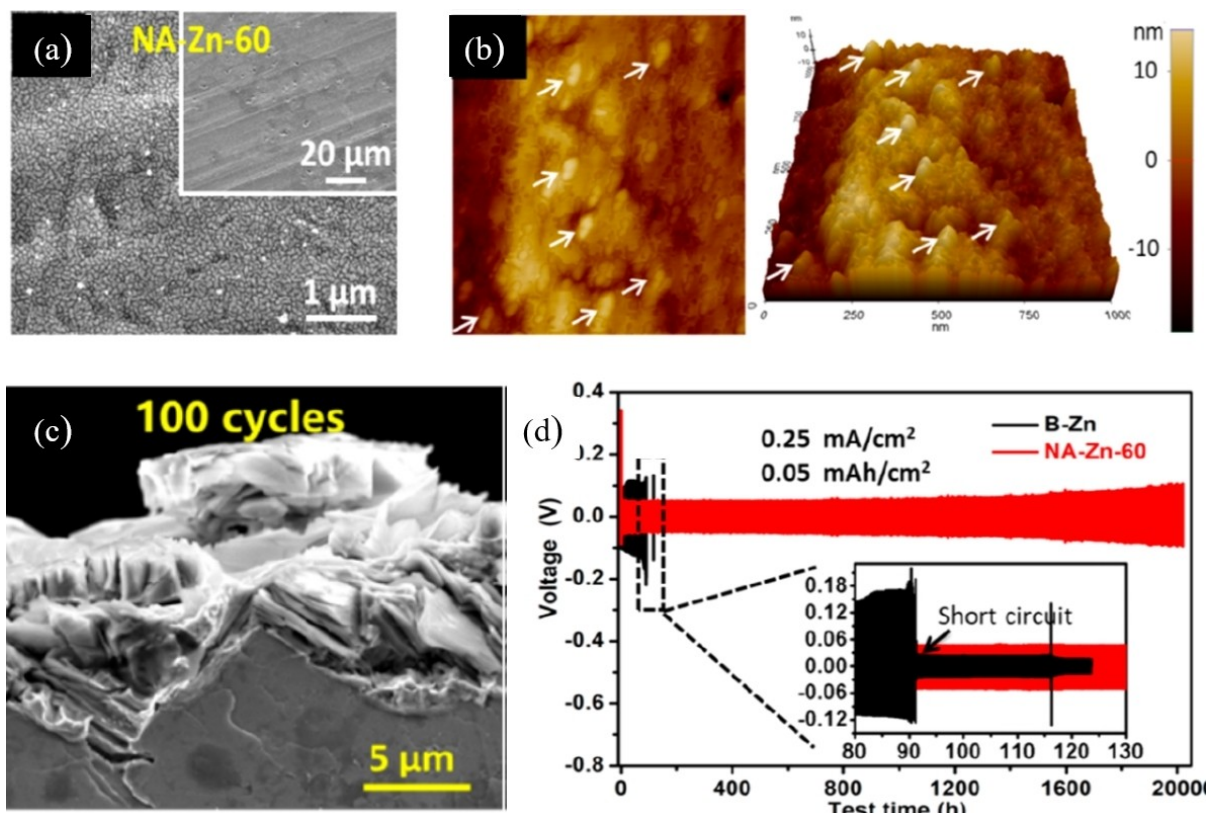


Figure 7. a) SEM images of Zn anode with sputtered Au particles; b) AFM images of Zn anode after sputtering; c) SEM images of Zn–Au anode after cycling; d) galvanostatic cycling performance of Zn–Zn symmetric cell with the sputter coated Au at a current density of 0.25 mA cm^{-2} and areal capacity of 0.05 mAh cm^{-2} .^[54] Reproduced with permission from Ref. [54]. Copyright (2019) America Chemical Society.

of inexpensive metals with superior tolerance in high current and capacity conditions would be desirable. Tin-modified 3D carbon host (SH), fabricated by magnetron sputtering, can tightly adhere to Zn substrate due to high adsorption energies and electronic interaction with Zn, endowing a modified Zn electrode with lower nucleation overpotential and dendrite-free feature.^[55] Morphology evolution for bare carbon felt host (PH) and SH was visualized by super depth surface profile measurement microscope (SDM) (Figure 8), which revealed uneven deposition and aggregation of Zn for the former. In contrast, the deposited Zn particles without local increase in

height during cycling unequivocally confirmed the dendrite-free deposition. This strategy not only benefits from the facile fabrication and low cost of tin but also manifests excellent cycling performance under an extremely high current density and areal capacity (up to 300 cycles at 40 mA cm^{-2} and 40 mAh cm^{-2}).

The carbon-decorated Zn electrode has also attracted much attention due to its high conductivity and structural diversity. Modifying the anode with a carbon of high conductivity can lower the overpotential and provide ample sites for Zn nucleation in the same way as the metal interface.^[56] For

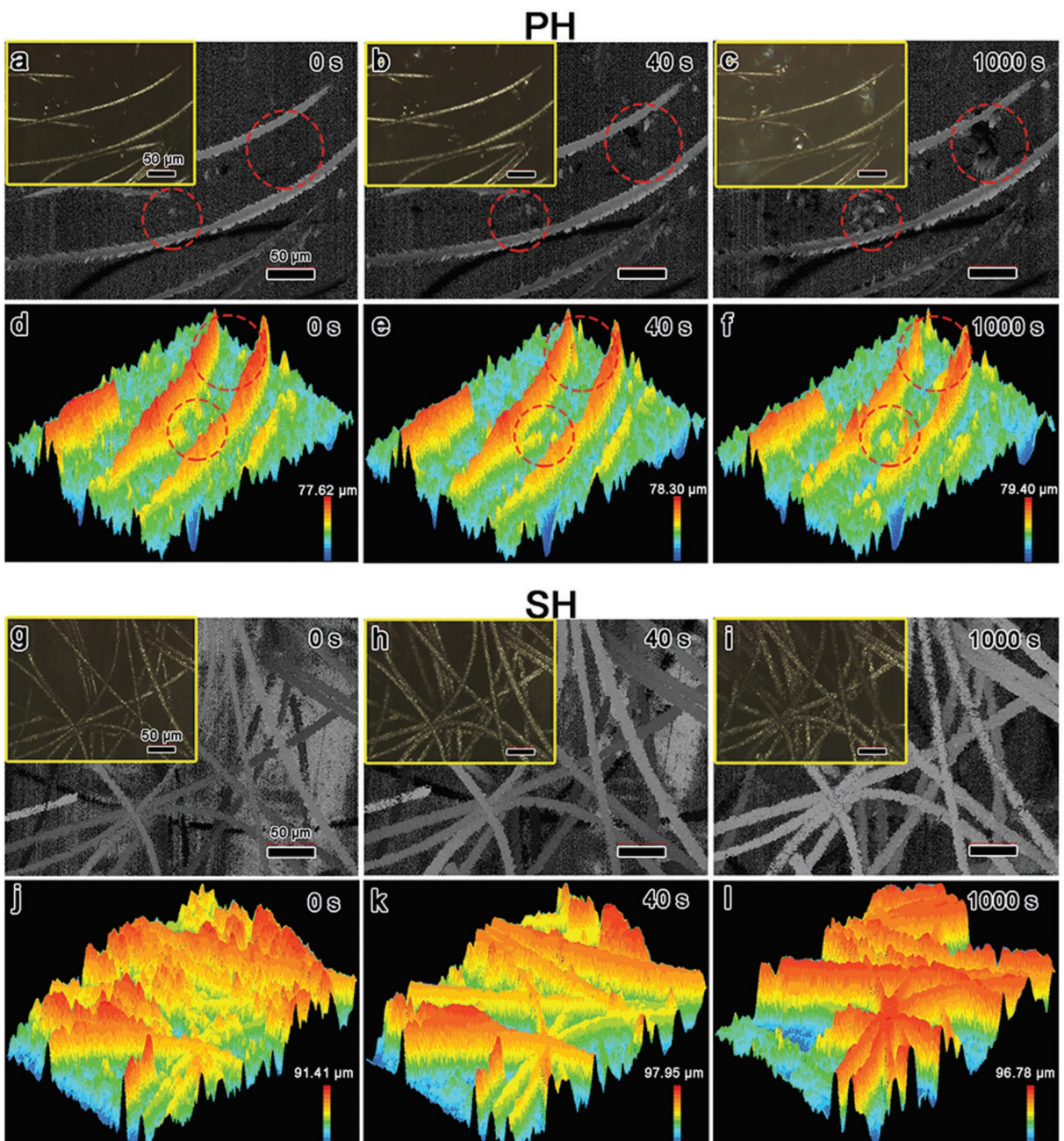


Figure 8. The in situ SDM images of Zn electrode with different hosts during cycling. a–f) The morphology evolution of bare carbon felt host (PH) as a function of cycling time to visualize the severe Zn aggregation and growth into large particles. (g–l) The more compact and uniform morphology of Zn electrode with Sn modified 3D carbon felt anodic host (SH).^[55] Reproduced with permission from Ref. [55]. Copyright (2019) Wiley-VCH.

instance, the commercial activated carbon can be directly applied by mixing with binder and Zn powder.^[57] This Zn-carbon composite anode rendered Zn to preferentially deposit in the pores of the activated carbon, leading to homogeneous nucleation and enhanced cycle life. Similarly, carbon black (CB) coating with high chemical stability, numerous voids, and excellent electrical conductivity can provide continuous conductive channels to facilitate uniform Zn nucleation inside the holes (Figure 9a).^[58]

In both strategies, a binder was employed to ensure adhesion and structural stability, preventing detachment of the coating from the Zn surface. The addition of the binder diminishes the gravimetric energy density, making the strategies less attractive for practical utilization. In this context, Shen et al.^[59] and Xia et al.^[60] have proposed the use of reduced graphene oxide (rGO) layer to realize the binder-free coating. The GO was spontaneously reduced to layered rGO on a Zn substrate, exhibiting a robust connection with Zn anode due to

strong chemical bonding. The porous structure and large surface area can synergistically facilitate the transmission of Zn^{2+} and suppress heterogeneous metal deposition (Figure 9b).^[60] Owing to the high structural versatility and straightforward preparation process, carbon materials are the most popular candidates as conductive hosts. For instance, the multifunctional 3D CNT framework was used to construct a CNT/Zn electrode, delivering superior cyclability over 1000 cycles with 88.7% capacity retention in Zn/MnO₂ battery.^[61] Generally, the isolated Zn nuclei sites with a higher electric field than the vicinity of it drive the Zn^{2+} flux to the individual nucleation centers, which promotes the continuous deposition of Zn^{2+} on these lumps and finally grows in the form of Zn dendrite (Figure 10a). In sharp contrast, the surface functional groups from CNTs can effectively attract the Zn^{2+} in the electrolyte; meanwhile, the highly porous structure of CNTs introduces a well-distributed electric field, thereby homogenizing the deposition of Zn with a dendrite free morphology

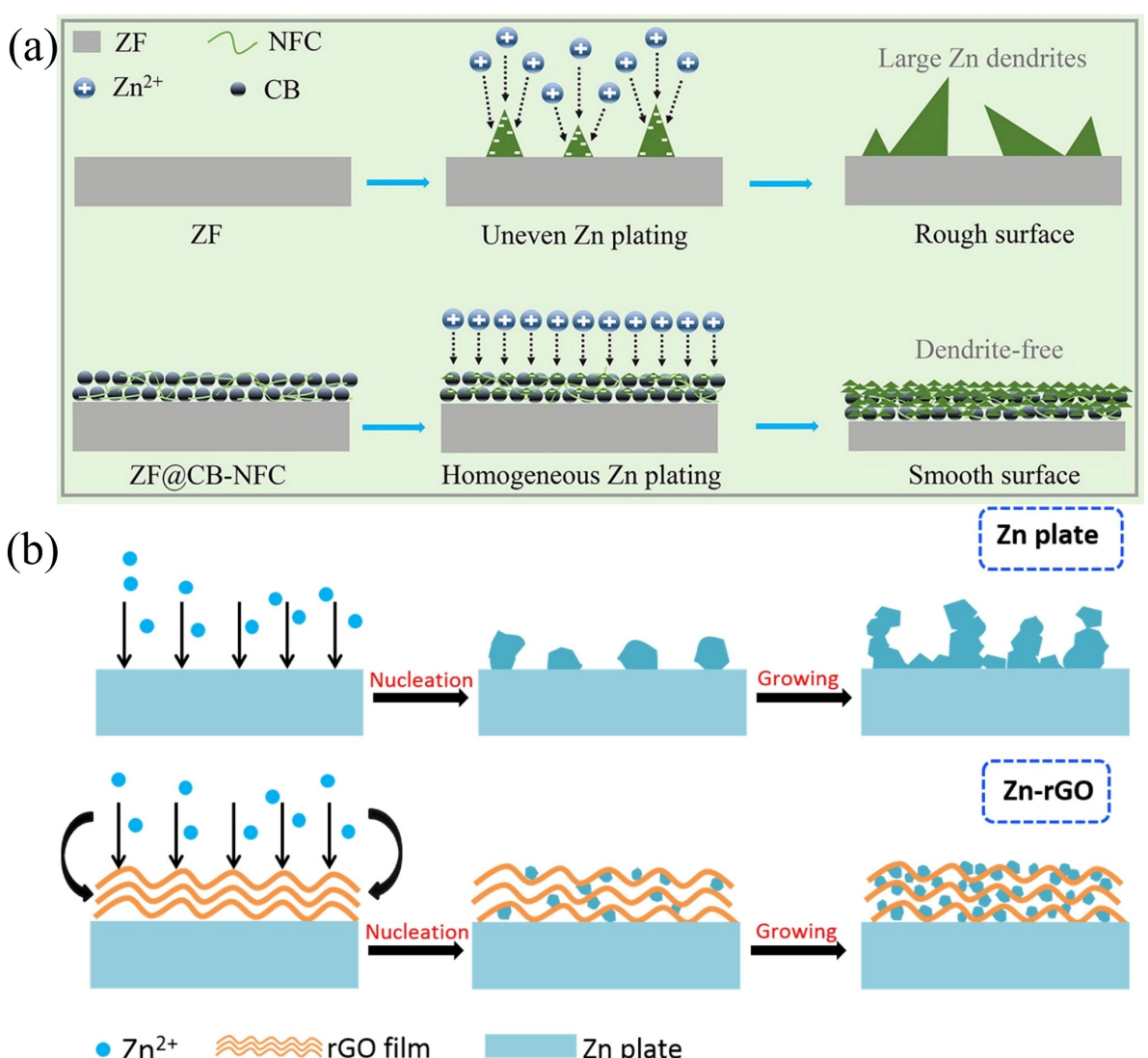


Figure 9. The schematic illustration of Zn stripping/plating on Zn with a) carbon black coating.^[58] Reproduced with permission from Ref. [58]. Copyright (2020) Elsevier. b) Reduced graphene oxide film.^[60] Reproduced with permission from Ref. [60]. Copyright (2019) Elsevier.

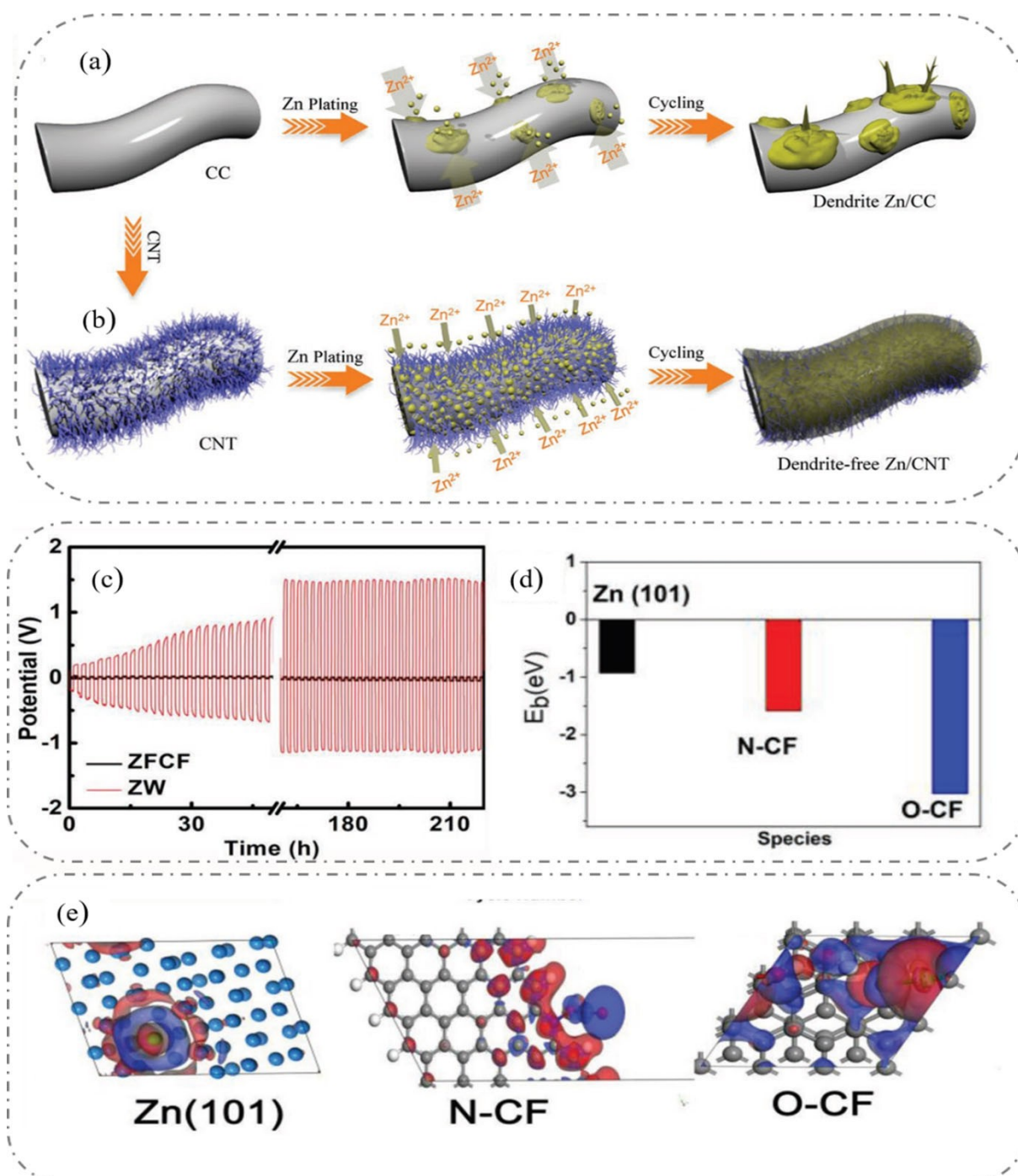


Figure 10. A schematic illustration of Zn nucleation on a) carbon cloth (CC), and b) Zn/CNT framework.^[61] Reproduced with permission from Ref. [61]. Copyright (2019) Wiley-VCH. c) Comparison of Zn cyclability in Zn/Zn cells for ZFCF and zinc wire electrode (ZW). d) The DFT calculated binding energy of a Zn atom on the Zn (101) facet and different N- and O-functional groups of carbon fiber. e) The electron density map at Zn atom adsorption site of Zn (101), N-functional, and O-functional groups of carbon fiber.^[64] Reproduced with permission from Ref. [64]. Copyright (2019) Wiley-VCH.

(Figure 10b). Analogous work employing carbon cloth^[62] and carbon fiber^[63] have also been conducted to solve the dendrite issue.

The performance of the carbon-scaffolded Zn electrode was further improved by anchoring 3D zinc flakes on the carbon fiber doped with zincophilic functional groups (ZFCF).^[64] After the acid treatment, the N- and O-functional groups were

introduced onto the carbon fiber, which can guarantee a uniform and stable Zn plating/stripping on ZFCF (Figure 10c) owing to the stronger binding of Zn^{2+} through the functional groups (Figure 10d). The zinc ions acted as electron-deficient Lewis acid, attracted by the unsaturated electron orbital in the surficial functional groups that serve as electron-rich Lewis base through acid-base interaction (Figure 10e).

3.2. Regulation of electric field inhomogeneity and ion diffusion

The driving force for the movement of Zn^{2+} in the electrolyte is the electric field between the two electrodes, which gets strongly affected by the mass transfer process. Microscopically, the distribution of the electric field is hard to maintain utterly uniform across the surface. Due to the preferential Zn deposition on spots with high field intensity (i.e., protrusions), the rapid consumption of Zn^{2+} triggers excessive Zn^{2+} movement from the neighboring regions into these spots. This uncontrolled diffusion is detrimental to the long-term stability of the electrode and further reinforces the preference for deposition on the protrusions. Thus, balancing and homogenizing the interfacial electric field is a potential approach to inhibit dendrite formation.

3.2.1. Shielding effect

The electrostatic shield mechanism is one effective way to inhibit dendrite formation and has been extensively studied in LIBs and ZIBs.^[65] As discussed before, during the deposition step, the sharp end of initial protuberances acts as the nucleation center due to the high intensity of the electric field, which is the main trigger for dendrite formation. The tip effect can be eliminated by an electrolyte additive with a lower reduction potential than Zn^{2+} , which can preferentially adsorb on the tips and keep the Zn^{2+} away. Based on this mechanism, a three-dimensional dendrite-free anode was designed by electroplating Zn on a 3D scaffold framework with the assistance of electrolyte additives. The Polyacrylamide (PAM)^[66] exhibit a strong adsorption onto zinc by the polar acyl group (adsorption energy of -1.25 eV). Hence, the PAM serves as an intermediate to uniformly move zinc from the electrolyte to the anode surface. Surfactant additives^[28,67] have also been extensively studied for Zn-ion batteries due to their facile adsorption on the zinc surface. Recently, tetrabutylammonium sulfate (TBA_2SO_4) – a cationic surfactant-type additive – was found to play a positive role in the uniform electrodeposition of Zn.^[68] Typically, during the nucleation step, the lateral diffusion and aggregation of Zn^{2+} on the electrode surface can be restrained by screening layers formed by the adsorption of TBA^+ (Figure 11a). Additionally, owing to its zincophobicity, (Figure 11b) TBA^+ serves as the diffusion barrier, preventing the transportation of hydrated Zn^{2+} towards screening layers and repelling the undesired diffusion of Zn^{2+} . The combined effect of shielding and zincophobic repulsion render a homogeneous and dendrite-free Zn anode. Notably, the low concentration of the optimal TBA_2SO_4 additive (0.029 g L^{-1}) is quite practical considering toxicity, price, and energy density. Not just surfactants, other organic additives like polyethylene glycol,^[69] polyethylene oxide,^[70] and diethyl ether^[71] have also been widely used to regulate the diffusion of Zn^{2+} and suppress the dendrite formation.

Unfortunately, the considerable energy barrier for nucleation (nucleation overpotential) caused by the introduction of

additives may lead to sluggish kinetics for Zn deposition, and thus an improved life performance is achieved at the expense of rate capability. Therefore, it is crucial to take the polarization into consideration when designing electrolyte additives. Recently, an *in situ* protective layer employing lithium chloride (LiCl) additive was demonstrated to improve the long-term performance,^[72] where both cation (Li^+) and anion (Cl^-) play a role. Owing to the inclusion of LiCl, an *in situ* solid-electrolyte interface (SEI) of Li_2O/Li_2CO_3 formed on the surface and served as a shielding layer to inhibit the rampant diffusion of Zn^{2+} , whereas the Cl^- can mitigate the polarization and induce uniform diffusion of Zn^{2+} through the passivation layer (Figure 11c). This synergistic mechanism broadly inhibits the dendrite formation at the Zn anode, extending the number of cycles. In another study, a eutectic Zn/Al alloy anode with a lamellar structure was also found to exert an electrostatic effect to prohibit the dendrite formation and improve the reversibility.^[73] The eutectic $Zn_{88}Al_{12}$ (at%) alloy was fabricated by alloying pure Zn and Al and the thickness of Zn or Al lamellas, namely interlamellar distance, by varying cooling rates. Notably, the formation of Al_2O_3 passivation shell on the Al lamella not only protects Al against dissolution but also blocks the electron transfer from the Al lamella to Zn^{2+} . These factors endow the anode with a positive electrostatic shielding on the Al/ Al_2O_3 lamella, enabling this novel structure to guide the uniform deposition of Zn (Figure 11d).^[73] As a result, the $Zn_{88}Al_{12}$ anode can operate for over 2000 h with dendrite-free Zn striping/plating and high Coulombic efficiency at current density of 0.5 mA cm^{-2} .

3.2.2. Ion sieving to control the diffusion of Zn^{2+}

The Zn^{2+} diffusion at the electrolyte/electrode interface is highly related to the concentration polarization, which is defined as the deviation of the electrochemical potential from its equilibrium value owing to the difference of ion concentration between the electrode surface and neighboring region of the electrolyte. The concentration gradient can accelerate the 2D diffusion of Zn^{2+} on the Zn surface, exerting detrimental effects on the homogeneous deposition. A protective layer on the Zn surface with sub-nanometer channels can provide an ion-sieving effect to inhibit the lateral diffusion of Zn^{2+} . This idea was demonstrated with a sieve-containing and uniformly porous Kaolin layer (KL) coated on the Zn anode.^[74] The kaolin with layered structure connected by hydrogen-oxygen bonds is composed of Si–O tetrahedron and Al–O octahedron sheets (Figure 12a). These functional groups and narrow pores facilitate selective channels for homogeneous Zn^{2+} migration. In this case, the ion-sieve adsorption of Zn^{2+} goes through two sequential steps: fast adsorption of Zn^{2+} at the external surface layer followed by intra-particle diffusion of Zn^{2+} guided by the functional groups in the interior layer. Chemically coupled hydrogen-substituted graphdiyne (HsGDY) with Zn electrode can also serve as a buffer layer to mediate the redistribution of Zn^{2+} concentration and substantially regulate the ion migration.^[75] The concentration polarization and tangled 2D

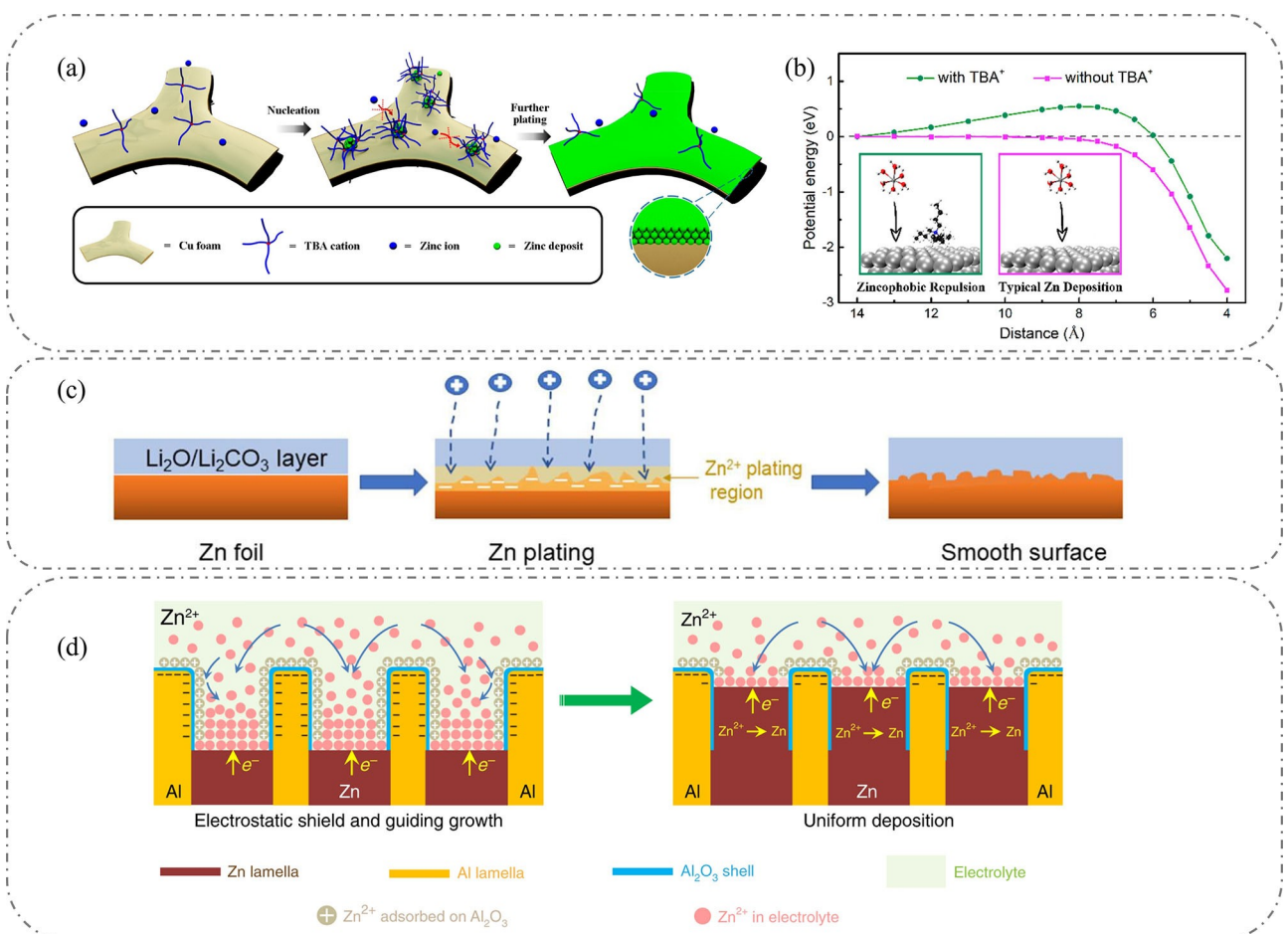


Figure 11. a) Schematic illustration of Zn deposition with or without TBA⁺. b) The potential energy of Zn²⁺ adsorption onto Zn surface at different distances with and without TBA⁺.^[68] Reproduced with permission from Ref. [68]. Copyright (2020) American Chemical Society. c) Schematic illustration of in situ SEI formation with LiCl electrolyte additive and Zn plating through the SEI layer.^[72] Reproduced with permission from Ref. [72]. Copyright (2021) American Chemical Society. d) Schematic illustration of the effect of electrostatic shield exhibited by lamella anode.^[73] Reproduced from Ref. [73]. Copyright (2020) The authors, published by Springer Nature.

diffusion of Zn²⁺ are both confined, even under the influence of an uneven electric field (Figure 12b). This well-balanced migration is attributed to the special layer structure where sub-units consisting of alkynyl groups and benzene rings are alternately connected to form the organic network of HsGDY (Figure 12c). This unique structure with sub-nanometer tunnels can selectively let in Zn²⁺ by blocking the diffusion of molecules and other ions with a larger radius.

However, the protection layer with ion-selective channels cannot exclusively prevent all molecules with small radius from permeating.^[76] Instead of blocking the movement of other ions and molecules, the shifting of the ion transport mechanism in the protective layer appears to be another potential strategy to achieve homogeneous Zn²⁺ diffusion. For instance, a composite passivation layer was constructed by applying Nafion solution and Zn–X zeolite nanoparticles.^[77] The exterior Nafion layer with a relatively wide ion channel (4 nm) would allow the permeation of small molecules and ions. In the inner layer, the inorganic filter (Zn–X layer) with nanopore size (0.74 nm) can further restrain undesired transport of anion and enable the free migration of Zn²⁺ at the organic/inorganic interface by

hopping mechanism. This unique composite layer shifts the transport mechanism from channel transport in Nafion layer to hopping transport across the interface, endowing the Nafion-Zn–X coated anode with long cycle life (over 1000 cycles) under deep cycling (1 mA cm⁻² and 10 mAh cm⁻²).

Owing to the inherent porous structure of metal-organic frameworks (MOFs), they have attracted significant attention in exploring their potential application in AZIBs.^[78] However, according to previous studies, the deficiencies of MOFs, such as complicated preparation process,^[78] utterly disappointing cycling performance,^[79] and instability at room temperature,^[80] are some practical concerns. Nevertheless, in an interesting study, an in situ zeolitic imidazolate framework-8 (ZIF-8) layer was grown on Zn foil by a one-step solvent thermal method where the Zn foil is immersed in the ZIF precursor solution and heated in an autoclave to obtain the Zn@ZIF anode.^[81] Due to abundant N species, the ZIF-8 layer exhibits strong zincophilicity compared to the Zn (001) facet (Figure 13a and b), suggesting that during cycling, a certain amount of Zn²⁺ ions are immobilized around the layer, thereby mitigating the concentration gradient at the interface. Besides, the ZIF-8 with

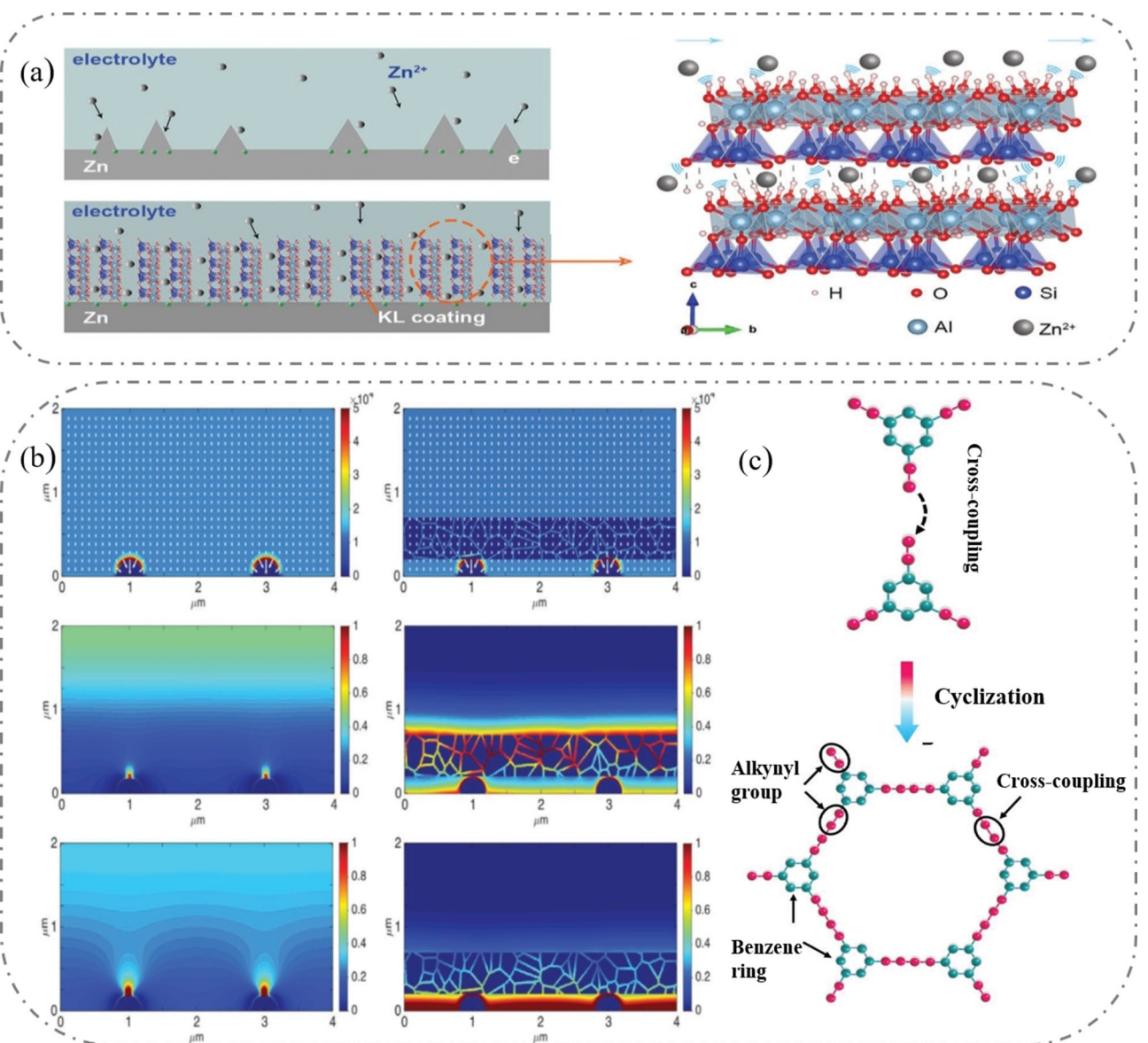


Figure 12. a) Schematic illustration of the crystal structure of kaolin and the channel for Zn^{2+} transport.^[74] Reproduced with permission from Ref. [74]. Copyright (2020) Wiley-VCH. b) Simulated electric and concentration fields for bare and HsGDY-coated Zn electrodes. c) Schematic illustration of the synthesis of HsGDY and its organic network.^[75] Reproduced with permission from Ref. [75]. Copyright (2020) Wiley-VCH.

a considerably high diffusion barrier (1.38 eV) prevent the instantaneous diffusion of Zn^{2+} onto the Zn (001) surface (Figure 13c), functioning as a buffer to guide the Zn^{2+} flux. In this way, the well-organized nanosized ZIF-8 layer, can harmonize the rampant 2D diffusion of Zn^{2+} on the substrate with an impressive capacity retention of 101% for a LaVO_4/Zn full cell after 10000 cycles.

3.2.3. Regulating Zn^{2+} transport in the electrolyte

The electrolyte plays a vital role in the electrochemical performance and charge storage mechanism of the battery due to its inherent physicochemical properties.^[84] Generally, the ionic conductivity of the electrolyte, regarded as a critical parameter,

can conspicuously affect the migration of Zn^{2+} in the bulk electrolyte and the rate performance of the battery.^[85] The aqueous electrolyte with lower viscosity and ion solvation energy typically possess higher conductivity than organic and ionic electrolytes.^[86] Among the aqueous varieties, mildly acidic electrolytes ($\text{pH}=3\text{--}6$) that are neither too acidic nor alkaline are particularly attractive as they can avoid the critical problems related to the formation of byproducts.^[87] Thus, not surprisingly, research and development of AZIBs based on mildly acidic electrolytes have made significant progress in a rather short time. Several different mildly acidic electrolytes have been developed with varying degrees of solvation effect, viscosity, and salt concentration, all of which affect the ionic conductivity.^[88] For example, the higher concentration of $\text{Zn}(\text{CF}_3\text{SO}_3)_2$ (zinc trifluoromethanesulfonate or zinc triflate)

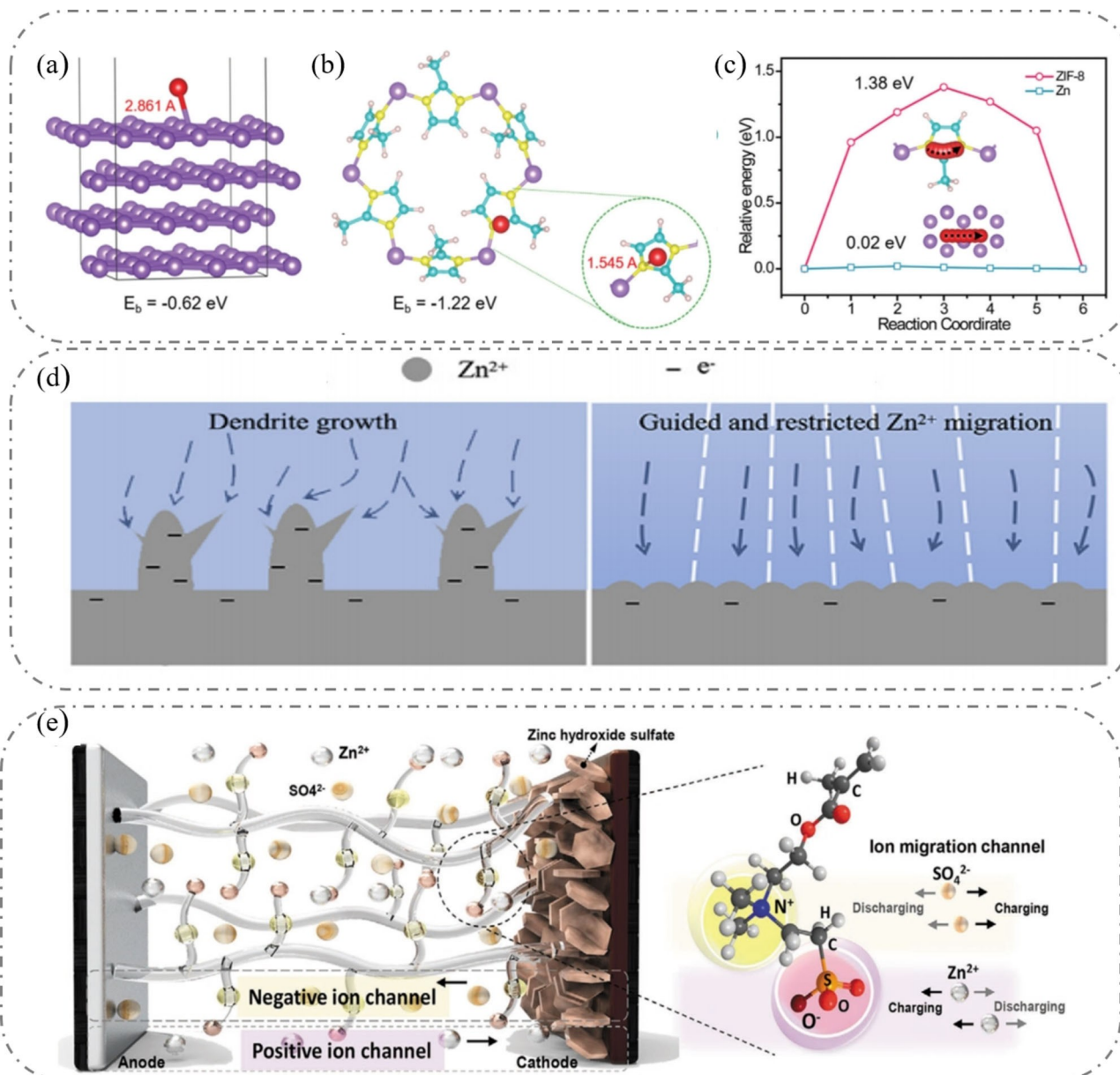


Figure 13. The binding energy of Zn^{2+} ion onto a) Zn (001) facet and b) ZIF-8 layer. c) The activation energy of Zn^{2+} migration through Zn (001) and ZIF-8.^[81] Reproduced from Ref. [81]. Copyright (2020) The authors, published by Wiley-VCH. d) Schematic illustration of the mechanism of Zn plating/stripping guided by Alg-Zn gel electrolyte.^[82] Reproduced with permission from Ref. [82]. Copyright (2020) Elsevier. e) Schematic diagram of separate ion channels provided by ZSC-hydrogel electrolyte under an external electric field.^[83] Reproduced with permission from Ref. [83]. Copyright (2020) Wiley-VCH.

proportionally increases the viscosity of the corresponding electrolyte, accompanied by the reduction of ionic conductivity.^[41] In this regard, 3 M $Zn(CF_3SO_3)_2$ strikes the right balance of viscosity, solvation and transport behavior of hydrated Zn^{2+} to exhibit superior stability and kinetics during cycling.^[41]

The gel electrolytes and quasi-solid electrolytes, typically synthesized by combining polymer or inorganic compounds with liquids, can provide the physical framework to manipulate the ion transport in electrolytes.^[89] Gel electrolytes display a similar mechanism of ion transport as the liquid ones but suffer from an inferior ionic conductivity due to lower fluidity and

chemical incompatibility between the electrolytic ions and functional groups. In this respect, the electrolyte framework that can preferentially interact with Zn^{2+} via suitable functional groups and possesses sufficient migration channels for the transport of Zn^{2+} , can endow the gel electrolytes with a sufficiently high ionic conductivity.^[11f] For instance, the zinc alginate gel electrolyte (Alg-Zn) was fabricated via a direct ion crosslinking method and provides a hierarchically three-dimensional transport network for Zn ions.^[82] Here, the carboxylate groups of alginates strongly interact with Zn^{2+} and exhibit the ion-confinement effect, thereby guiding the migration of Zn^{2+} in the electrolyte through the polymer chains (Figure 13d). This

electrolyte can mitigate the tip effect by rendering the uniform migration of Zn^{2+} and displays considerably high ionic conductivity ($1.83 \times 10^{-2} \text{ S cm}^{-1}$) at room temperature. Recently, a zwitterionic sulfobetaine/cellulose (ZSC) hydrogel electrolyte was found to effectively increase the ionic transport via ion diffusion pathways formed by aligned zwitterionic side groups.^[83] As shown in Figure 13(e), owing to the unique structure, the ZSC electrolyte can separately facilitate the cation and anion movement through specific ion channels, delivering a high ionic conductivity of $24.6 \times 10^{-2} \text{ S cm}^{-1}$. Moreover, the as-fabricated Zn-MnO₂ battery can provide an astounding rate performance of up to 10000 cycles at 30 C with an average capacity of 62 mAh g^{-1} . Although the gel electrolytes can provide the continuous transport path for the movement of Zn ions, they would not remarkably improve the electrochemical performances of the battery, especially for capacity retention and lifespan.

3.3. Controlling crystallographic orientation of zinc growth

At the initial stage of electroplating, Zn crystallites nucleate with random crystalline orientation – typically in the form of hexagonal platelets. However, growth tends to happen via the preferential addition of zinc on specific crystallographic facets. While zinc deposition on the (002) facet would lead to large pillar-like structures that can physically pierce the separator and rapidly shut down the battery, this is not typically observed. The Zn plates can also parallelly grow on the substrate via the addition of zinc to the (100) facets, leading to flat and uniform deposition, and this is often what is observed when dendritic inhibition is in play. Under the dendritic regime, instead of the vertical growth, small hexagonal flakes deposit on top of each other and pile up as porous structures, rising vertically from the substrate forcing a short circuit. Consequently, strategies have been explored to tune Zn electrodeposition to render parallel growth or smooth film like growth as a viable method to optimize the electrochemical performance of the Zn metal anode.

3.3.1. Epitaxial growth of Zn crystals

Based on the previous studies from alkaline media, it was known that the Zn (002) facet possesses stronger corrosion-resistance than Zn (101) and (100) facets, which can be ascribed to the higher activation energy for Zn dissolution for the (002) facet with higher packing density, and thus low surface energy.^[90] The same has also been verified in mildly acidic sulphate electrolytes.^[91] This (002) exposed facet in parallel with the substrate can also favor the compact and glossy deposition of Zn and eliminate dendrite formation. To construct this specific texture, the epitaxial electrodeposition of Zn on a substrate appears to be a feasible way. For the epitaxial growth, a coherent or semi-coherent lattice interface is needed between the epitaxial substrate and epilayer; afterwards, the orientation of the newly formed crystalline phase (epilayer) has

a direct relationship to the substrate.^[92] Following this principle, the graphene layer that exhibits a low lattice mismatch with Zn metal was found to induce epitaxial electroplating of Zn.^[93] Considering the minor lattice mismatch between graphene and Zn, the as-formed epilayer of Zn is horizontal to the substrate to minimize lattice strain and energy barrier, resulting in the preferential growth of the (002) facet. This heteroepitaxial Zn anode can exhibit high tolerability under high current density and areal capacity.

Similarly, MOF materials were recently applied to facilitate a dendrite-free anode via homoepitaxy. The regulation of initial nucleation stages via homoepitaxy can effectively influence the subsequent growth of Zn crystals and deliver the desirable textured Zn plates.^[78,79,94] As a result, compared to Li metal, the Zn metal anode can eliminate the concern of SEI formation at the metal surface, which facilitates the home/heteroepitaxial growth of Zn with uniform plating/stripping manner on specific substrates.

3.3.2. Optimization of the electrolyte

Both salt and solvent of the electrolyte determine the chemical and coordination environment of Zn^{2+} , and thus the manner of zinc nucleation by influencing the solvated Zn^2 structure and through interaction with the target Zn surface.^[95] In this context, some electrolytes have been explored that can endow selective deposition of textured Zn to enable dendrite free operation. For instance, the zinc trifluoromethanesulfonate [Zn(OTf)₂] can alter the zinc coordination in the salt-in-water electrolyte and further prompt the formation of Zn (002) texture via the strong OTf anion-Zn²⁺ interaction.^[96] The proposed mechanism is that at the onset of electrodeposition, the OTf⁻ anions, propelled by the enormous adsorption energy of -13.9 eV with the Cu substrate, promote the stabilization of adsorbed Zn ions (or adions) on the flat surface sites of the substrate. Subsequently, this stabilization leads to sufficient coverage of Zn adions on the surface of the substrate, which facilitates the formation of hexagonal nuclei (Figure 14a). As a result, the hexagonally arranged nuclei further aggregate and parallelly grow along the (002) facet till touching the neighboring nuclei to form a continuous film (Figure 14b).^[96] In another work, Cong et al. showed that poly(2-acrylamide-2-methyl-1-propane sulfonate) zinc (PAMPSZn) hydrogel electrolyte is highly beneficial to achieve ultra-stable and highly reversible Zn anode thanks to a uniform regulation of the Zn²⁺ movement by the polyanionic chain to achieve homogeneous stripping and plating (Figure 14c).^[97] Simultaneously, the appearance of the prominent (002) diffraction peak during cycling indicates the preferential deposition of zinc with the flat (002) facet exposed (Figure 14d). Hence, the Zn/Zn symmetric cell with PAMPSZn electrolyte can deliver a long-term performance of up to 4500 h at 1 mA cm^{-2} and 1.0 mAh cm^{-2} current density and areal capacity, respectively. Similarly, inorganic and organic electrolyte additives such as polyethylene-glycol (PEG-8000),^[28] sodium dodecyl sulfate (SDS),^[28] and nickel triflate^[98] can also regulate the crystallographic orientation of Zn deposition.

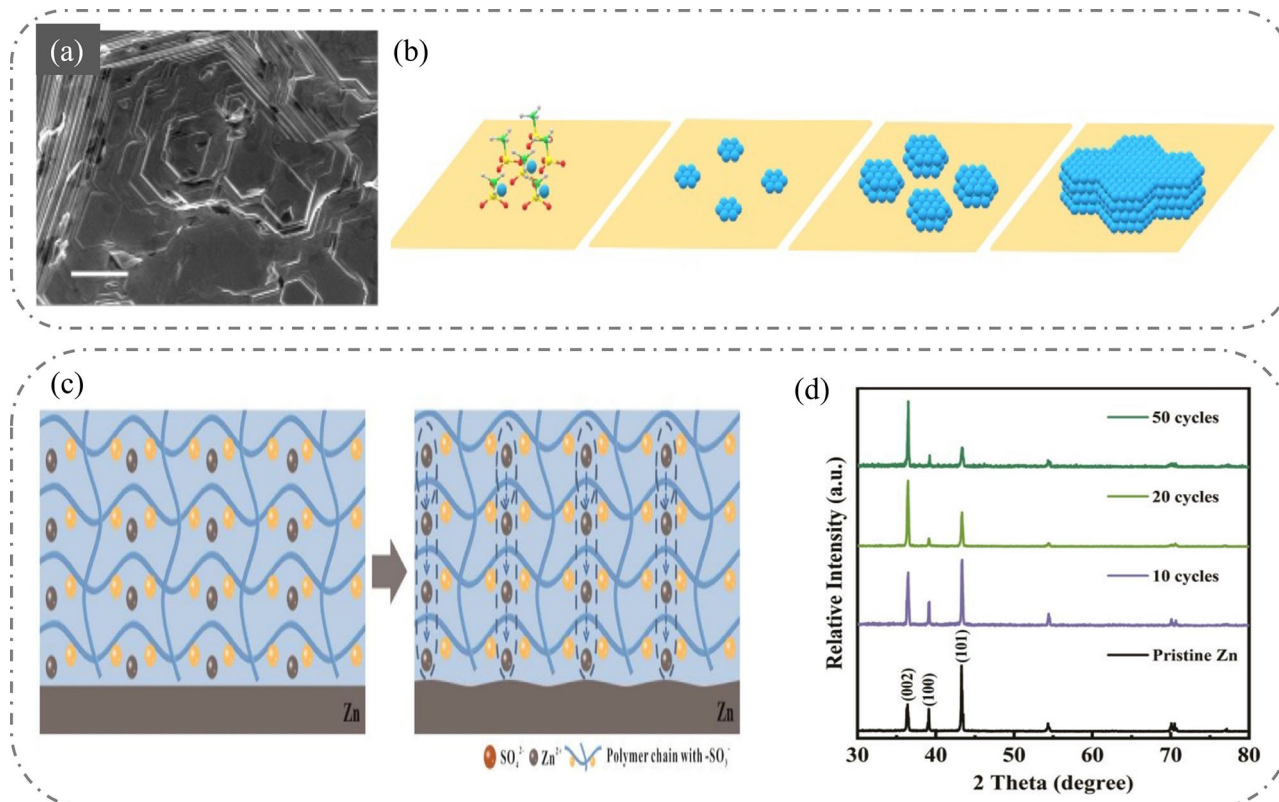


Figure 14. a) SEM images of Zn electrode with the hexagonally packed feature of (002) textured facet after cycling in the $\text{Zn}(\text{OTf})_2$ electrolyte. b) Schematic illustration of the proposed mechanism for the OTf^- anion.^[96] Reproduced with permission from Ref. [96]. Copyright (2020) Wiley-VCH. c) The scheme of the proposed mechanism of the PAMPSZn hydrogel electrolyte; d) XRD patterns of pristine Zn and the Zn anode with the PAMPSZn electrolyte after 10, 20, and 50 cycles.^[97] Reproduced with permission from Ref. [97]. Copyright (2020) Elsevier.

Notably, large rolling deformation can successfully construct a (002) textured Zn surface, which provides a potential path for achieving large-scale industrial production.^[99]

Of late, there has been a flurry of reports exploring various mechanisms to inhibit Zn dendrite, whereas the electrochemical performances of these strategies are still unsatisfactory to realize commercial viability. To achieve convincing improvement in AZIB performance for practical application, more in-depth investigations are necessary while paying attention to the cycling conditions and parameters.

4. Recent Advances in Inhibiting HER and Corrosion

The gas pressure build-up and corrosion of the Zn anode because of HER are exceedingly harmful for the long-term performance and reversibility of AZIBs. Furthermore, it is apparent that HER and dendrite can mutually impact the electrochemical performance of the Zn anode as both are sensitive to the surface state of the Zn metal. Their strong interrelation makes it impossible to bypass HER while addressing the dendrite problem. Until now, the strategies to mitigate HER mainly involve two mechanisms: (1) reducing the chemical

activity of Zn or water and (2) avoiding direct contact between water and Zn.

4.1. Reducing chemical activity

Several studies^[32,33] agree that the adsorption of H atom on the Zn surface is a prerequisite for hydrogen evolution. Therefore, the surface state and activity of Zn play a decisive role in the HER process. Besides, in aqueous batteries, water determines the coordination environment of Zn^{2+} and can directly react with Zn. Consequently, various strategies have been developed to restrain the chemical activity of Zn and water.^[100]

4.1.1. Reducing water activity via hydrogen bonding

In an aqueous ZnSO_4 electrolyte, Zn^{2+} is typically surrounded by 6 water molecules in an octahedral configuration as $[\text{Zn}(\text{H}_2\text{O})_6]^{2+}$. The water solvation shell introduces abundant water molecules to the surface of the anode and makes the reduction of H_2O to H_2 more likely during zinc plating.^[101] Simultaneously, the H^+ removal through H_2 evolution results in an increase in local pH, which perpetuates an alkaline environment near the anode, and thus corrodes Zn to form Zn(OH)_2 and ZnO . Recently, the taming of activity of free water

molecules through hydrogen bond formation between water and electrolyte additives has been explored as one feasible strategy to inhibit HER. For instance, methanol was investigated by Hao et al., and they demonstrated that the stable solvation structure of Zn^{2+} with water is weakened by methanol due to the methanol-H₂O H-bond formation.^[102] As illustrated in Figure 15(a), initially, the free water molecules in the solvation structure are repulsed out by methanol as a result of H-bond

formation. Thus, methanol molecules gradually insert into the outer and inner shell of solvated Zn^{2+} with increasing volume fraction of methanol in the electrolyte. Ultimately, the coordination balance between H₂O and Zn^{2+} in the inner solvation shell is disrupted, and Zn^{2+} tends to combine with SO₄²⁻. With such modification of Zn^{2+} solvation, H₂ evolution and corrosion are significantly suppressed, and the transference number of Zn^{2+} gets a boost. As a result, the anti-freeze methanol additive

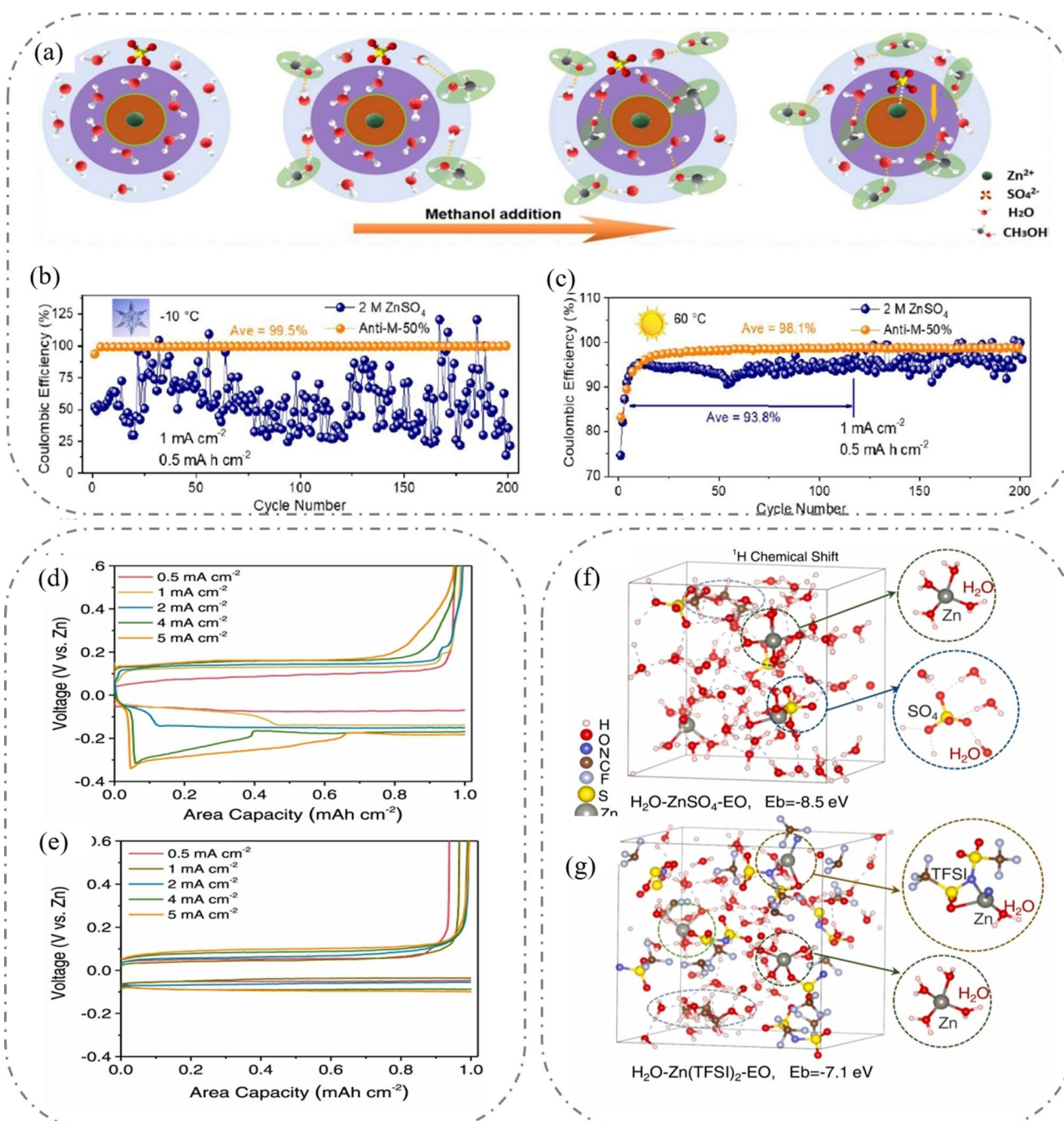


Figure 15. a) The evolution of solvation sheath of Zn^{2+} in $ZnSO_4$ electrolyte when increasing the volume ratio of methanol additive. The Zn reversibility comparison in Zn/Cu asymmetric cells with $ZnSO_4$ electrolyte and 50 vol% methanol additives at b) $-10^{\circ}C$ and c) $60^{\circ}C$.^[102] Reproduced with permission from Ref. [102]. Copyright (2020) Wiley-VCH. Voltage profiles of Zn–Cu symmetric cells under different current densities with d) 1 M $ZnSO_4$ + 0.2 wt% PEO and e) 1 M $Zn(TFSI)_2$ + 0.2 wt% PEO electrolytes. Snapshot of the MD simulation for the solvation shell of f) H_2O – $ZnSO_4$ –EO and g) H_2O – $Zn(TFSI)_2$ –EO.^[102] Reproduced with permission from Ref. [105]. Copyright (2021) Elsevier.

endows the Zn electrode with an average CE of 99.5% and 98.1% under nonambient temperatures of -10°C and 60°C , respectively (Figure 15b and c). Analogous studies employing ethylene glycol (EG)^[28f,103] and glycerol^[104] additives have also been found to exhibit similar performance improvement.

Polyethylene oxide (PEO) polymer was also reported to significantly prolong the cycling performance of commercial Zn foil anode with a small weight percentage (0.5 wt%).^[106] Most recently, Yan et al.^[105] demonstrate that PEO as the electrolyte additive can effectively stabilize the Zn anode in both ZnSO_4 and zinc di[bis(trifluoromethylsulfonyl)imide] $[\text{Zn}(\text{TFSI})_2]$ electrolyte, but exhibits different voltage hysteresis for these two electrolytes during plating and stripping (Figure 15d and e).^[105] This is because the salt anion can have unique interactions with the additive, thereby affecting the Zn dissolution-deposition behavior. In ZnSO_4 electrolyte, instead of direct chemical bonding with Zn^{2+} , PEO tends to tightly interact with Zn^{2+} through surrounding H-bonds with high binding energy, suggesting higher de-solvation energy of Zn^{2+} during plating and stripping (Figure 15f).^[105] In contrast, TFSI^- anion directly bonds with Zn^{2+} and PEO in the form of $\text{H}_2\text{O}-\text{Zn}(\text{TFSI})_2-\text{EO}$ (Figure 15g). This different solvation complex with a higher overall binding energy of -7.1 eV than that in ZnSO_4 electrolyte (-8.5 eV) suggests much easier de-solvation of Zn^{2+} ions in aqueous electrolyte with TFSI^- than SO_4^{2-} anion, thereby clearly explaining the underlying mechanism of facile Zn plating/stripping in $[\text{Zn}(\text{TFSI})_2]$ electrolyte from the molecular perspective^[105]. Therefore, this work highlights the importance of appropriate electrolyte salt and additives, providing detailed insight into the interplay between salt anion and additive.

4.1.2. Restraining water activity through high salt concentration

High salt concentration in the electrolyte can effectively restrain the HER. Like electrolyte additives, increasing salt concentration can regulate the Zn^{2+} coordination environment and even reduce the free water molecules in the electrolyte. For example, in the ZnSO_4 electrolyte, increasing the concentration of ZnSO_4 from 2 to 4.2 M with a fixed 0.1 M MnSO_4 concentration in the electrolyte alters the Zn^{2+} coordination sphere.^[107] At high ZnSO_4 concentration, sulfate anions (SO_4^{2-}) start to occupy the interior shell of Zn^{2+} and expel the water molecules out due to the higher affinity to Zn^{2+} .

Apart from directly increasing the concentration of Zn salt, adding other salts – i.e., by using a highly concentrated hybrid electrolyte – can also tune the coordination environment of Zn^{2+} . For example, a well-known “water-in-salt” (WIS) electrolyte composed of 1 m $\text{Zn}(\text{TFSI})_2$ and 20 m LiTFSI ^[108] [where m is molality (mol kg^{-1})] can reshape the Zn^{2+} solvation sheath and effectively prevent the H_2 evolution. Molecular Dynamics (MD) simulation predicted equilibrium Zn^{2+} -solvation-sheath structure illustrates that by increasing the concentration of LiTFSI, the anion replaces the water molecules from the inner shell of Zn^{2+} (Figure 16a). In the most concentrated electrolyte [1 m $\text{Zn}(\text{TFSI})_2 + 20\text{ m LiTFSI}$], the solvation shell of Zn^{2+} is domi-

nated by TFSI^- , with all six oxygens in the coordination sphere being from TFSI.

Leveraging this coordination structure, this intriguing electrolyte can effectively curb HER by suppressing the water activity and enable stable cycling of the Zn/LiMn₂O₄ full cell with 99.9% CE. However, the high price and toxicity of fluorinated salts are unfavorable for large-scale utilization; hence, replacing them with low-cost salts is another direction for the concentrated electrolyte.^[110] In this regard, ZnCl_2 based water-in-salt electrolyte of 30 m concentration was proposed by Zhang et al.,^[111] which can tame the electrochemical water reactivity owing to the presence of a hydrated shell of $[\text{ZnCl}_4]^{2-}$ instead of $[\text{Zn}(\text{H}_2\text{O})_6]^{2+}$. In addition to using cheap water-in-salt electrolytes, a super-saturated electrolyte with a moderate 3.3 M ZnSO_4 concentration, combined with MOF coating layer, exhibits different Zn^{2+} solvation structures between the bulk electrolyte and MOF channels.^[109] As depicted in Figure 16(b), inside of the MOF layer, the oversized solvated ion complex was partially desolvated in advance due to the porous features of the layer. Afterwards, a super-saturated electrolyte formed inside MOF channels with a solvation structure of $\text{H}_2\text{O}-\text{Zn}^{2+}\cdot\text{OSO}_3^{2-}$ which can pass through the MOF channels (Figure 16c). This ion association gives rise to an astounding lifespan in symmetric Zn half cells of up to 3000 h at $2\text{ mA}\cdot 2\text{ mAh cm}^{-2}$.

4.1.3. Regulation of the zinc-anode activity

Constricting the anode activity through modification of the surface state of the Zn anode is another option to achieve higher corrosion resistance and HER overpotential. Typically, alloying of Zn with other metals possessing stronger corrosion resistivity in aqueous media than Zn can remarkably improve the corrosion resistance of the Zn anode. In alkaline media, binary alloys such as Zn–Cr,^[112] Zn–Ni,^[31d,113] and Zn–Pb^[114] have been commonly employed to mitigate corrosion. Inspired by the previous studies, the anti-corrosive metallic Cu with a positive electrode potential ($+0.34\text{ V}$ vs. SHE) was introduced to Zn anode to form a uniform Zn–Cu alloy with superior chemical stability in an aqueous environment (Figure 17a).^[115] The excellent corrosion protection was verified by the Tafel plot, where more positive corrosion potential and lower corrosion current both confirm its excellent corrosion-resistant capability in ZnSO_4 electrolyte (Figure 17b). More importantly, compared to the bare Zn anode, after dwelling 30 days in the electrolyte, the Zn–Cu composite anode in a symmetric configuration still presents ultra-stable longevity of 1500 h at $1\text{ mA}\cdot 0.5\text{ mAh cm}^{-2}$ (Figure 17c).

Similarly, a 3D Zn₃Mn alloy anode with a novel crystalline structure (Figure 17d) not only provides a preferable ion-migration path for Zn ions but also effectively controls the surface reaction thermodynamics.^[116] The Zn₃Mn alloy anode is compatible with seawater-based electrolytes and exhibits a wide electrochemical window of up to 2.6 V, thereby effectively suppresses the water dissociation. Even in the harsh seawater environment with interference from hetero-ions, the 3D Zn–Mn

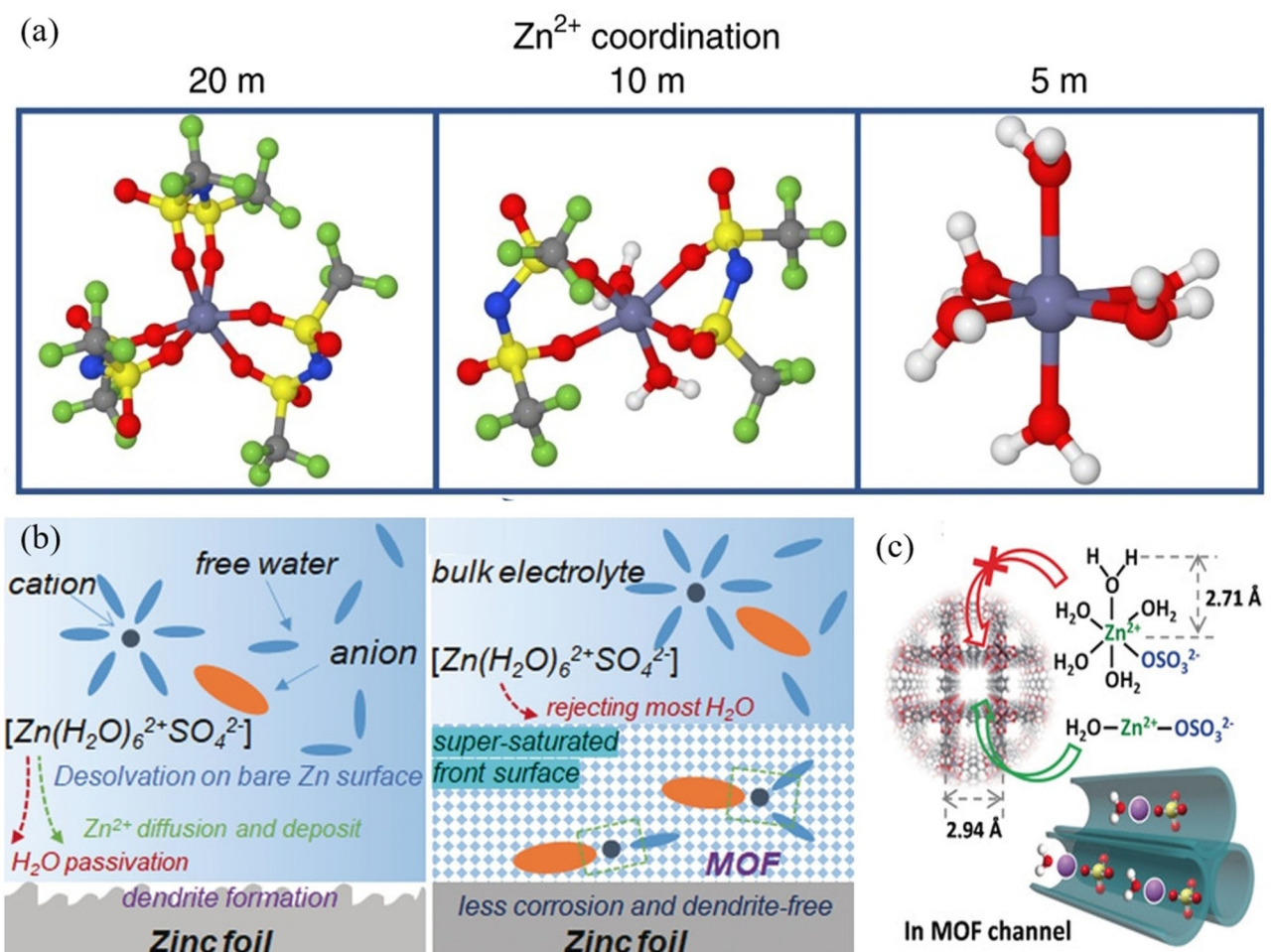


Figure 16. a) The evolution of coordinating structure of hydrated Zn^{2+} in the 1 M $\text{Zn}(\text{TFSI})_2$ electrolyte with different concentrations of LiTFSI .^[108] Reproduced with permission from Ref. [108]. Copyright (2018) The authors, published by Springer Nature. b) Working mechanism of the MOF coating layer in constructing a super-saturated electrolyte at the front surface. c) The schematic illustration of the coordination structure of $\text{H}_2\text{O}-\text{Zn}^{2+}-\text{OSO}_3^{2-}$ in the super-saturated electrolyte and the migration path inside the MOF channel.^[109] Reproduced with permission from Ref. [109]. Copyright (2020) Wiley-VCH.

alloy anode maintains an outstanding lifetime (700 hours) with an extremely high current density of 80 mA cm^{-2} and an areal capacity of 16 mAh cm^{-2} (Figure 17e). This rationally designed electrode is promising for industrial-level applications owing to universal electroplating fabrication and the low cost of the solvent.

In another work, a ternary Zn–Sn–Pb alloy was proposed to reduce the self-corrosion and HER significantly in an aqueous electrolyte.^[117] Thanks to enhanced hydrogen evolution overpotential and lower HER potential of Pb and Sb metals, the Zn–Sb–Pb anode displays a robust tolerance to side reactions with a highly reservable capacity. Hence, tuning the electrochemical property of the electrode by alloying chemically inactive components with Zn metal can offer a viable option for designing ultra-stable zinc metal electrodes. However, it must be noted that the formation of galvanic cells due to inhomogeneous distribution of alloying elements is possible to exacerbate the chemical corrosion of the anode and electrolyte in turn.^[118]

4.2. Avoiding direct Zn-electrolyte contact

The interface between the Zn anode and the electrolyte plays a decisive role in the anode's corrosion behavior. Not only Zn (in contact with aqueous electrolytes) cannot form a compact solid-electrolyte interphase (SEI) like Li (in contact with non-aqueous electrolyte) to prevent further side reactions, the porous passivation layer formed by corrosion on the Zn surface (e.g., ZnO , Zn(OH)_2 , and $\text{Zn}_2(\text{OH})_2\text{SO}_4$) fails to prevent further HER and to some extent even accelerates the corrosion rate.^[119] The insulating passivation layer on Zn is likely to increase the impedance of the anode and lead to sluggish charge transfer kinetics. Thus, applying a physical barrier at the interface between Zn and electrolytes has been proposed as a feasible approach to overcome the HER related corrosion.

4.2.1. Ex-situ formed surface coating layer

It has been shown that oxide (e.g., CaCO_3 ,^[44] ZrO ,^[48] ZnO ^[50] and Sc_2O_3 ^[120] etc.) and MOF coating layer^[109] can function as a

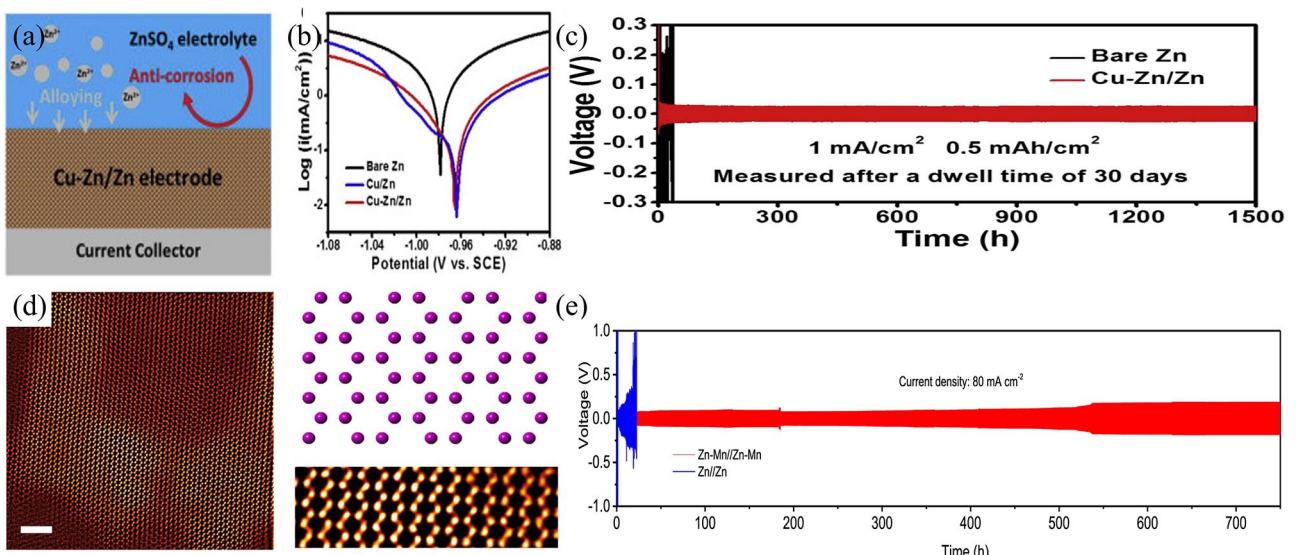


Figure 17. a) Schematic illustration of the functioning of the Cu–Zn/Zn electrode. b) The Tafel plots of Zn, Cu–Zn alloy electrode, and Cu–Zn/Zn electrode (the Cu–Zn electrode after cycling) in 3 M ZnSO₄ electrolyte.^[115] Reproduced with permission from Ref. [115]. Copyright (2020) Elsevier. c) Life performance of bare Zn electrode and Cu–Zn alloying electrode in symmetric Zn/Zn cells after dwelling time of 30 days in the electrolyte.^[115] Reproduced with permission from Ref. [115]. Copyright (2020) Elsevier. d) High-angle annular dark-field (HAADF) scanning transmission electron microscopy (STEM) image of the Zn–Mn alloy. e) Comparison of Zn reversibility in Zn/Zn cells between Zn–Mn alloy electrode and bare Zn electrode at a current density of 80 mA cm⁻² and areal capacity of 16 mAh cm⁻².^[116] Reproduced with permission from Ref. [116]. Copyright (2021) The authors, published by Springer Nature.

physical barrier to alleviate the hydrogen evolution on Zn in aqueous electrolytes. Furthermore, unlike the conventional solid-liquid interface of the anode, a liquid-liquid interlayer^[121] was recently proposed to solve corrosion and dendrite-related issues. A liquid-liquid interface was firstly established by liquid Ga–In–Zn alloy according to the ternary phase diagram (Figure 18a and b).^[121b] The liquid alloying interlayer demonstrates dendrite-free morphology during long-term operation as the alloy with high affinity to Zn and high electrical conductivity can endow fast charge transfer. This regulation of the zinc plating was confirmed by *in situ* synchrotron X-ray tomography investigation during zinc plating, which showed no dendrite (Figure 18d) compared to the uneven distribution of zinc dendrite observed on the surface of the bare Zn anode (Figure 18c). Besides, Ga and In metal both exhibit higher HER overpotential than Zn metal, hence provide considerable corrosion resistance in the ZnSO₄ aqueous electrolyte. Similarly, the traditional solid-liquid interfaces formed by anti-corrosion material such as In,^[48] Sn,^[122] and Bi₂O₃^[123] also endow the Zn anode with enhanced resistance to self-corrosion and HER.

A compact passivation layer composed of zinc hydroxycarbonate [Zn₅(CO₃)₂(OH)₆ or Zn₄CO₃(OH)₆·H₂O] is spontaneously formed on the surface of Zn metal when it is exposed to air, and this dense layer can retard the corrosion by blocking the moisture and oxygen from Zn metal.^[124] Lately, an in-depth study about the surface chemistry of Zn metal was conducted by Hao et al.^[125] and attest that this self-corrosion layer is thermodynamically unstable in mild electrolytes and is unable to protect Zn metal against corrosion. Therefore, they intricately deposited a dense ZnS layer on the Zn metal surface to prevent the Zn anode from side reactions. The merits of the ZnS coating layer are mainly attributed to the formation of

Zn–S polar bonds at the interface of ZnS and Zn metal, which reshape the charge distribution at the interface and enhance the adhesion of the protective layer to the Zn metal. In contrast to the bare Zn anode that suffers from inhomogeneous deposition with severe agglomeration during plating (Figure 18e), the ZnS@Zn electrode with strong stability can guide the homogeneous deposition under the film and maintain a smooth morphology (Figure 18f).

To some extent, most of the protective layers stabilize the Zn anode leading to extended lifespan, but cracking of the layer due to drastic volume change during the long-term operation would severely influence the practical implementation of this strategy. Therefore, instead of delaying corrosion and dendrite growth, having an in-depth understanding of the Zn anode is a requisite to find a way to inherently improve the reversibility and corrosion-resistance properties. The ZnF₂ coating layer that serves as a fast Zn²⁺ conductor is an excellent alternative with fast transport of Zn²⁺ to achieve strong protection against H₂O-related corrosion and a dendrite-free anode (Figure 18g).^[126] Here, the lower Zn²⁺ insertion barrier (0.52 eV) on Zn@ZnF₂ reduces the energy barrier of nucleation, and thus ensures higher charge-transfer kinetic than bulk ZnF₂ (4.08 eV) and metallic Zn surface (0.67 eV). Most notably, the hydrogen gas production was also quantified by gas chromatography mass spectrometry (GC-MS) analysis to *in situ* monitor the gas evolution. Compared to a large H₂ flux for the bare Zn anode (Figure 18h), ZnF₂ layer almost exclusively suppressed the H₂ evolution (Figure 18i) during the charging process. The HER suppression was found to stem from a higher adsorption Gibbs free energy of hydrogen adsorption (ΔG_H) for Zn@ZnF₂ (Figure 18j), implying weaker hydrogen binding on Zn@ZnF₂, and thus hydrogen-repulsing surface chemistry.

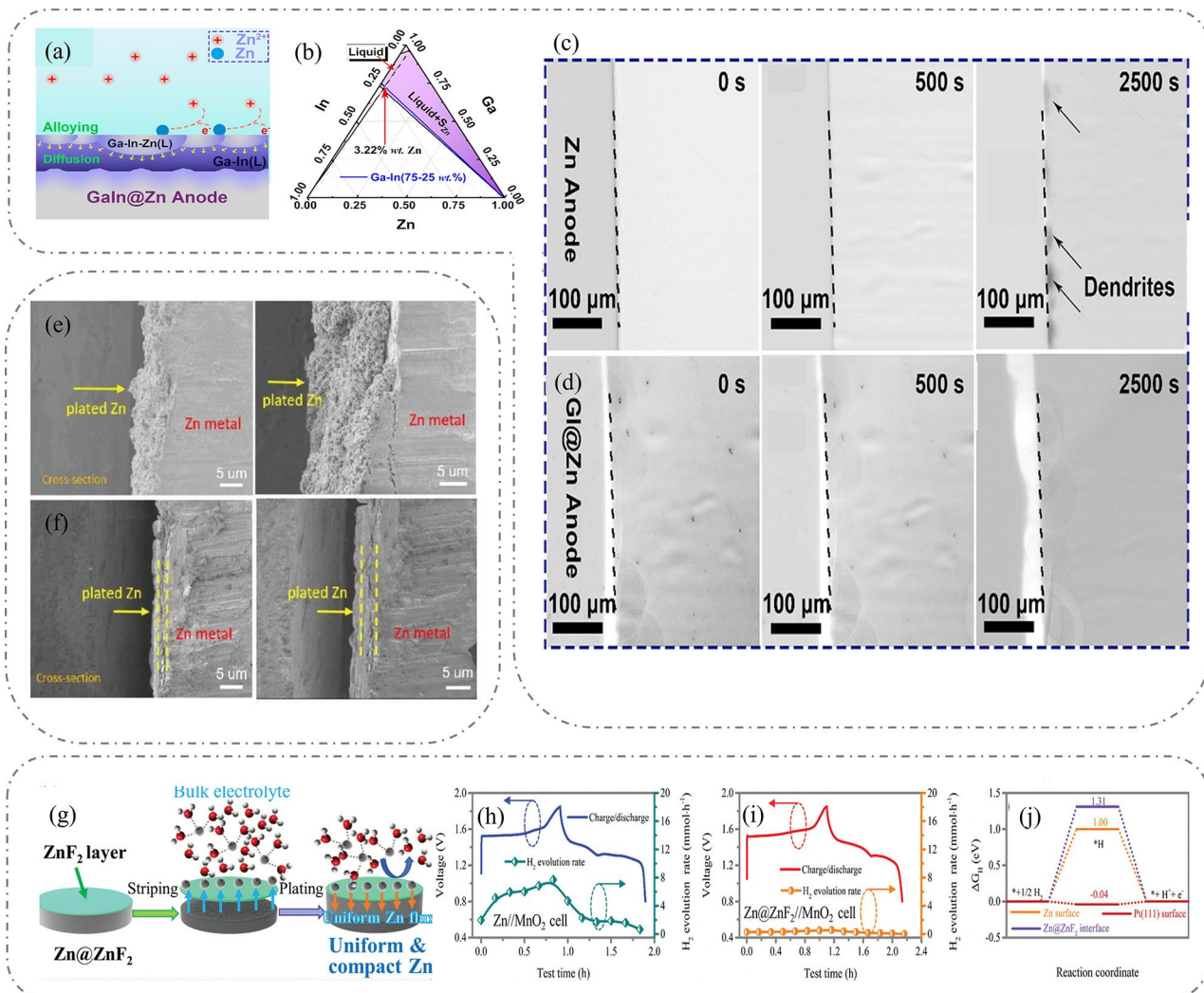


Figure 18. a) Schematic illustration of the functioning of the liquid Ga–In coated Zn anode. b) The isothermal phase diagram of Ga–In–Zn ternary. The cross-section image obtained by in situ synchrotron X-ray tomography at a current density of 10 mA cm^{-2} for c) the symmetric cells with bare Zn electrodes and d) Ga–In coated Zn electrodes.^[121b] Reproduced with permission from Ref. [121b]. Copyright (2021) American Chemical Society. Cross-section SEM images of Zn deposition e) on bare Zn anode and f) on Zn electrode with ZnS protective layer.^[125] Reproduced with permission from Ref. [125]. Copyright (2020) Wiley-VCH. g) Schematic illustration of the working mechanism of the ZnF_2 coating layer. h) In situ monitoring of hydrogen evolution flux for Zn/MnO_2 full battery and i) $\text{ZnF}_2/\text{MnO}_2$ full battery. j) The Gibbs free energy diagram for HER on $\text{ZnF}_2@Zn$ electrode and Zn (002).^[126] Reproduced with permission from Ref. [126]. Copyright (2021) Wiley-VCH.

4.2.2. In situ formed surface layer

Lithium-metal batteries also face a similar dilemma of intrinsic corrosion at the Li anode. But it also has an intrinsic solution, which is in situ formation of SEI that is highly permeable to Li^+ and can keep out the reactive solvent. The high redox potential of Zn (-0.76 V vs. SHE) implies that conventional electrolyte anions and organic solvents are difficult to chemically reduce as a protective SEI layer before zinc plating. Therefore, alternative solvents and electrolytes must be looked at to design Zn anodes with a robust in situ formed SEI. In this regard, a new deep eutectic solvent (DES) consisting of acetamide (Ac) and $\text{Zn}(\text{TFSI})_2$ was found to be effective.^[127] Due to strong cation-anion interaction, this DES can induce the formation of zinc complexes $\{[\text{ZnTFSI}_m(\text{Ac})_n]^{(2-m)+}, m=1-2, n=1-3\}$ that become reductively unstable below 0.37 V (vs. Zn/

Zn^{2+} , Figure 19a), suggesting preferential decomposition of TFSI^- to form an SEI on the Zn surface. As indicated by X-ray photoelectron spectroscopy (XPS, Figure 19b), an SEI, composed of rigid ZnF_2 and S/N-rich organic compounds, successfully forms on the Zn surface. Time-of-flight secondary ion mass spectrometry (TOF-SIMS, Figure 19c) revealed an even distribution of Zn, F, N, and S on the cycled Zn surface, confirming the uniformity of the SEI layer. This Zn^{2+} -permeable SEI passivation layer can guide the Zn^{2+} diffusion in the layer and repel the free water molecules.

The stability of the SEI layer during plating/stripping plays a crucial role in the water repulsion. Disruption of the SEI layer or formation of hydrophilic interphase is incapable of preventing water penetration during long-term cycling. Based on this consideration, an ultra-stable and self-repairable SEI protective layer was in situ constructed on the Zn metal surface through

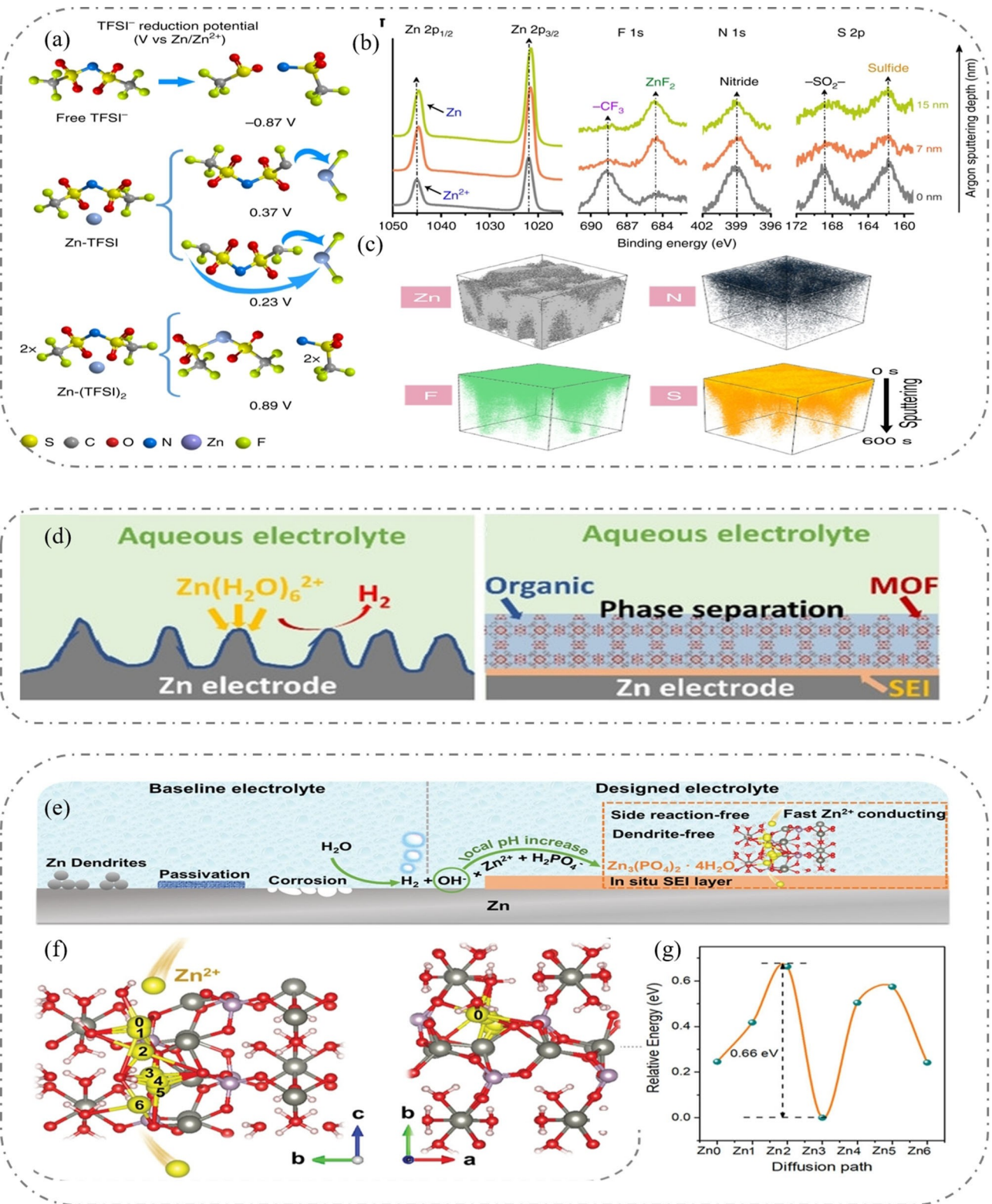


Figure 19. a) DFT calculated reduction potentials of different TFSI^- solvation structure. b) XPS spectra for Zn, F, N, and S elements in SEI film for different Ar sputtering depth. c) Three-dimensional view of Zn, N, F, and S elemental distribution of the SEI in (TOF-SIMS) sputtered volumes.^[127] Reproduced with permission from Ref. [127]. Copyright (2019) The authors, published by Springer Nature. d) Illustration of the surface structure of bare Zn anode and SEI formation in MOF-coated Zn anode.^[128] Reproduced with permission from Ref. [128]. Copyright (2020) Wiley-VCH. e) Schematic illustration of the Zn surface evolution in the reference Zn anode and the optimized electrolytes. f) DFT calculations of the optimum Zn-ion diffusion pathway in the SEI layer, and g) the corresponding migration energy barrier.^[129] Reproduced with permission from Ref. [129]. Copyright (2021) Wiley-VCH.

the assistance of $\text{Zn}(\text{TFSI})_2\text{-tris}(2,2,2\text{-trifluoroethyl})\text{phosphate}$ (TFEP) organic electrolyte and an organophilic MOF layer (Figure 19d).^[128] The MOF layer with highly ordered microporous channels (9 Å) can not only effectively confine organic TFEP electrolyte (<6.6 Å) in the layer but also enable the fast migration of zinc ions (0.74 Å). Furthermore, the TFEP is immiscible with bulk $\text{Zn}(\text{TFSI})_2$ aqueous electrolyte, hence completely blocks water by phase separation. During plating/stripping, the $\text{Zn}(\text{TFSI})_2\text{-TFEP}$ electrolyte is decomposed to an ionic-conductor $\text{ZnF}_2\text{-Zn}_3(\text{PO}_4)_2$ SEI layer with strong chemical stability. The hydrophobicity of this layer repels any residual water molecules in the organic electrolyte.

As discussed above, the hydrogen evolution on the Zn surface during cycling will release hydroxyl anions into the electrolyte and increase the local pH value, thereby induce the formation of undesirable byproducts. To turn this drawback into an advantage, Zeng et al. proposed an *in situ* formed SEI layer with a compact and well-arranged structure, composed of $\text{Zn}_3(\text{PO}_4)_2\cdot 4\text{H}_2\text{O}$, through the addition of a tiny amount of $\text{Zn}(\text{H}_2\text{PO}_4)_2$ salt (Figure 19e).^[129] Unlike the conventional construction of SEI involving the decomposition of solvent and/or salt, the $\text{Zn}_3(\text{PO}_4)_2\cdot 4\text{H}_2\text{O}$ SEI film can form and coat the Zn surface via the reaction between H_2PO_4^- and OH^- . The anti-corrosion property of the SEI was confirmed by linear polarization, indicating less propensity to corrosion with more positive corrosion potential. In striking contrast to the bare Zn anode, the SEI-coating with a high Zn-ion transference number of 0.75 can effectively retard the undesirable ions and facilitate Zn^{2+} diffusion. This superior ion-transport property was attributed to the presence of multiple Zn^{2+} diffusion channels (tagged from Zn0 to Zn6 in Figure 19f). The corresponding Zn^{2+} diffusion barrier for this channel was calculated to be 0.66 eV (Figure 19g), indicating facile diffusion kinetics.

It is highly unlikely to find an interlayer material with Zn^{2+} conductivity comparable to that of aqueous electrolytes, and therefore, besides blocking HER, the interlayer is likely to add to the zinc plating/stripping overpotential and will slow down zinc reaction kinetics. In reality, rarely the interlayer is perfectly compact and pore free. Therefore, the zinc ion (hence, the electrolyte) primarily transports through the cracks and/or pores, which compromises the HER suppression effect.

5. Summary and Future Directions

Here, we have discussed the chemistry and electrochemistry of the Zn metal anode and the HER on Zn in alkaline and mildly acidic media, zinc dendrite formation and associated mechanisms, and highlighted the fundamental challenges facing Zn anodes while presenting notable research efforts in mitigating the dendrite formation and HER in AZIBs. Thanks to some innovative and effective strategies, dendrite and corrosion-free Zn anode in AZIB electrolytes is to some extent achievable on a lab scale. However, in those studies, often attention was not paid to practical considerations required for the development of a reliable solution. There remain significant gaps between functional requirements and lab-scale investigation, but some

of those can be easily tackled. Most concerningly, often, there is substantial variation in the performance across studies, including noticeable ambiguities, which boils down to diverse cycling conditions and cell parameters that are applied without much consideration. Below we discuss some of the crucial factors to consider for the overall evaluation of approaches toward mitigating the dendrite/HER corrosion problems of the Zn anode in AZIBs. In addition, a brief analysis of the influence of several cell parameters on the gravimetric and volumetric energy densities is also presented, which should provide guidance in selecting potential strategies and future directions.

5.1. Influence of current density and areal capacity

The current density and areal capacity applied during cycling are important parameters of consideration. Figure 20 summarizes lifespans and corresponding cycling conditions for Zn plating/stripping in Zn–Zn symmetric cells for some of the approaches that drew attention.^[44,45,48,61,74,77,79,102,105,111,121b,125,130]

The selection of current density and areal capacity is rather arbitrary, and some are far from realistic criteria and conceal the factual lifespans and CE of batteries. This consideration is critical as it is now well established that lower capacities ($\leq 1 \text{ mAh cm}^{-2}$) and high current densities ($\geq 2 \text{ mA cm}^{-2}$), can significantly delay the dendritic failure of the Zn anode in AZIB electrolytes.^[29] At current densities exceeding 4 mA cm^{-2} the Zn anode cyclability can extend over 1000 cycles (2000 h), albeit subject to the thickness of the separator (discussed below), with the regular aqueous ZnSO_4 electrolyte and without any modification of the Zn. Such long-term Zn cycling stems from the formation of flat and dense (002) textured morphology at high currents. While excellent performance at high current densities is appealing for certain applications, keeping the intended applications of AZIBs in mind, which would be renewable and residential storage coupled with wind and rooftop solar, good performance at low power, and thus at relatively low current densities is more desirable. It is easy to show that a 12 V/10 kWh home battery connected to 6.6 kW rooftop solar would be typically charged at a C/3 rate (full charge in 3 h). This means if the AZIB type home battery has an areal capacity of $2\text{--}4 \text{ mAh cm}^{-2}$, it would charge (when Zn is deposited back at the Zn anode) at a maximum current density of $\sim 0.6\text{--}1.3 \text{ mA cm}^{-2}$. Therefore, the evaluation of any approaches toward enabling prolonged Zn anode cycle life in AZIBs is recommended to be performed at $0.5\text{--}2 \text{ mA cm}^{-2}$ for $2\text{--}4 \text{ mAh cm}^{-2}$ areal capacity. Applications like load leveling would though require operation at relatively higher currents, but the cycled areal capacity, which is dictated by the cathode capacity, would still be in the same range.

5.2. Assessment of Coulombic efficiency

Coulombic efficiency is another important parameter that reveals invaluable info about the reversibility of the involved electrochemical reactions. Despite some claims of 100 % CE for

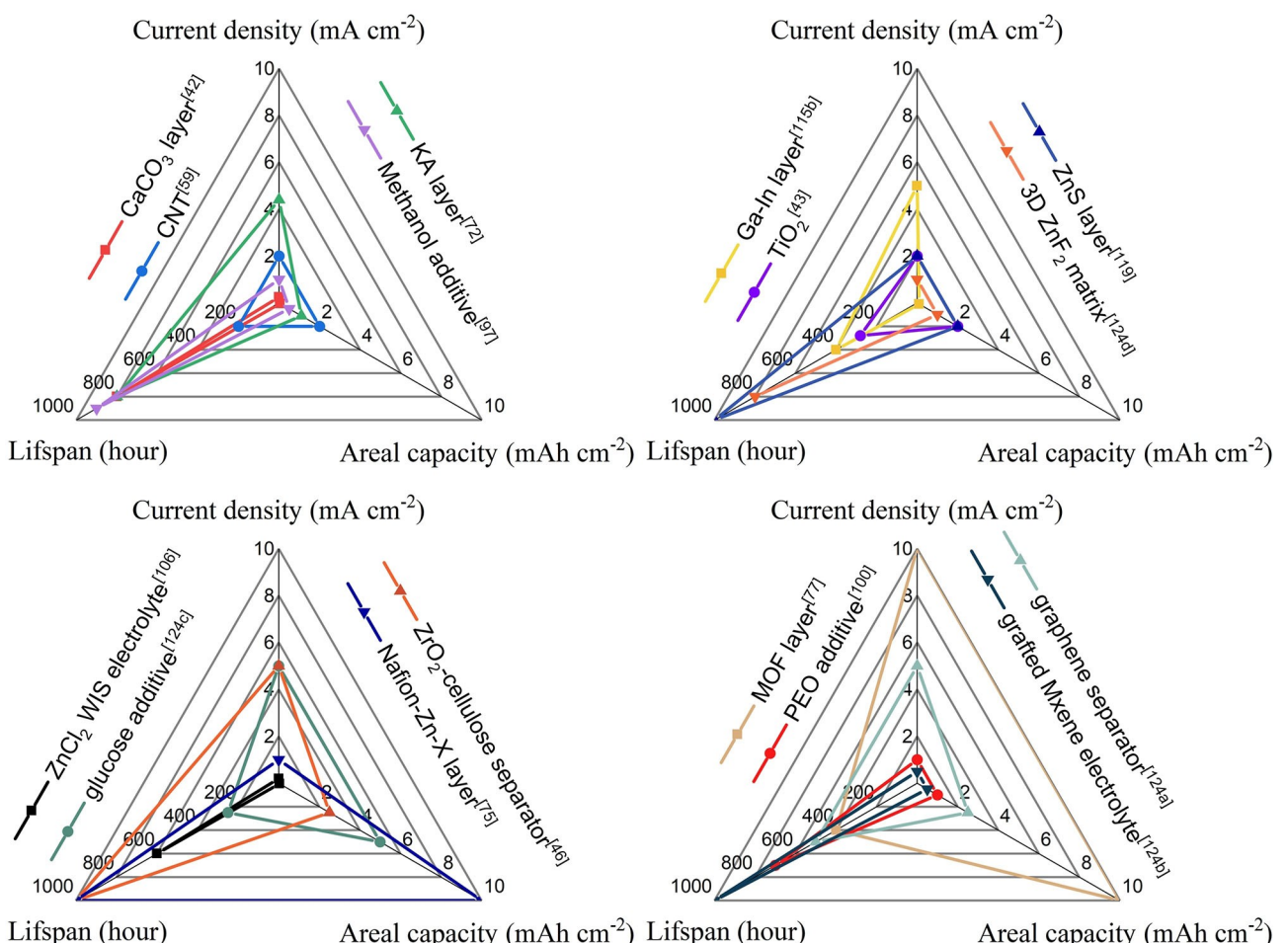


Figure 20. Summary of testing conditions (current density and areal capacity) for different strategies and corresponding life performance.

Zn metal batteries in some electrolytes with some innovative strategies, the lack of consistency between different studies is a major concern. Such discrepancy can be attributed to the different testing protocols employed for the measurement of CE and sometimes unrealistic testing conditions. Cyclic voltammetry (CV) and galvanostatic cycling have been commonly employed to quantify the Zn reversibility. However, as Ma et al.^[131] pointed out, CV measurement can potentially misinterpret the reversibility due to the inaccurate measurement of the charge passed during stripping (anodic cycle) vs. plating (cathodic cycle), which is sensitive to the scan rate, salt concentration in the electrolyte, ion diffusion coefficient, etc. Therefore, galvanostatic cycling that gives a more realistic description of the battery operation is recommended as a standard protocol to quantify CE.^[132] This is typically done in an asymmetric configuration with Ti/Cu employed as the working electrode against Zn, and an average CE is often reported based on hundreds of striping/plating cycles. Several factors like the surface texture of Ti/Cu, the purity of the metals, the presence of specific impurities in Zn that can suppress HER, and even the nature of the glass fiber type separator may influence the CE value and result in variation between studies. In this regard, a method proposed by Auerbach et al. for Li can

eliminate the Ti/Cu metal surface effect. This protocol involves the deposition of a fixed amount of Zn (Q_r) on the working electrode as a reservoir, followed by the cycling of a small fraction (Q_s) for n cycles between the two electrodes, and a final exhaustive strip (Q_f) to remove all the deposited Zn off the working electrode. The average CE is then obtained from $\text{CE}_{\text{ave}} = (nQ_s + Q_f)/(nQ_s + Q_r)$. It is important to note that the current density has a significant influence on the CE, with the higher current density leading to higher CE.^[29] This is not surprising as HER related corrosion are kinetically subdued at high current densities. Besides, different current densities for plating and stripping and the cycled capacity may also have an effect, but these have not been investigated so far.

5.3. Evaluation of Zn cyclability

While Zn–Zn symmetric cycling is the protocol regularly employed to investigate the long-term zinc cyclability, asymmetric cycling is only used to probe the CE. A sudden drop in polarization voltage detects a short circuit cell failure. However, a soft short – when the two electrodes get connected by only a single (or a few) dendritic protrusion of small cross-section –

may only lead to a very small change in polarization in symmetric voltage profiles and would be extremely difficult to detect. Often it is challenging to pinpoint the failure mode in many studies as an increase in polarization is associated with cell failure. This can happen due to factors like zinc depletion and electrolyte consumption, but it is impossible for the failure mode to vary between studies for the same electrolyte, as is typically observed for the aqueous ZnSO_4 reference electrolyte. Since zinc is mostly used in large excess relative to the cycled capacity, the variation points to the significant difference in electrolyte volume applied across studies. The electrolyte volume is often not reported, which raises the question of whether care is taken to use the same electrolyte volume for the reference and the optimized cell for a fair comparison and accurate evaluation of the performance improvement. Nevertheless, the short circuit, including soft shorts, can be comprehensively detected by asymmetric cycling where an internal short is reflected by a longer than expected stripping profile, which unlike in the symmetric cycling, is limited by the stripping voltage, not time.^[29,133] Interestingly, the short circuit events exclusively occur during the stripping of zinc from the Ti/Cu electrode, i.e., during zinc plating on Zn, which mimics the same event in a full AZIB cell and nullifies any influence of the Ti/Cu surface. Therefore, asymmetric cycling that also reveals the CE as a function of cycling is recommended as a more comprehensive protocol to probe the Zn anode cycle life.

5.4. Inter electrode distance

The thickness of the separator is a factor that is rarely mentioned but can account for disparities in Zn cycling stability between studies. When a thick separator is employed, the Zn dendrites are less likely to grow as large and pierce through the whole distance, and thus short circuit events are deferred, which not only gives a false impression of the performance but also make the results hard to compare and critically evaluate. A thick separator will significantly reduce the volumetric capacity of AZIBs (see below), ruining one of the most significant merits of the Zn metal anode. Therefore, along with current density and areal capacity, the inter-electrode distance should be explicitly provided to avoid ambiguous comparison across different studies and facilitate standard testing protocols for performance assessment.^[134] In addition, considering that the Zn dendrite in AZIBs is typically loose and flaky platelets that pile up as columnar structures to induce electrical short, the porosity of the separator may have some influence and is thus worth noting.

5.5. Considerations for full-cell cyclability assessment

In validating Zn anode cycle life enhancement, a small cathode loading of around 0.5 mAh cm^{-2} (corresponding to 1–3 mg of active material loading) is often applied even if the Zn cyclability is established at a higher areal capacity. At the same time, a very high current density is employed, which favors

stable cathode cycling.^[134] A high current density combined with a low areal capacity avoids short circuit mediated cell failure (see above) for even the reference cell that is simply demonstrated to undergo faster capacity decay compared to the optimized cell. Such an observation does not necessarily testify to dendritic inhibition in the full cell, and the reason for the faster capacity decay in the reference cell remains ambiguous. Since typically a large volume of electrolyte and a significantly large excess of zinc is employed, corrosion related loss of zinc/electrolyte would not lead to a major capacity fading in the reference cell. Besides, the excellent long-term cyclability reported with the unoptimized electrolyte/Zn in every seminal materials discovery study cannot suddenly become unachievable in the context of Zn dendrite/corrosion inhibition studies. This ambiguity deserves particular attention from the AZIB research community to ensure consistency across reports.

5.6. Analysis of gravimetric and volumetric energy density

Accounting for the practically relevant parameters such as separator thickness, electrode loading, zinc excess, and electrolyte amount into consideration is essential for a realistic and balanced assessment of any innovative breakthrough approaches promising improvement in performance. A shallow utilization of Zn metal (or low depth of discharge) artificially leads to an extended performance, but it does not translate into a high energy density.^[135] The same is true for the separator thickness, and the electrolyte volume, which are somewhat intertwined as a thicker separator requires a greater volume of the electrolyte to soak the separator or fill the separator pores. In this regard, here we present an analysis of the gravimetric (E_G) and volumetric (E_V) energy density of a single layer AZIB stack – consisting of only one cathode and one zinc anode layer – as a function of zinc excess, separator thickness and electrolyte volume relative to the cycled capacity. To simplify the calculation, we did not consider the packaging material or a multilayer stack that would otherwise allow double-sided use of the current collectors and lead to a slightly higher energy density. Here $\alpha\text{-MnO}_2$ has been chosen as the representative cathode with an average voltage of 1.3 V and a capacity of 285 mAh g^{-1} that is typically obtained at a C/5 current rate.^[136] 80 wt% active material along with 15 wt% conducting carbon (Super P) and 5 wt% binder make up the cathode composite, assuming a nominal cathode porosity of 20%. For the electrolyte, the most commonly employed aqueous ZnSO_4 electrolyte of 1 M concentration has been chosen, and for the separator the glass microfiber filter paper (Whatman GF/A® type) has been selected, which has a porosity of 90%, and the thickness has been varied. The contribution of the electrolyte volume to the total stack volume is calculated as: *electrolyte volume – cathode pore volume – separator pore volume* since electrolyte is going to spread inside the cathode and separator pores. This, in turn, leads to very little to no contribution of the electrolyte volume to the volume of the overall stack. The cathode collector, a 5 μm thick Ti foil, is fixed

for all the calculations. Finally, the Zn anode is considered as a pure metal foil and is assumed to remain fully dense and maintain the thickness for simplification. Based on these assumptions, E_G and E_V values for a single layer $Zn|\alpha\text{-MnO}_2$ cell stack can be calculated based on the following equations. The parameters used here are further summarized in the supporting information.

$$E_G = \frac{V \times Q}{m_e + m_b + m_c + m_{am} + m_{Zn} + m_s + m_{Ti}} \quad (27)$$

where V is the average discharge voltage and Q is the specific discharge capacity of $\alpha\text{-MnO}_2$ cathode at a C/5 rate, m_e , m_b , m_c , m_{am} , m_{Zn} , m_s , m_{Ti} are the mass of electrolyte, binder additive, conductive carbon, active cathode material, Zn electrode, separator, and Ti current collector, respectively.

$$V_{cathode} = V_b + V_c + V_{am} + V_{pore} \quad (28)$$

$$V_e = V'_e - V_s \times \rho_s - V_{pore} \quad (29)$$

$$\begin{aligned} E_V = & \frac{V \times Q}{V_{cathode} + V_e + V_{Zn} + V_s + V_{Ti}} = \\ & \frac{V \times Q}{(V_b + V_c + V_{am} + V_{pore}) + (V'_e - V_s \times \rho_s - V_{pore}) + V_{Zn} + V_s + V_{Ti}} \end{aligned} \quad (30)$$

where $V_{cathode}$ is the actual volume of the cathode, V_b , V_c , V_{am} are the theoretical volume of binder additive, conductive carbon, and active material, respectively. V_{pore} is the pore volume of the cathode. V_e is the surplus electrolyte volume after soaking into the pore of the separator and cathode, V'_e is the actual volume of electrolyte, V_s and ρ_s are the electrolyte and porosity of the separator, respectively. V_{Zn} and V_{Ti} are the volume of Zn anode and Ti current collector.

The energy density values, as approximated by the above two equations, are presented in Figure 21, and the corresponding data can be found in the accompanying spreadsheet (Supporting Information). Since the cathode capacity (the cathode loading), which is also the cycled capacity, has the most profound impact on the energy density, the influence of the parameters has been assessed as a function of the capacity. It is apparent that a capacity of $\sim 3 \text{ mAh cm}^{-2}$ would be critical to achieving considerable energy densities for practical applications. This also means that the Zn cycling studies in Zn anode stabilization related works should be performed at

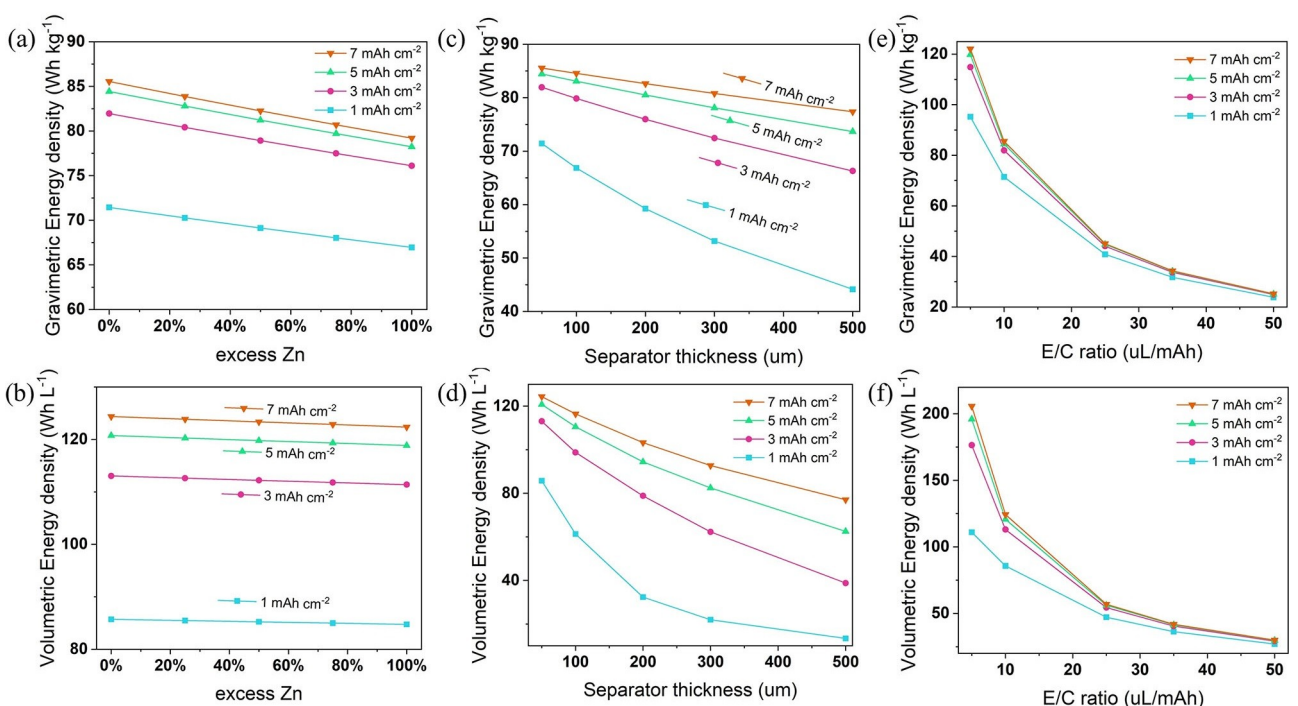


Figure 21. Gravimetric and volumetric energy density variation of a single layer $Zn|\alpha\text{-MnO}_2$ cell stack as a function of a, b) excess Zn, c, d) separator thickness, and e, f) electrolyte to cathode ratio (E/C ratio) in terms of volume per mAh capacity. For all calculations active material proportion at the cathode was fixed at 0.8 (or 80%) and the porosity of the cathode was fixed at 0.2. The thickness of the separator was fixed at 50 μm (for a, b, c, e, f) and its porosity was fixed at 90% based on the data available for commercial glass fiber membrane filter (Whatman GF/A). For (1, b, c, d) the E/C ratio was fixed at 10 $\mu\text{L mAh}^{-1}$, which is equivalent to $\sim 2.85 \mu\text{L}$ of electrolyte per mg of $\alpha\text{-MnO}_2$ loading at the cathode. The Zn excess was fixed at zero for (c–f). Further details regarding the calculation and the datasheet are provided as the Supporting Information.

>1 mAh cm⁻² to have any practical relatability. Notably, as increasing the capacity beyond 3 mAh cm⁻² has little effect on the energy density, the AZIB cell chemistry must be optimized for 3–4 mAh cm⁻² areal capacity cycling. Among the three cell parameters probed here, Zn excess and separator thickness have a relatively small effect on the E_G (Figure 21a and c). The E_V variation is even less with Zn excess in the 0 to 100% range (Figure 21b). This is understandable as zinc is a high-density metal, and excess zinc would not proportionately add to the volume increase. Yet, assuming the observed linear trend, the E_G and E_V are anticipated to drop to 59.2 Wh kg⁻¹ and 105.2 Wh l⁻¹ at 500% Zn excess. Therefore, it can be concluded that for practical development, the Zn excess must be contained below 100%, which is a rather steep target considering that almost all the Zn anode works are conducted with over 1000% Zn excess if not more, and the Zn loss with cycling due to corrosion and dendrite formation remains unassessed. The separator thickness is found to have a strong influence on the E_V – dropping from 113 Wh l⁻¹ for 100 µm thickness to 38.7 Wh l⁻¹ for 500 µm – as a high degree of porosity (90%) leads to a rapid increase in volume with increasing thickness (Figure 21d). Even though the volumetric energy density is not a major concern for stationary applications, the large separator thickness can completely nullify the positive E_V contribution of the Zn anode, and a larger dimension would add to the ancillary (packaging, infrastructure, etc.) cost. Electrolyte to cycled capacity ratio (E/C in µL mAh⁻¹) has the most severe consequence on E_G and E_V (Figure 21e and f). Increasing E/C from 10 µL mAh⁻¹ to 25 µL mAh⁻¹, i.e., from 2.28 µL mg⁻¹ to 5.7 µL mg⁻¹ in terms of the total cathode loading, the E_G dramatically drops from 114.9 Wh kg⁻¹ to 44.1 Wh kg⁻¹. The corresponding drop in E_V is from 176.4 Wh l⁻¹ to 54.4 Wh l⁻¹. This sensitivity to the E/C ratio can be particularly concerning if an excess volume of electrolyte is deemed necessary to cover for the electrolyte loss due to corrosion. In fact, corrosion mediated electrolyte decomposition, which is suspected to primarily occur in the form of HER during Zn deposition, needs to be eliminated for the practical viability of the AZIB technology. This means particular attention must be dedicated to accurately quantifying water (electrolyte) related corrosion at the Zn anode and conducting Zn anode cyclability assessment at low E/C ratios. Interestingly, the low volume of electrolyte implementation indirectly necessitates that a thin separator is employed as a thicker separator (with high porosity) would require a larger volume of electrolyte for sufficient wetting.

The E_G of ~80 Wh kg⁻¹ and E_V of ~100 Wh l⁻¹ of the Zn/MnO₂ AZIB technology surpasses the lead-acid technology and appears to catch up with nonaqueous LiFePO₄-graphite and sodium-ion technologies in terms of the energy density,^[137] which are potential competitions for stationary storage applications. However, those energy values are only achievable under relatively stringent conditions, namely 3–4 mAh cm⁻² areal capacity, <100% Zn excess, ≤100 µm separator thickness and ≤10 µL mAh⁻¹ electrolyte utilization. Understandably, such strict requirements cannot suddenly be applied in lab-scale investigations, mainly because the effect of all the different

factors on cell stability remains unclear. But progressive steps should still be taken to elucidate the Zn anode performance under near practical conditions, which would help benchmark the innovative strategies in a relatable and reproducible framework.

5.7. Concluding remarks

Despite the significantly large volume of studies on Zn anode for AZIBs in the last few years, its development is still in an early stage, and considerable focus must be directed toward fundamental understanding without which achieving good performance under practically relevant conditions would remain a long shot. For example, Zn dendrites growth resulting from the inhomogeneous nucleation at the initial nucleation stage is considered to be a diffusion-controlled process and susceptible to the crystalline structure of Zn. However, deeper fundamental investigations are needed to shed light on the origin of the rampant ion diffusion and the role of the crystallographic orientation (texture) on the growth morphology. Similarly, HER corrosion, which may not only lead to electrolyte dry out mediated cell failure but is also suspected of inducing dendritic deposition, must be thoroughly probed to unravel the factors that can promote and suppress it. The stabilization of the Zn anode electrochemistry, key for the realization of the AZIB technology, has witnessed many efforts as innovation breakthrough with inflated expectations. It is now time to push into the slope of enlightenment through deeper understanding and rigorous assessment in a practically relevant framework, essential to avoid falling into a slump and render the early promise into a reality.

Acknowledgements

Open access publishing facilitated by University of New South Wales, as part of the Wiley - University of New South Wales agreement via the Council of Australian University Librarians.

Conflict of Interest

The authors declare no conflict of interest.

Keywords: aqueous zinc-ion batteries • energy density analysis • zinc anode • zinc dendrite • corrosion inhibition

- [1] B. Obama, *Science* **2017**, *355*, 126.
- [2] a) S. Chu, Y. Cui, N. Liu, *Nat. Mater.* **2016**, *16*, 16; b) M. Armand, J.-M. Tarascon, *Nature* **2008**, *451*, 652.
- [3] J.-M. Tarascon, M. Armand, in *Materials for sustainable energy: a collection of peer-reviewed research and review articles from Nature Publishing Group* (Eds: V. Dusastre), World Scientific, Montréal, Canada **2011**, p. 171.
- [4] X. Wu, A. Markir, Y. Xu, C. Zhang, D. P. Leonard, W. Shin, X. Ji, *Adv. Funct. Mater.* **2019**, *29*, 1900911.

- [5] G. A. Elia, K. Marquardt, K. Hoeppner, S. Fantini, R. Lin, E. Knipping, W. Peters, J. F. Drillet, S. Passerini, R. Hahn, *Adv. Mater.* **2016**, *28*, 7564.
- [6] Y. Li, J. Fu, C. Zhong, T. Wu, Z. Chen, W. Hu, K. Amine, J. Lu, *Adv. Energy Mater.* **2019**, *9*, 1802605.
- [7] a) B. Jiang, C. Xu, C. Wu, L. Dong, J. Li, F. Kang, *Electrochim. Acta* **2017**, *229*, 422; b) D. Kundu, B. D. Adams, V. Duffort, S. H. Vajargah, L. F. Nazar, *Nat. Energy* **2016**, *1*, 16119; c) H. Pan, Y. Shao, P. Yan, Y. Cheng, K. S. Han, Z. Nie, C. Wang, J. Yang, X. Li, P. Bhattacharya, K. T. Mueller, J. Liu, *Nat. Energy* **2016**, *1*, 16039; d) F. Tang, J. Gao, Q. Ruan, X. Wu, X. Wu, T. Zhang, Z. Liu, Y. Xiang, Z. He, X. Wu, *Electrochim. Acta* **2020**, *353*, 136570.
- [8] a) S. Guo, G. Fang, S. Liang, M. Chen, X. Wu, J. Zhou, *Acta Mater.* **2019**, *180*, 51; b) L. Wang, S. Yan, C. D. Quilty, J. Kuang, M. R. Dunkin, S. N. Ehrlich, L. Ma, K. J. Takeuchi, E. S. Takeuchi, A. C. Marschilok, *Adv. Mater. Interfaces* **2021**, *8*, 2002080; c) P. Oberholzer, E. Tervoort, A. Bouzid, A. Pasquarello, D. Kundu, *ACS Appl. Mater. Interfaces* **2018**, *11*, 674; d) H. Liang, Z. Cao, F. Ming, W. Zhang, D. H. Anjum, Y. Cui, L. Cavallo, H. N. Alshareef, *Nano Lett.* **2019**, *19*, 3199.
- [9] a) M. S. Chae, J. W. Heo, H. H. Kwak, H. Lee, S.-T. Hong, *J. Power Sources* **2017**, *337*, 204; b) L. Zhang, L. Chen, X. Zhou, Z. Liu, *Adv. Energy Mater.* **2015**, *5*, 1400930; c) D. Selvakumaran, A. Pan, S. Liang, G. Cao, *J. Mater. Chem. A* **2019**, *7*, 18209.
- [10] C. Xie, Y. Li, Q. Wang, D. Sun, Y. Tang, H. Wang, *Carbon Energy* **2020**, *2*, 540.
- [11] a) C. Han, W. Li, H. K. Liu, S. Dou, J. Wang, *Nano Energy* **2020**, *74*, 104880; b) Z. Cao, P. Zhuang, X. Zhang, M. Ye, J. Shen, P. M. Ajayan, *Adv. Energy Mater.* **2020**, *10*, 2001599; c) F. Wan, X. Zhou, Y. Lu, Z. Niu, J. Chen, *ACS Energy Lett.* **2020**, *5*, 3569; d) M. Fayette, H. J. Chang, I. A. Rodríguez-Pérez, X. Li, D. Reed, *ACS Appl. Mater. Interfaces* **2020**, *12*, 42763; e) S. Huang, J. Zhu, J. Tian, Z. Niu, *Chem. Eur. J.* **2019**, *25*, 14480; f) D. Han, S. Wu, S. Zhang, Y. Deng, C. Cui, L. Zhang, Y. Long, H. Li, Y. Tao, Z. Weng, Q.-H. Yang, F. Kang, *Small* **2020**, *16*, 2001736; g) B. Li, X. Zhang, T. Wang, Z. He, B. Lu, S. Liang, J. Zhou, *Nano-Micro Lett.* **2021**, *14*, 6.
- [12] C. Zhao, X. Wang, C. Shao, G. Li, J. Wang, D. Liu, X. Dong, *Sustain. Energy Fuels* **2021**, *5*, 332.
- [13] T. Wang, C. Li, X. Xie, B. Lu, Z. He, S. Liang, J. Zhou, *ACS Nano* **2020**, *14*, 16321.
- [14] B. Beverskog, I. Puigdomenech, *Corros. Sci.* **1997**, *39*, 107.
- [15] L. M. Baugh, A. Higginson, *Electrochim. Acta* **1985**, *30*, 1163.
- [16] R. W. Powers, M. W. Breiter, *J. Electrochem. Soc.* **1969**, *116*, 719.
- [17] V. N. Flerov, *Zh. Prikl. Khim.* **1959**, *32*, 132.
- [18] M. F. Bell, Anodic Dissolution of Zinc. Doctoral dissertation, University of Newcastle upon Tyne, **1976**.
- [19] S. Thomas, N. Birbilis, M. S. Venkatraman, I. S. Cole, *Corrosion, J. Sci. Eng.* **2012**, *68*, 015009.
- [20] K. Wippermann, J. W. Schultze, R. Kessel, J. Penninger, *Corros. Sci.* **1991**, *32*, 205.
- [21] a) C. Cachet, B. Saidani, R. Wiart, *J. Electrochem. Soc.* **1991**, *138*, 678; b) C. Cachet, B. Saidani, R. Wiart, *J. Electrochem. Soc.* **1992**, *139*, 644; c) C. Cachet, U. Ströder, R. Wiart, *Electrochim. Acta* **1982**, *27*, 903.
- [22] a) J. Hendrikx, A. van der Putten, W. Visscher, E. Barendrecht, *Electrochim. Acta* **1984**, *29*, 81; b) T. P. Dirkse, N. A. Hampson, *Electrochim. Acta* **1972**, *17*, 135; c) T. P. Dirkse, N. A. Hampson, *Electrochim. Acta* **1972**, *17*, 1113; d) T. P. Dirkee, N. A. Hampson, *J. Electroanal. Chem. Interfacial Electrochem.* **1972**, *35*, 7.
- [23] S. K. Sharma, M. D. Reed, *J. Inorg. Nucl. Chem.* **1976**, *38*, 1971.
- [24] M. C. H. McKubre, D. D. Macdonald, *J. Electrochem. Soc.* **1981**, *128*, 524.
- [25] M. Mokaddem, P. Volovitch, K. Ogle, *Electrochim. Acta* **2010**, *55*, 7867.
- [26] T. Yamamoto, T. Shoji, M. Hishinuma, *J. Appl. Electrochem.* **1988**, *18*, 521.
- [27] a) T. Hurlen, K. P. Fischer, *J. Electroanal. Chem. Interfacial Electrochem.* **1975**, *61*, 165; b) L. M. Baugh, *Electrochim. Acta* **1979**, *24*, 669; c) L. M. Baugh, *Electrochim. Acta* **1979**, *24*, 657; d) R. D. Armstrong, M. F. Bell, J. *Electroanal. Chem. Interfacial Electrochem.* **1974**, *55*, 201.
- [28] a) Y. Xiao, J. Shi, F. Zhao, Z. Zhang, W. He, *J. Electrochim. Soc.* **2018**, *165*, A47; b) K. Wang, P. Pei, Z. Ma, H. Chen, H. Xu, D. Chen, X. Wang, *J. Mater. Chem. A* **2015**, *3*, 22648; c) Z. Zhao, X. Fan, J. Ding, W. Hu, C. Zhong, J. Lu, *ACS Energy Lett.* **2019**, *4*, 2259; d) M.-H. Lin, C.-J. Huang, P.-H. Cheng, J.-H. Cheng, C.-C. Wang, *J. Mater. Chem. A* **2020**, *8*, 20637; e) Y. Zhang, Y. Wu, W. You, M. Tian, P.-W. Huang, Y. Zhang, Z. Sun, Y. Ma, T. Hao, N. Liu, *Nano Lett.* **2020**, *20*, 4700; f) N. Chang, T. Li, R. Li, S. Wang, Y. Yin, H. Zhang, X. Li, *Energy Environ. Sci.* **2020**, *13*, 3527; g) A. Mitha, *Polyethylene Glycol as an Electrolyte Additive for Rechargeable Hybrid Aqueous Batteries*. Master thesis, University of Waterloo, **2018**; h) A. Wang, W. Zhou, A. Huang, M. Chen, Q. Tian, J. Chen, *J. Colloid Interface Sci.* **2021**, *586*, 362; i) Z. Hou, X. Zhang, X. Li, Y. Zhu, J. Liang, Y. Qian, *J. Mater. Chem. A* **2017**, *5*, 730; j) K. E. K. Sun, T. K. A. Hoang, T. N. L. Doan, Y. Yu, X. Zhu, Y. Tian, P. Chen, *ACS Appl. Mater. Interfaces* **2017**, *9*, 9681.
- [29] H. Glatz, E. Tervoort, D. Kundu, *ACS Appl. Mater. Interfaces* **2019**, *12*, 3522.
- [30] B. Tang, L. Shan, S. Liang, J. Zhou, *Energy Environ. Sci.* **2019**, *12*, 3288.
- [31] a) A. Rami, A. Lasia, *J. Appl. Electrochem.* **1992**, *22*, 376; b) L. Chen, A. Lasia, *J. Electrochem. Soc.* **1992**, *139*, 3214; c) R. K. Shervedani, A. Lasia, *J. Electrochem. Soc.* **1997**, *144*, 2652; d) L. Chen, A. Lasia, *J. Electrochem. Soc.* **1991**, *138*, 3321.
- [32] R. Ichino, C. Cachet, R. Wiart, *Electrochim. Acta* **1996**, *41*, 1031.
- [33] T. Trišović, L. Gajić Krstajić, N. Krstajić, M. Vojnović, *J. Serb. Chem. Soc.* **2001**, *66*, 811.
- [34] H. Li, Q. Yang, F. Mo, G. Liang, Z. Liu, Z. Tang, L. Ma, J. Liu, Z. Shi, C. Zhi, *Energy Storage Mater.* **2019**, *19*, 94.
- [35] V. Yufit, F. Tariq, D. S. Eastwood, M. Bitton, B. Wu, P. D. Lee, N. P. Brandon, *Joule* **2019**, *3*, 485.
- [36] A. Pei, G. Zheng, F. Shi, Y. Li, Y. Cui, *Nano Lett.* **2017**, *17*, 1132.
- [37] S. Xu, Y. Zhu, D. Xiong, L. Wang, P. Yang, P. K. Chu, *J. Phys. Chem.* **2017**, *121*, 3938.
- [38] Q. Yang, G. Liang, Y. Guo, Z. Liu, B. Yan, D. Wang, Z. Huang, X. Li, J. Fan, C. Zhi, *Adv. Mater.* **2019**, *31*, 1903778.
- [39] L. Schoeman, K. C. Sole, *J. S. Afr. Inst. Min. Metall.* **2017**, *117*, 622.
- [40] a) Z. Zhao, J. Zhao, Z. Hu, J. Li, J. Li, Y. Zhang, C. Wang, G. Cui, *Energy Environ. Sci.* **2019**, *12*, 1938; b) H. Liu, Y. Zhang, C. Wang, J. N. Glazer, Z. Shan, N. Liu, *ACS Appl. Mater. Interfaces* **2021**, *13*, 32930.
- [41] N. Zhang, F. Cheng, Y. Liu, Q. Zhao, K. Lei, C. Chen, X. Liu, J. Chen, *J. Am. Chem. Soc.* **2016**, *138*, 12894.
- [42] K. S. Nagy, S. Kazemiabnabi, K. Thornton, D. J. Siegel, *ACS Appl. Mater. Interfaces* **2019**, *11*, 7954.
- [43] a) Q. Zhang, J. Luan, Y. Tang, X. Ji, H. Wang, *Angew. Chem. Int. Ed.* **2020**, *59*, 13180; b) L. Li, J. Xue, C. Han, N. Liu, K. Ma, R. Zhang, X. Wu, L. Dai, L. Wang, Z. He, *J. Colloid Interface Sci.* **2021**, *599*, 467.
- [44] L. Kang, M. Cui, F. Jiang, Y. Gao, H. Luo, J. Liu, W. Liang, C. Zhi, *Adv. Energy Mater.* **2018**, *8*, 1801090.
- [45] K. Zhao, C. Wang, Y. Yu, M. Yan, Q. Wei, P. He, Y. Dong, Z. Zhang, X. Wang, L. Mai, *Adv. Mater. Interfaces* **2018**, *5*, 1800848.
- [46] Q. Zhang, J. Luan, X. Huang, Q. Wang, D. Sun, Y. Tang, X. Ji, H. Wang, *Nat. Commun.* **2020**, *11*, 3961.
- [47] H. He, J. Liu, *J. Mater. Chem. A* **2020**, *8*, 22100.
- [48] P. Liang, J. Yi, X. Liu, K. Wu, Z. Wang, J. Cui, Y. Liu, Y. Wang, Y. Xia, J. Zhang, *Adv. Funct. Mater.* **2020**, *30*, 1908528.
- [49] X. Xie, S. Liang, J. Gao, S. Guo, J. Guo, C. Wang, G. Xu, X. Wu, G. Chen, J. Zhou, *Energy Environ. Sci.* **2020**, *13*, 503.
- [50] J. Y. Kim, G. Liu, G. Y. Shim, H. Kim, J. K. Lee, *Adv. Funct. Mater.* **2020**, *30*, 2004210.
- [51] a) O. Borodin, X. Ren, J. Vatamanu, A. von Wald Cresce, J. Knap, K. Xu, *Acc. Chem. Res.* **2017**, *50*, 2886; b) F. Wang, O. Borodin, M. S. Ding, M. Gobet, J. Vatamanu, X. Fan, T. Gao, N. Eidsom, Y. Liang, W. Sun, *Joule* **2018**, *2*, 927; c) C. Yan, H.-R. Li, X. Chen, X.-Q. Zhang, X.-B. Cheng, R. Xu, J.-Q. Huang, Q. Zhang, *J. Am. Chem. Soc.* **2019**, *141*, 9422.
- [52] Z. Zhou, Y. Zhang, P. Chen, Y. Wu, H. Yang, H. Ding, Y. Zhang, Z. Wang, X. Du, N. Liu, *Chem. Eng. Sci.* **2019**, *194*, 142.
- [53] A. Naveed, H. Yang, J. Yang, Y. Nuli, J. Wang, *Angew. Chem. Int. Ed.* **2019**, *58*, 2760.
- [54] M. Cui, Y. Xiao, L. Kang, W. Du, Y. Gao, X. Sun, Y. Zhou, X. Li, H. Li, F. Jiang, C. Zhi, *ACS Appl. Energ. Mater.* **2019**, *2*, 6490.
- [55] Y. Yin, S. Wang, Q. Zhang, Y. Song, N. Chang, Y. Pan, H. Zhang, X. Li, *Adv. Mater.* **2020**, *32*, 1906803.
- [56] J. Liang, Z.-H. Sun, F. Li, H.-M. Cheng, *Energy Storage Mater.* **2016**, *2*, 76.
- [57] H. Li, C. Xu, C. Han, Y. Chen, C. Wei, B. Li, F. Kang, *J. Electrochem. Soc.* **2015**, *162*, A1439.
- [58] A. Wang, W. Zhou, A. Huang, M. Chen, J. Chen, Q. Tian, J. Xu, *J. Colloid Interface Sci.* **2020**, *577*, 256.
- [59] C. Shen, X. Li, N. Li, K. Xie, J.-g. Wang, X. Liu, B. Wei, *ACS Appl. Mater. Interfaces* **2018**, *10*, 25446.
- [60] A. Xia, X. Pu, Y. Tao, H. Liu, Y. Wang, *Appl. Surf. Sci.* **2019**, *481*, 852.
- [61] Y. Zeng, X. Zhang, R. Qin, X. Liu, P. Fang, D. Zheng, Y. Tong, X. Lu, *Adv. Mater.* **2019**, *31*, 1903675.
- [62] Y. Qian, C. Meng, J. He, X. Dong, *J. Power Sources* **2020**, *480*, 228871.
- [63] W. Dong, J.-L. Shi, T.-S. Wang, Y.-X. Yin, C.-R. Wang, Y.-G. Guo, *RSC Adv.* **2018**, *8*, 19157.

- [64] Q. Guan, Y. Li, X. Bi, J. Yang, J. Zhou, X. Li, J. Cheng, Z. Wang, B. Wang, J. Lu, *Adv. Energy Mater.* **2019**, *9*, 1901434.
- [65] F. Ding, W. Xu, G. L. Graff, J. Zhang, M. L. Sushko, X. Chen, Y. Shao, M. H. Engelhard, Z. Nie, J. Xiao, *J. Am. Chem. Soc.* **2013**, *135*, 4450.
- [66] Q. Zhang, J. Luan, L. Fu, S. Wu, Y. Tang, X. Ji, H. Wang, *Angew. Chem. Int. Ed.* **2019**, *58*, 15841.
- [67] a) R. K. Ghavami, Z. Rafiei, S. M. Tabatabaei, *J. Power Sources* **2007**, *164*, 934; b) J. Zhu, Y. Zhou, C. Gao, *J. Power Sources* **1998**, *72*, 231.
- [68] A. Bayaguud, X. Luo, Y. Fu, C. Zhu, *ACS Energy Lett.* **2020**, *5*, 3012.
- [69] A. Mitha, H. Mi, W. Dong, I. S. Cho, J. Ly, S. Yoo, S. Bang, T. K. A. Hoang, P. Chen, *J. Electroanal. Chem.* **2019**, *836*, 1.
- [70] D. Zhang, A. J. Warren, G. Li, Z. Cheng, X. Han, Q. Zhao, X. Liu, Y. Deng, L. A. Archer, *Macromolecules* **2020**, *53*, 2694.
- [71] W. Xu, K. Zhao, W. Huo, Y. Wang, G. Yao, X. Gu, H. Cheng, L. Mai, C. Hu, X. Wang, *Nano Energy* **2019**, *62*, 275.
- [72] X. Guo, Z. Zhang, J. Li, N. Luo, G.-L. Chai, T. S. Miller, F. Lai, P. Shearing, D. J. L. Brett, D. Han, Z. Weng, G. He, I. P. Parkin, *ACS Energy Lett.* **2021**, *6*, 395.
- [73] S.-B. Wang, Q. Ran, R.-Q. Yao, H. Shi, Z. Wen, M. Zhao, X.-Y. Lang, Q. Jiang, *Nat. Commun.* **2020**, *11*, 1634.
- [74] C. Deng, X. Xie, J. Han, Y. Tang, J. Gao, C. Liu, X. Shi, J. Zhou, S. Liang, *Adv. Funct. Mater.* **2020**, *30*, 2000599.
- [75] Q. Yang, Y. Guo, B. Yan, C. Wang, Z. Liu, Z. Huang, Y. Wang, Y. Li, H. Li, L. Song, J. Fan, C. Zhi, *Adv. Mater.* **2020**, *32*, 2001755.
- [76] T. D. Gierke, G. Munn, F. Wilson, *J. Polym. Sci. Polym. Phys. Ed.* **1981**, *19*, 1687.
- [77] Y. Cui, Q. Zhao, X. Wu, X. Chen, J. Yang, Y. Wang, R. Qin, S. Ding, Y. Song, J. Wu, *Angew. Chem. Int. Ed.* **2020**, *132*, 16737.
- [78] Z. Wang, J. Huang, Z. Guo, X. Dong, Y. Liu, Y. Wang, Y. Xia, *Joule* **2019**, *3*, 1289.
- [79] R. Yuksel, O. Buyukcakir, W. K. Seong, R. S. Ruoff, *Adv. Energy Mater.* **2020**, *10*, 1904215.
- [80] Y. An, Y. Tian, Y. Li, C. Wei, Y. Tao, Y. Liu, B. Xi, S. Xiong, J. Feng, Y. Qian, *Chem. Eng. J.* **2020**, *400*, 125843.
- [81] X. Liu, F. Yang, W. Xu, Y. Zeng, J. He, X. Lu, *Adv. Sci.* **2020**, *7*, 2002173.
- [82] Y. Tang, C. Liu, H. Zhu, X. Xie, J. Gao, C. Deng, M. Han, S. Liang, J. Zhou, *Energy Storage Mater.* **2020**, *27*, 109.
- [83] F. Mo, Z. Chen, G. Liang, D. Wang, Y. Zhao, H. Li, B. Dong, C. Zhi, *Adv. Energy Mater.* **2020**, *10*, 2000035.
- [84] M. Zhou, Y. Chen, G. Fang, S. Liang, *Energy Storage Mater.* **2022**, *45*, 618.
- [85] S. Huang, J. Zhu, J. Tian, Z. Niu, *Chem. Eur. J.* **2019**, *25*, 14480.
- [86] D. Kundu, S. H. Vajargah, L. Wan, B. Adams, D. Prendergast, L. F. Nazar, *Energy Environ. Sci.* **2018**, *11*, 881.
- [87] a) W. Sun, F. Wang, S. Hou, C. Yang, X. Fan, Z. Ma, T. Gao, F. Han, R. Hu, M. Zhu, *J. Am. Chem. Soc.* **2017**, *139*, 9775; b) F. Wan, Y. Zhang, L. Zhang, D. Liu, C. Wang, L. Song, Z. Niu, J. Chen, *Angew. Chem. Int. Ed.* **2019**, *58*, 7062.
- [88] T. Zhang, Y. Tang, S. Guo, X. Cao, A. Pan, G. Fang, J. Zhou, S. Liang, *Energy Environ. Sci.* **2020**, *13*, 4625.
- [89] a) D. Wang, H. Li, Z. Liu, Z. Tang, G. Liang, F. Mo, Q. Yang, L. Ma, C. Zhi, *Small* **2018**, *14*, 1803978; b) T. K. A. Hoang, M. Acton, H. T. H. Chen, Y. Huang, T. N. L. Doan, P. Chen, *Mater. Today* **2017**, *4*, 34; c) W. Xiong, D. Yang, T. K. A. Hoang, M. Ahmed, J. Zhi, X. Qiu, P. Chen, *Energy Storage Mater.* **2018**, *15*, 131; d) T. K. A. Hoang, T. N. L. Doan, J. H. Cho, J. Y. J. Su, C. Lee, C. Lu, P. Chen, *ChemSusChem* **2017**, *10*, 2816.
- [90] D. Abayarathna, E. Hale, T. O'Keeffe, Y.-M. Wang, D. Radovic, *Corros. Sci.* **1991**, *32*, 755.
- [91] K. E. K. Sun, T. K. A. Hoang, T. N. L. Doan, Y. Yu, P. Chen, *Chem. Eur. J.* **2018**, *24*, 1667.
- [92] E. Fahrenkrug, J. Gu, S. Jeon, P. A. Veneman, R. S. Goldman, S. Maldonado, *Nano Lett.* **2014**, *14*, 847.
- [93] J. Zheng, Q. Zhao, T. Tang, J. Yin, C. D. Quilty, G. D. Renderos, X. Liu, Y. Deng, L. Wang, D. C. Bock, *Science* **2019**, *366*, 645.
- [94] M. Liu, L. Yang, H. Liu, A. Amine, Q. Zhao, Y. Song, J. Yang, K. Wang, F. Pan, *ACS Appl. Mater. Interfaces* **2019**, *11*, 32046.
- [95] J. Zheng, L. A. Archer, *Sci. Adv.* **2021**, *7*, 2.
- [96] D. Yuan, J. Zhao, H. Ren, Y. Chen, R. Chua, E. T. J. Jie, Y. Cai, E. Edison, W. Manalastas Jr., M. W. Wong, M. Srinivasan, *Angew. Chem. Int. Ed.* **2020**, *13*, 133.
- [97] J. Cong, X. Shen, Z. Wen, X. Wang, L. Peng, J. Zeng, J. Zhao, *Energy Storage Mater.* **2021**, *35*, 586.
- [98] Z. Liu, T. Cui, G. Pulletikurthi, A. Lahiri, T. Carstens, M. Olschewski, F. Endres, *Angew. Chem. Int. Ed.* **2016**, *55*, 2889.
- [99] M. Zhou, S. Guo, J. Li, X. Luo, Z. Liu, T. Zhang, X. Cao, M. Long, B. Lu, A. Pan, G. Fang, J. Zhou, S. Liang, *Adv. Mater.* **2021**, *33*, 2100187.
- [100] J. Cao, D. Zhang, R. Chanajaree, Y. Yue, Z. Zeng, X. Zhang, J. Qin, *Adv. Powder Mater.* **2021**, DOI: <https://doi.org/10.1016/j.apmater.2021.09.007>.
- [101] M. Xu, T. Zhu, J. Z. Zhang, *J. Phys. Chem.* **2019**, *123*, 6587.
- [102] J. Hao, L. Yuan, C. Ye, D. Chao, K. Davey, Z. Guo, S. Qiao, *Angew. Chem. Int. Ed.* **2021**, *13*, 7336.
- [103] a) N. Wang, Y. Yang, X. Qiu, X. Dong, Y. Wang, Y. Xia, *ChemSusChem* **2020**, *13*, 5556; b) R. Qin, Y. Wang, M. Zhang, Y. Wang, S. Ding, A. Song, H. Yi, L. Yang, Y. Song, Y. Cui, J. Liu, Z. Wang, S. Li, Q. Zhao, F. Pan, *Nano Energy* **2021**, *80*, 105478.
- [104] Y. Zhang, M. Zhu, K. Wu, F. Yu, G. Wang, G. Xu, M. Wu, H.-K. Liu, S.-X. Dou, C. Wu, *J. Mater. Chem.* **2021**, *9*, 4253.
- [105] M. Yan, C. Xu, Y. Sun, H. Pan, H. Li, *Nano Energy* **2021**, *82*, 105739.
- [106] Y. Jin, K. S. Han, Y. Shao, M. L. Sushko, J. Xiao, H. Pan, J. Liu, *Adv. Funct. Mater.* **2020**, *30*, 2003932.
- [107] B. W. Olbasa, F. W. Fenta, S.-F. Chiu, M.-C. Tsai, C.-J. Huang, B. A. Jote, T. T. Beyene, Y.-F. Liao, C.-H. Wang, W.-N. Su, H. Dai, B. J. Hwang, *ACS Appl. Energ. Mater.* **2020**, *3*, 4499.
- [108] F. Wang, O. Borodin, T. Gao, X. Fan, W. Sun, F. Han, A. Faraone, J. A. Dura, K. Xu, C. Wang, *Nat. Mater.* **2018**, *17*, 543.
- [109] H. Yang, Z. Chang, Y. Qiao, H. Deng, X. Mu, P. He, H. Zhou, *Angew. Chem. Int. Ed.* **2020**, *59*, 9377.
- [110] a) J. Zhao, Y. Li, X. Peng, S. Dong, J. Ma, G. Cui, L. Chen, *Electrochem. Commun.* **2016**, *69*, 6; b) X. Wu, Y. Xu, C. Zhang, D. P. Leonard, A. Markir, J. Lu, X. Ji, *J. Am. Chem. Soc.* **2019**, *141*, 6338; c) L. Zhang, I. A. Rodríguez-Pérez, H. Jiang, C. Zhang, D. P. Leonard, Q. Guo, W. Wang, S. Han, L. Wang, X. Ji, *Adv. Funct. Mater.* **2019**, *29*, 1902653; d) J. Zheng, T. Tang, Q. Zhao, X. Liu, Y. Deng, L. A. Archer, *ACS Energy Lett.* **2019**, *4*, 1349; e) X. Zhong, F. Wang, Y. Ding, L. Duan, F. Shi, C. Wang, *J. Electroanal. Chem.* **2020**, *867*, 114193; f) X. Song, H. He, M. H. A. Shiraz, H. Zhu, A. Khosrozadeh, J. Liu, *Chem. Commun.* **2021**, *57*, 1246.
- [111] C. Zhang, J. Holoubek, X. Wu, A. Daniyar, L. Zhu, C. Chen, D. P. Leonard, I. A. Rodríguez-Pérez, J.-X. Jiang, C. Fang, *Chem. Commun.* **2018**, *54*, 14097.
- [112] V. Chakarova, T. Boiadjieva-Scherzer, D. Kovacheva, H. Kronberger, M. Monev, *Corros. Sci.* **2018**, *140*, 73.
- [113] a) A.-R. El-Sayed, H. S. Mohran, H. M. Abd El-Lateef, *Metall. Mater. Trans. A* **2012**, *43*, 619; b) H. S. Kim, Y. N. Jo, W. J. Lee, K. J. Kim, C. W. Lee, *Electroanalysis* **2015**, *27*, 517.
- [114] C. W. Lee, S. W. Eom, K. Sathiyanarayanan, M. S. Yun, *Electrochim. Acta* **2006**, *52*, 1588.
- [115] Z. Cai, Y. Ou, J. Wang, R. Xiao, L. Fu, Z. Yuan, R. Zhan, Y. Sun, *Energy Storage Mater.* **2020**, *27*, 205.
- [116] H. Tian, Z. Li, G. Feng, Z. Yang, D. Fox, M. Wang, H. Zhou, L. Zhai, A. Kushneria, Y. Du, Z. Feng, X. Shan, Y. Yang, *Nat. Commun.* **2021**, *12*, 237.
- [117] D. Chao, W. Zhou, F. Xie, C. Ye, H. Li, M. Jaroniec, S.-Z. Qiao, *Sci. Adv.* **2020**, *6*, 21.
- [118] X. G. Zhang, *J. Electrochem. Soc.* **1996**, *143*, 1472.
- [119] I. O. Wallinder, C. Leygraf, C. Karlen, D. Heijerick, C. Janssen, *Corros. Sci.* **2001**, *43*, 809.
- [120] M. Zhou, S. Guo, G. Fang, H. Sun, X. Cao, J. Zhou, A. Pan, S. Liang, *J. Energy Chem.* **2021**, *55*, 549.
- [121] a) H. Jia, Z. Wang, M. Dirican, S. Qiu, C. Y. Chan, S. Fu, B. Fei, X. Zhang, *J. Mater. Chem. A* **2021**, *9*, 5597; b) C. Liu, Z. Luo, W. Deng, W. Wei, L. Chen, A. Pan, J. Ma, C. Wang, L. Zhu, L. Xie, X.-Y. Cao, J. Hu, G. Zou, H. Hou, X. Ji, *ACS Energy Lett.* **2021**, *6*, 675.
- [122] W. Guo, Y. Zhang, X. Tong, X. Wang, L. Zhang, X. Xia, J. Tu, *Mater. Today* **2021**, *20*, 100675.
- [123] M. Schmid, M. Willert-Porada, *Electrochim. Acta* **2018**, *260*, 246.
- [124] N. S. Sangaj, V. Malshe, *Prog. Org. Coat.* **2004**, *50*, 28.
- [125] J. Hao, B. Li, X. Li, X. Zeng, S. Zhang, F. Yang, S. Liu, D. Li, C. Wu, Z. Guo, *Adv. Mater.* **2020**, *32*, 2003021.
- [126] L. Ma, Q. Li, Y. Ying, F. Ma, S. Chen, Y. Li, H. Huang, C. Zhi, *Adv. Mater.* **2021**, *33*, 2007406.
- [127] H. Qiu, X. Du, J. Zhao, Y. Wang, J. Ju, Z. Chen, Z. Hu, D. Yan, X. Zhou, G. Cui, *Nat. Commun.* **2019**, *10*, 5374.
- [128] L. Cao, D. Li, T. Deng, Q. Li, C. Wang, *Angew. Chem. Int. Ed.* **2020**, *59*, 19292.
- [129] X. Zeng, J. Mao, J. Hao, J. Liu, S. Liu, Z. Wang, Y. Wang, S. Zhang, T. Zheng, J. Liu, P. Rao, Z. Guo, *Adv. Mater.* **2021**, *33*, 2007416.
- [130] a) Y. Yang, C. Liu, Z. Lv, H. Yang, Y. Zhang, M. Ye, L. Chen, J. Zhao, C. C. Li, *Adv. Mater.* **2021**, *33*, 2007388; b) C. Zhi, Z. Chen, X. Li, D. Wang, Q. Yang, L. Ma, Z. Huang, G. Liang, A. Chen, Y. Guo, B. Dong, X. Huang, C.

- Yang, *Energy Environ. Sci.* **2021**, *14*, 3492; c) P. Sun, L. Ma, W. Zhou, M. Qiu, Z. Wang, D. Chao, W. Mai, *Angew. Chem. Int. Ed.* **2021**, *60*, 18247.
- [131] L. Ma, M. A. Schroeder, O. Borodin, T. P. Pollard, M. S. Ding, C. Wang, K. Xu, *Nat. Energy* **2020**, *5*, 743.
- [132] a) D. Aurbach, Y. Gofer, *J. Electrochem. Soc.* **1991**, *138*, 3529; b) L. Ma, M. A. Schroeder, T. P. Pollard, O. Borodin, M. S. Ding, R. Sun, L. Cao, J. Ho, D. R. Baker, C. Wang, *Energy Environ. Mater.* **2020**, *3*, 516; c) B. D. Adams, J. Zheng, X. Ren, W. Xu, J. G. Zhang, *Adv. Energy Mater.* **2018**, *8*, 1702097.
- [133] B. D. Adams, J. Zheng, X. Ren, W. Xu, J.-G. Zhang, *Adv. Energy Mater.* **2018**, *8*, 1702097.
- [134] L. E. Blanc, D. Kundu, L. F. Nazar, *Joule* **2020**, *4*, 771.
- [135] J. Zhi, S. Li, M. Han, P. Chen, *Sci. Adv.* **2020**, *6*, eabb1342.
- [136] H. Pan, Y. Shao, P. Yan, Y. Cheng, K. S. Han, Z. Nie, C. Wang, J. Yang, X. Li, P. Bhattacharya, K. T. Mueller, J. Liu, *Nat. Energy* **2016**, *1*, 16039.
- [137] Y. E. Durmus, H. Zhang, F. Baakes, G. Desmaizieres, H. Hayun, L. Yang, M. Kolek, V. Küpers, J. Janek, D. Mandler, S. Passerini, Y. Ein-Eli, *Adv. Energy Mater.* **2020**, *10*, 2000089.

Manuscript received: December 15, 2021

Revised manuscript received: January 23, 2022

Accepted manuscript online: January 24, 2022

Version of record online: February 9, 2022